

Polydisperse polymer networks with irregular topologies I: Mechanics of cross-link distributions

Jason Mulderrig,^{1,2,*} Michael Buche,³ and Matthew Grasinger^{1,†}

¹*Materials & Manufacturing Directorate, Air Force Research Laboratory,
Wright-Patterson AFB, Ohio 45433, USA*

²*National Research Council (NRC) Research Associateship Programs,
The National Academies of Sciences, Engineering, and Medicine*

³*Materials and Failure Modeling, Sandia National Laboratories, Albuquerque, New Mexico 87185, USA*

The structure of polymer networks, defined by chain lengths and connectivity patterns, fundamentally influences their bulk properties. While existing polymer network models connect chain properties to emergent network behavior, they are often limited to monodisperse networks with regular connectivities. In this work, we introduce a novel modeling framework that shifts the focus from individual polymer chains to cross-links and their connected chains as the fundamental unit of analysis. The key features of this framework are the relaxation of the cross-link junction position to satisfy local force balance, and physically intuitive means for satisfying material frame indifference. We explore two distinct limiting behaviors for the orientation of the frame of a cross-link: (1) the free rotation limit, which assumes the cross-link rotates to minimize free energy, and (2) the frame averaging limit, which incorporates structural heterogeneity by averaging over all possible cross-link orientations. It is found that an increase in variance in monomer numbers generally leads to network softening, while in bimodal networks, the onset of strain stiffening is controlled by shorter chains and the stiffening response is modulated by the ratio of short to long chains. By deriving closed-form approximations for both limits valid in the regimes of small deformation or small polydispersity, we offer an efficient computational approach to modeling the mechanics of complex, polydisperse networks. An aim of this framework is to take a step toward the rational modeling and design of heterogeneous polymer networks with structures tailored for specific properties.

I. INTRODUCTION

Constitutive models for solid polymer networks fall into two main categories: (1) phenomenological models based on strain invariants and principal stretches, and (2) micromechanical models that connect macromolecular and network structural properties to the continuum scale. In the first category, there is the Neo-Hookean, Mooney-Rivlin [1, 2], and Ogden models [3]. In this work, we focus on micromechanical models. Statistical mechanics help to elucidate the entropic underpinnings of the elasticity of many polymers [4]. The continuum response of a broader polymer network can be constructed by using the single-chain elasticity in a polymer network model. Network models allow one to relate macroscopic variables, such as deformation, to individual chains within the network.

Many polymer network models exist in the literature. Some have a discrete number of chains arranged in a representative volume element (RVE) while others model the network via a probability density of polymer chains. There are also competing assumptions for how macroscopic deformation is related to the deformations of chains within the network. Traditional discrete network models include the 3-chain [5], the 4-chain [6–10] (i.e. Flory-Rehner model), and the 8-chain [11] models. Continuous network models began with the full network model of Wu and van der Giessen [12, 13] (inspired by [14]) which assumes that all chains in the network are of the same length (in the reference

* mulderrig.jason@gmail.com

† matthew.grasinger.1@us.af.mil

configuration) and that the directions of chains are uniformly distributed over the unit sphere. In response to the (at times) underwhelming fit of the full network model to benchmark data on rubber elasticity, it was improved upon by the microsphere model of Miehe et al. [15]. A key feature of the microsphere model was the development of a new assumption for how macroscopic deformation is related to chains within the network. The assumption involved a “stretch fluctuation field” in the unit sphere of chain directions. The stretch fluctuation field is determined by minimizing the average free energy of the network subject to homogenization-based constraints. For certain fitted parameters, the microsphere model recovers the 8-chain model exactly.

Since these earlier developments, a number of variants have been proposed that aim to retain much of the simplicity and physical-basis of earlier models while also providing a better fit to the ‘S’-shaped stress-strain curves of the well-known Treloar data for rubber elasticity [16–36]. Many of these variants decompose the free energy density of the network additively into a contribution which represents the “cross-linked network” – often modeled using the 8-chain or a full network model – and a topological constraint contribution due to chain entanglements within the network. The contribution of topological constraints has taken different forms: some based on chain statistics and micromechanics [16, 20, 21, 23–28] while others appear more phenomenological [17–19]. For full network type models, a new macro-to-micro kinematic assumption has recently been developed, based on an affine stretch projection and a microscale analog of the Biot stress, which performs well for capturing complex and multiaxial stress-strain relationships [22]. Many constitutive models for rubber-like elasticity exist in the literature that attempt to balance between competing objectives: (1) contain as few fitting parameters as possible, (2) have the ability to reproduce complex deformation behavior, and (3) in the interest of informing material design, have model parameters which are physically interpretable and can be reasonably connected to the underlying microstructure of the material.

Polymer network models have been applied to a vast number of different polymer networks related to adhesives [37], biomechanics [38–40], dynamically bonded polymer networks [41], magneto-active polymers [42] and electro-active polymers [43–47]. Network models have also been used for capturing phenomena such as viscoelasticity [37, 48], excluded volume induced strain-hardening and incompressibility [49], and chain scission and fracture [50–52]. As a result, continuous network models have been generalized to anisotropic chain distributions [40, 53] and polydisperse networks (i.e. networks consisting of chains of different lengths) [50]. However, many open questions persist regarding how to relate macroscopic deformation to chain-scale (or micro-) deformation in polydisperse polymer networks [50]. Some standard assumptions such as the affine deformation assumption [4], which assumes that chain end-to-end vectors get mapped under the deformation gradient, or equal stretch theories such as the 8-chain model [11], appear to overestimate the stiffness of polydisperse networks for small deformations, but under predict the onset of strain stiffening. Alternatively, equal-force theories assume that chains of different contour lengths that are aligned in the same direction sustain equal forces [50, 54–56]. Other interesting perspectives have emerged which consider more network-wide ensembles of monomers (as opposed to strictly chain-level ensembles) and take an Eulerian-inspired approach (as opposed to Lagrangian) at the continuum level [57, 58]. Certain aspects of these various approaches seem more suitable for polydisperse polymer networks, but all lack explicit consideration of how chains of different lengths are ultimately connected together at cross-links and how this gives rise to different distributions of stresses within the network. Connections cannot be made between network topology and continuum behavior.

There are alternative approaches that are also micromechanical in nature. Explicit discrete network models¹ offer a compelling alternative for connecting network topology and polydispersity to

¹ These are sometimes referred to as “discrete network models”. We add the word “explicit” to make clear that this class of models are distinct from the polymer network models that are the main focus of this work.

emergent bulk properties [59–73]. These models represent the material as a lattice-like structure, where individual structural members exhibit hyperelastic behavior. To probe the stress or failure response, the boundaries of a simulation box are deformed, and the system’s energy is minimized. Recently, this type of approach has been extended to include the concept of “tension blobs”, and utilizes statistical graph theory to characterize the trade-off between the coordination of the network in distributing loads, on the one hand, and entropy on the other [74]. Explicit discrete network models are particularly powerful for elucidating structure-property relationships, as they can capture complex, non-local interactions and detail how loads are transferred between disparate parts of the network, such as between regions with differing cross-link densities and functionalities. However, this non-local formulation results in a large system of coupled, nonlinear equations, making analytical solutions generally intractable and requiring (potentially computationally expensive) numerical methods. Another alternative evokes the concept of maximal advance paths, which makes a connection between a network’s macroscopic affine path and its microscopic averaged deformation [75–77]. Again, this method can characterize non-local interactions across the network, but at the cost of requiring numerics. In this work, we pivot to a more local description of polydisperse network mechanics. This allows us to make analytical progress and, where numerical solutions are still necessary, has the potential to result in a reduction in computational expense and complexity.

The primary focus of this work is on discrete polymer network models. In contrast to standard polymer network models, which treat polymer chains as fundamental units of the network, here we shift perspective to consider cross-links as more fundamental. In this context, a discrete network model is a direct analog of a cross-link. The standard macro-to-micro kinematic assumption for discrete polymer network models – motivated by coordinate system invariance – is that the RVE rotates such that its edges lie along the principal directions of stretch. However, recent theoretical work and experimental observations underscore the importance of treating the RVE orientation relative to a given deformation more carefully [43, 78–80]. In this work, we instead conceptualize the orientation of the RVE as thermally fluctuating. In other words, we consider the RVE as embedded in an elastic background which gives it a preferred orientation and a torsional stiffness. We explore and compare the new model in two limits that are both interesting and analytically tractable: (1) in the limit of negligible torsional stiffness, the kinematic behavior of the new model reduces to the recently developed free rotation assumption [80] – which assumes that the cross-link rotates into the frame that minimizes its free energy after deformation, and (2) in the limit of large torsional stiffness, the model is equivalent to averaging over an isotropic distribution of frames (i.e. cross-link orientations). Through this modeling framework, polydispersity in polymer chain length and cross-link connectivity can be related to the behavior of the broader polymer network.

Structure. The structure of the work is as follows:

- In Section II, as a prelude, some broadly used polymer chain models and concepts in continuum mechanics are reviewed.
- Section III develops a new framework for discrete polydisperse polymer network models by beginning with the statistical mechanics of a single cross-link embedded in an elastic background, and then following its implications up to the continuum scale through applications of statistical methods and approximations across scales.
- Section IV and Section V concern properties of, and approximation strategies for, the “free rotation” and “frame averaging” limits of the broader framework, respectively.
- Section VI explores the implications of polydispersity and topological differences on the elasticity of a bimodal network of Gaussian chains.

- Section VII considers how network structural properties give rise to different features in the characteristic ‘S’-shape stress-strain curves of polymer network elasticity out to large deformation regimes.
- Section VIII concludes the work.

II. PRELUDE

Polymer chain statistical mechanics. A statistical mechanics-based approach is often used as the foundation for the micromechanical modeling of polymer chain elasticity. Consider a freely jointed chain (FJC) of n rigid monomers² bonded end-to-end, each with a length b . This chain has a contour length, $\ell = nb$. This chain also has an associated end-to-end vector, \mathbf{r} (i.e. the vector from the beginning of the chain to its end), and its magnitude, $r = |\mathbf{r}|$, is called the end-to-end chain length. The ratio of r to ℓ defines the (absolute) chain stretch, $\gamma = r/\ell$. A statistical mechanics description begins by defining a probability density of polymer chain conformations, $p(r)$. For freely-jointed Gaussian chains,

$$p_G(r) = \exp\left(-\frac{3r^2}{2nb^2}\right). \quad (2.1)$$

For freely-jointed chains statistically described by the Kuhn and Grün approach [81],

$$p_{KG}(r) = \exp\left(-n\left(\frac{r}{\ell}\mathcal{L}^{-1}\left(\frac{r}{\ell}\right) + \ln\left(\mathcal{L}^{-1}\left(\frac{r}{\ell}\right)\operatorname{csch}\mathcal{L}^{-1}\left(\frac{r}{\ell}\right)\right)\right)\right), \quad (2.2)$$

where \mathcal{L}^{-1} is the inverse of the Langevin function, $\mathcal{L}(x) = \coth x - 1/x$.³ Notably, the Kuhn and Grün approach captures the finite extensibility of the chain; that is, $p_{KG}(r) \rightarrow 0$ as $r \rightarrow \ell$. Additional formulations for $p(r)$ have also been derived for the extensible freely jointed chain [82] and the primitive chain from the tube model [83] (to name a few).

To determine the most probable end-to-end chain length from $p(r)$, we first need to consider the probability of finding the end of a polymer chain within a spherical shell (centered about the chain beginning at the origin) of radius r and thickness dr [4]. We denote this probability as $P(r)dr$,

$$P(r)dr = 4\pi r^2 p(r)dr. \quad (2.3)$$

The most probable end-to-end chain length has been conventionally associated with the root-mean-square chain conformation; the corresponding r_{rms} is given by

$$r_{rms} = \sqrt{\frac{\int_0^{r_{crit}} r^2 P(r)dr}{\int_0^{r_{crit}} P(r)dr}}. \quad (2.4)$$

Note that $P(r)$ is defined over the domain $r \in [0, r_{crit}]$: for Gaussian chains, $r_{crit} = \infty$; for Kuhn and Grün chains, $r_{crit} = \ell$; for extensible freely jointed chains, $r_{crit} \gtrsim \ell$ (e.g., [82]). For Gaussian chains, $r_{rms} = \sqrt{nb}$ (found as the expectation of the distance from the origin for a random walk of n steps, each of length b) [4]. For other chain models, r_{rms} can be obtained by evaluating Eq. (2.4) numerically.

² We here use the term “monomers”, not in the chemical sense, but in the mechanical sense where the term is often used interchangeably with “Kuhn segments” or “links”.

³ The details behind the numerical implementation of the inverse Langevin function are provided in Appendix A.

Chain energetics. With a statistical description of polymer chain conformations at hand, we employ the principal thermodynamic connection formula $w(r) = -k_B T \ln p(r)$ to yield the chain free energy w . For Gaussian chains and Kuhn and Gr \ddot{u} n chains, the free energy is respectively given by,

$$w_G(r) = \frac{3}{2} k_B T \frac{r^2}{nb^2}, \quad (2.5)$$

$$w_{KG}(r) = nk_B T \left(\frac{r}{\ell} \mathcal{L}^{-1} \left(\frac{r}{\ell} \right) + \ln \left(\mathcal{L}^{-1} \left(\frac{r}{\ell} \right) \operatorname{csch} \mathcal{L}^{-1} \left(\frac{r}{\ell} \right) \right) \right), \quad (2.6)$$

where k_B is Boltzmann's constant and T is the absolute temperature. In agreement with the finite extensibility of the Kuhn and Gr \ddot{u} n chain, $w_{KG} \rightarrow \infty$ as $r \rightarrow \ell$.

In addition to w_G and w_{KG} , there are a myriad of other chain free energies in the literature that are applicable to different types of polymers under various loading conditions: extensible freely jointed chains [50, 52, 82, 84] have been an important development for understanding the large deformation and fracture of polymer networks; tube and slip-link chain models (see relevant overviews in [85, 86]) have played an important role in capturing the effect of topological constraints – e.g., entanglements – in rubber elasticity; the worm-like chain [78, 87, 88] has found many applications in biopolymers; and electrically responsive chains [44, 46, 47, 89–91] have been used to model to soft robotics, wearable electronics, etc. (to name a few).⁴

Chain mechanics. Given the free energy response of a single chain, its mechanical response (i.e., the force along the chain) can be obtained directly by differentiation:

$$\mathbf{f} = \frac{\partial w}{\partial \mathbf{r}}. \quad (2.7)$$

The choice of a chain mechanics model (given the choice of chain free energy) along with the specification of a polymer network model are the basis for many multiscale models of polymer networks. Such models seek to make connections between molecular-/meso-scale features and corresponding continuum-scale behaviors.

Continuum mechanics. To establish notation, we introduce some fundamental concepts in continuum solid mechanics. Let \mathbf{X} be a material point of a solid body in the reference configuration and $\mathbf{x} = \mathbf{\Phi}(\mathbf{X})$ its corresponding point in the deformed configuration. Here $\mathbf{\Phi}$ is the mapping that describes the deformation of the solid body. The deformation gradient, $\mathbf{F} = \nabla \mathbf{\Phi}$, maps line elements – which are infinitesimal changes in position, $\delta \mathbf{x}$ – from the reference to the current configuration, i.e. $\delta \mathbf{x} = \mathbf{F} \delta \mathbf{X}$. The right Cauchy-Green tensor, $\mathbf{C} = \mathbf{F}^T \mathbf{F}$, describes the stretches of line elements under \mathbf{F} . Physically, we require that $\det \mathbf{F} > 0$. Then by the polar decomposition theorem, \mathbf{F} can be uniquely decomposed into $\mathbf{F} = \mathbf{R} \mathbf{V}$ where $\mathbf{R} \in SO(3)$, $\mathbf{V} = \sqrt{\mathbf{C}}$ is positive definite, and $SO(3)$ is the group of three-dimensional rotations (i.e., proper orthogonal transformations). Moving forward, we refer to \mathbf{V} as the right stretch tensor and its eigenvalues and eigenvectors as the principal stretches, λ_i , and principal directions, $\hat{\mathbf{v}}_i$, respectively. Because \mathbf{V} is symmetric, the principal directions can be chosen such that $\hat{\mathbf{v}}_i \cdot \hat{\mathbf{v}}_j = \delta_{ij}$ and this set of directions constitutes a principal frame. The tensor

$$\mathbf{P} = \begin{pmatrix} | & | & | \\ \hat{\mathbf{v}}_1 & \hat{\mathbf{v}}_2 & \hat{\mathbf{v}}_3 \\ | & | & | \end{pmatrix} \quad (2.8)$$

⁴ For chains interacting with external fields, the symmetry of the free energy response may be broken such that its functional dependence is on \mathbf{r} as opposed to r . However, in this work, we restrict our attention to chains with isotropic elasticity.

is a rotation that diagonalizes the stretch tensor, $\mathbf{\Lambda} = \mathbf{PVP}^T = \text{diag}(\lambda_1, \lambda_2, \lambda_3)$.

Analogous to the single chain case, the elasticity of the solid polymer network can be modeled via a free energy density $\mathcal{W} = \mathcal{W}(\mathbf{F})$ where the nominal stress (i.e. first Piola–Kirchhoff stress) is given by $\mathbf{\Sigma} = \partial\mathcal{W}/\partial\mathbf{F}$.

III. POLYDISPERSE POLYMER NETWORK MODELS

Consider a polydisperse polymer network, such as the one depicted in Fig. 1. Polydispersity arises in polymer networks from the cross-linking procedure taken to synthesize these materials. From this, polydispersity manifests in several different physical phenomena, as follows: (1) scattered chain orientations, (2) unequal chain contour lengths, (3) dispersity in initial chain conformations (e.g., chain pre-stretches [60, 61]), and (4) variation in the number of chains connected together at cross-linker sites (i.e., variation in cross-linker site topology). To simplify the scope of this work, we will explicitly account for phenomena (1), (2), and (4) in our modeling formulation. Incorporating phenomenon (3) into our formulation remains an open problem for future research.

We begin our modeling approach by first characterizing the space of polydisperse polymer network cross-links. We do so by the set $\mathcal{C} = \{c_i\}_{i=1}^{|\mathcal{C}|}$,⁵ where each cross-link, c , is a representative volume element (RVE). We further characterize each individual cross-link with its own set, which consists of the chains that it connects. For FJCs, this takes the form $c = \{(n_i, \ell_i, \mathbf{X}_i, w_i)\}_{i=1}^k$, where n_i is the number of monomers of the i th chain, ℓ_i is its contour length, \mathbf{X}_i is its end position (in the undeformed body), w_i is its free energy function (which will depend, in general, on n_i, ℓ_i , etc.), and where k is the number of chains that are connected at the junction point, \mathbf{y} . It is required that $|\mathbf{X}_i - \mathbf{X}_j| \leq \ell_i + \ell_j$ for all $i \neq j$. Let Ω_0 be the domain of the RVE associated with the cross-link in its undeformed reference state; and, as such, it is defined as the convex hull of the chain ends, $\{\mathbf{X}_i\}_{i=1}^k$: $\Omega_0 = \text{Conv}(\{\mathbf{X}_i\}_{i=1}^k) \subset \mathbb{R}^3$. Note an otherwise implicit assumption: which end of the chain is its “beginning” and which its “end” is arbitrary. By convention, we say the chain ends are at the boundary of the RVE while the chain beginnings are taken to be at the junction point itself. Then each chain end-to-end vector in the RVE is given by $\mathbf{r}_i = \mathbf{X}_i - \mathbf{y}$. The stochastic structure of the network is then encoded by a probability density function, $\rho_c : c \mapsto [0, \infty)$, that describes the likelihood of the network having a cross-link structure, $c \in \mathcal{C}$. The function is normalized such that $\int dc \rho_c = 1$.

A. Cross-link mechanics

The crux of our discrete polymer network modeling approach is that we treat each cross-link as an RVE, which responds to external loads, and then model the response of the network as an average over the statistical distribution of cross-links. Three major conceptual challenges remain: (1) How should the probability density function, ρ_c , be parameterized in practice? (2) How should a cross-link, c , be physically instantiated? And (3) given some c , how does it response to external loads? To make progress, we make the following assumptions:

- (1) The (average) chain ends connected to a cross-link, c , are well-defined and at $\{\mathbf{X}_i\}_{i=1}^k$ in the undeformed body. Further, the restraints imposed on a particular cross-link c by the remainder

⁵ The set notation used here is shorthand for $\{x_i\}_{i=1}^n \equiv \{x_i : 1 \leq i \leq n\} = \{x_1, x_2, \dots, x_n\}$. We use this shorthand set notation throughout this work, and also analogously employ this shorthand notation to tuples where convenient.

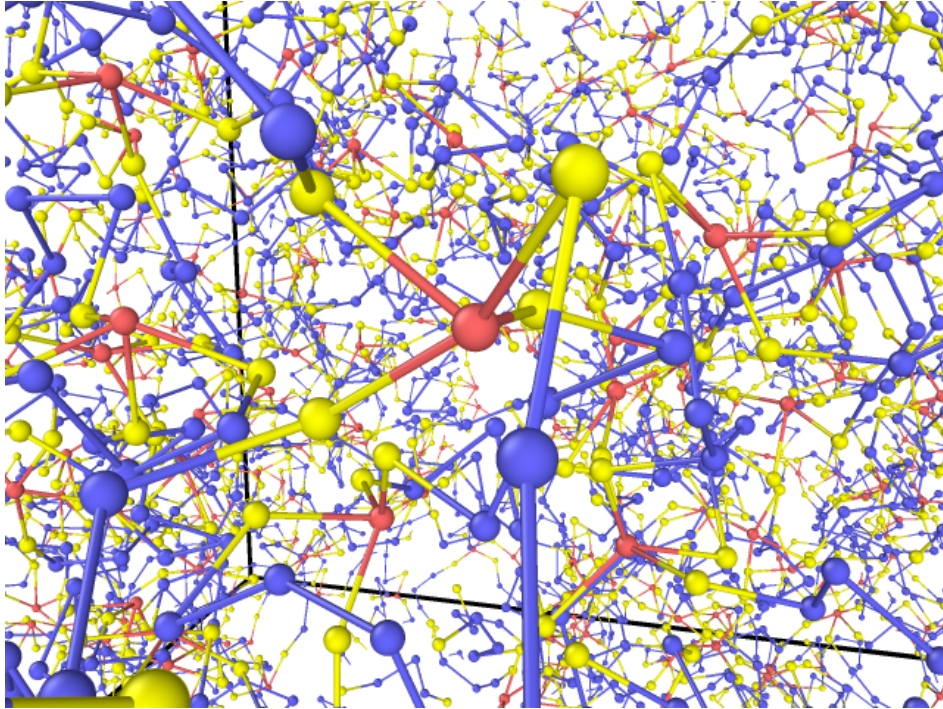


FIG. 1. *Computational rendering of a polydisperse polymer network microstructure.* Chains differ in monomer number, meet at cross-link junctions with differing number of chains, and have varying local connectivities. The polydisperse polymer network microstructure displayed here is generated via end-linking coarse-grained precursor chains in the LAMMPS molecular dynamics simulation package [92, 93]. These simulations are modified from those developed by Riggleman and colleagues [94–96]. In the figure, the red beads represent cross-linker sites, yellow beads represent precursor chain end monomers with the capability of bonding to cross-linker sites, and blue beads represent inner-chain monomers.

of the polymer network can be accurately captured by fixing the nearest neighbor cross-links to their average positions.⁶

- (2) When a cross-link forms, (a) chain conformations have their expected length (given by their r_{rms}) from the initial junction point, and (b) due to entropic and excluded volume effects, chains orientations are “maximally spaced out” (provided that the orientations may also achieve a force balance, i.e., are not linearly independent); this is made more precise in Section III D and Appendix B, where details regarding instantiating the chain end positions are discussed.
- (3) The chain properties and RVE geometry of a cross-link are independent of its orientation; that is,

$$\rho_c \left(\{ (n_i, \ell_i, \mathbf{Q}_0 \mathbf{X}_i, w_i) \}_{i=1}^k \right) = \rho_{\mathbf{Q}_0} (\mathbf{Q}_0) \rho \left(\{ (n_i, \ell_i, \mathbf{X}_i, w_i) \}_{i=1}^k \right) = \rho_{\mathbf{Q}_0} (\mathbf{Q}_0) \rho(c) \quad (3.1)$$

where $\rho_{\mathbf{Q}_0} (\mathbf{Q}_0)$ is the probability density of the cross-link having some orientation, $\mathbf{Q}_0 \in SO(3)$, relative to a reference set of chain end positions, $\{ \mathbf{X}_i \}_{i=1}^k$. Here, when referring to the “orientation” of a cross-link, we mean its preferred orientation within an elastic background; that is, it

⁶ In general, the nearest neighbor cross-links may not be nearest in space, but rather, they are nearest with respect to the continuous network topological structure. Conversely, it is conceivable that cross-links that are distantly connected along the network structure may interpenetrate the same physical space. For a rich discussion of chain interpenetration in polymer networks, see [97, 98].

is the ground state of its orientation. It is important that $\rho_{\mathbf{Q}_0}(\mathbf{Q}_0)$ satisfy frame indifference and the underlying symmetry of the material. We are interested in isotropic materials in this work and, thus, we will restrict our attention to

$$\rho_{\mathbf{Q}_0}(\mathbf{Q}_0) = \text{const.} = \frac{1}{|SO(3)|} = \frac{1}{8\pi^2} \quad (3.2)$$

such that all cross-link orientations are assumed equally likely.

At this point, the parameterization of $\rho(c)$ remains unspecified. We discuss a methodology for parameterizing $\rho(c)$ in Section III E.

- (4) Macroscopic network deformation affinely displaces the relative positions of the chain ends (and, as a consequence, neighboring cross-links), $\{\mathbf{X}_i\}_{i=1}^k \rightarrow \{\mathbf{F}\mathbf{X}_i\}_{i=1}^k$. Meanwhile, the cross-link junction is allowed to occupy all possible physically-permissible positions in response to random thermal fluctuations of the connected chains.
- (5) Thermal fluctuations of the network can be characterized through
 - (a) fluctuations of the internal degrees of freedom of each chain (e.g. for a FJC, the link orientations),
 - (b) rigid rotations of the cross-link such that $\{\mathbf{X}_i\}_{i=1}^k \rightarrow \{\mathbf{Q}\mathbf{X}_i\}_{i=1}^k$ for $\mathbf{Q} \in SO(3)$ in the undeformed body, and $\{\mathbf{F}\mathbf{X}_i\}_{i=1}^k \rightarrow \{\mathbf{F}\mathbf{Q}\mathbf{X}_i\}_{i=1}^k$ in the deformed body, and
 - (c) displacements of the junction point, \mathbf{y} .

These fluctuation modes are depicted in Fig. 2. It is assumed that all other fluctuation modes have a negligible contribution to the network behavior (e.g., because they are effectively inaccessible due to higher energy or other constraints).

- (6) Cross-links are embedded in an elastic background that gives them a preferred orientation and a torsional stiffness with respect to the preferred orientation.
- (7) The internal degrees of freedom of each of the chains thermalize much more quickly than network fluctuations; that is, fluctuations due to rotations of the cross-link or displacements of the junction point. This assumption is justified by observing that rotating the cross-link or displacing its junction point is coupled to all of the degrees of freedom of the chains. The cross-link is a larger, more complex structure than its individual chains. Relaxation times of polymers often scale with their size and the complexity of their structure [99, 100]. Thus, one would expect that deformation modes of the RVE related to the global structure of the cross-link should have longer relaxation times. The result of this assumption is two-fold: (1) the free energy contributions from the chains can be taken as a sum of their individual free energies, $\sum_{i=1}^k w_i$, and (2) in the statistical mechanics formulation of the network, the internal chain degrees of freedom can be treated separately before averaging over fluctuating cross-link rotations and junction positions.

Assumptions 1-3 will facilitate the construction of cross-links and associated cross-link probability density function, ρ_c . Assumptions 4-7 will facilitate modeling the mechanical response of a cross-link.

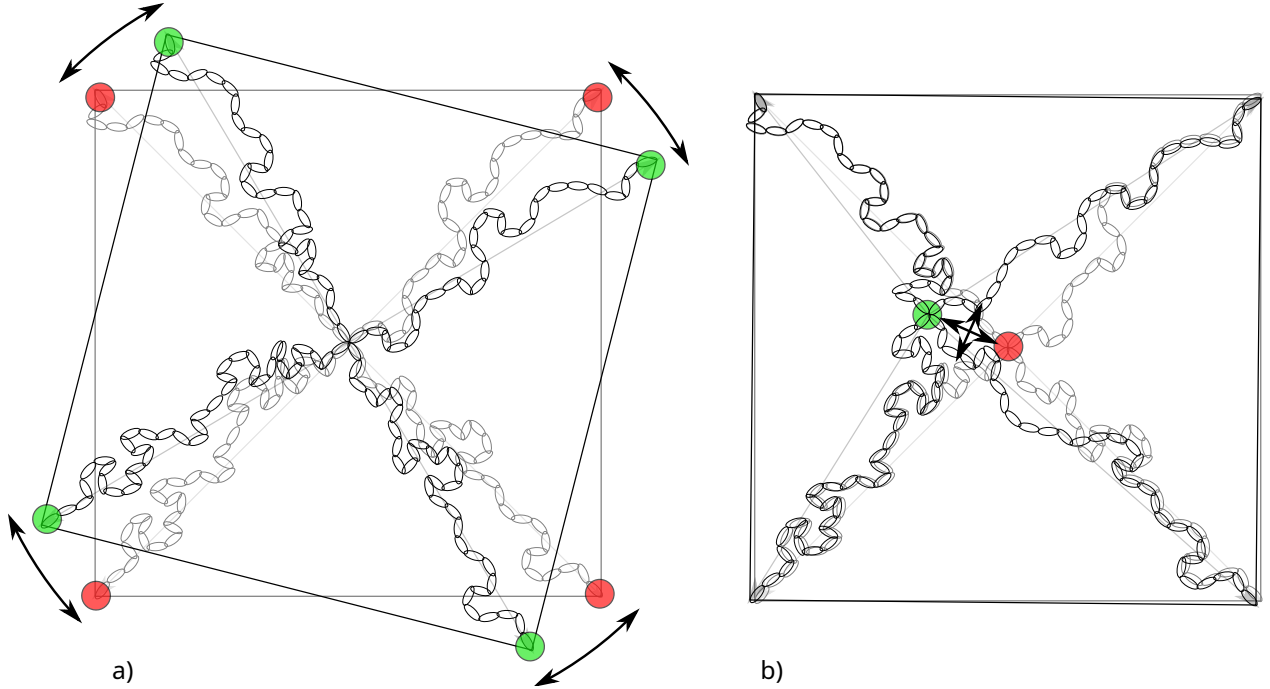


FIG. 2. *Thermal fluctuations of cross-links.* Thermal fluctuations cause a) rigid rotations of the end positions of the cross-link, $\mathbf{X} \rightarrow \mathbf{Q}\mathbf{X}$ and b) perturbations of the junction position, \mathbf{y} .

Statistical mechanics of a cross-link. The free energy of a thermally fluctuating system at constant temperature is obtained (via the principal thermodynamic connection formula) as $-k_B T \ln \mathcal{Z}$ where \mathcal{Z} is the partition function. Let $\Omega = \text{Conv}(\{\mathbf{F}\mathbf{Q}\mathbf{X}_i\}_{i=1}^k) \subset \mathbb{R}^3$ be the rotated and deformed RVE domain. Given Assumptions 4-7, the partition function of a cross-link is given by

$$\mathcal{Z}(\mathbf{F}, \mathbf{Q}_0) = \int_{\mathbf{y} \in \Omega} d\mathbf{y} \int_{\mathbf{Q} \in SO(3)} d\mathbf{Q} \exp\left(-\frac{1}{k_B T} \sum_{i=1}^k w_i (|\mathbf{F}\mathbf{Q}\mathbf{X}_i - \mathbf{y}|) - \frac{U_{\text{net}}(\mathbf{Q})}{k_B T}\right) \quad (3.3)$$

where $U_{\text{net}}(\mathbf{Q})$ is the torsional elastic energy from the surrounding network when rotating the cross-link by some amount \mathbf{Q} prior to deformation. Here we assume a simple form for the torsional elasticity as

$$U_{\text{net}}(\mathbf{Q}) = \frac{\kappa}{2} \|\mathbf{Q} - \mathbf{Q}_0\|^2 \quad (3.4)$$

where κ is some torsional stiffness modulus, and recall: \mathbf{Q}_0 is the preferred orientation of the cross-link in the undeformed body relative to the reference positions, $\{\mathbf{X}_i\}_{i=1}^k$. Even with this simplified form of U_{net} , exact evaluation of Eq. (3.3) is prohibitively difficult. Instead, we use saddle point approximation to explore two interesting limits that are both more analytically tractable. Towards approximating Eq. (3.3), let

$$\{\mathbf{Q}^*, \mathbf{y}^*\} = \arg \inf_{\mathbf{Q} \in SO(3), \mathbf{y} \in \Omega} \sum_{i=1}^k w_i (|\mathbf{F}\mathbf{Q}\mathbf{X}_i - \mathbf{y}|), \quad (3.5)$$

$$\mathbf{y}_{\mathbf{Q}_0}^* = \arg \inf_{\mathbf{y} \in \Omega} \sum_{i=1}^k w_i (|\mathbf{F}\mathbf{Q}_0\mathbf{X}_i - \mathbf{y}|). \quad (3.6)$$

The two limits of interest are: (1) the *free rotation limit* where, for each $\mathbf{Q}_0 \in SO(3)$, there exists a \mathbf{Q}^* such that Eq. (3.5) and

$$\frac{\kappa}{2k_B T} \|\mathbf{Q}^* - \mathbf{Q}_0\|^2 \ll 1, \quad (3.7)$$

are both satisfied⁷; and (2) the *frame averaging limit* where

$$\frac{\kappa}{2k_B T} \gg 1. \quad (3.8)$$

In the free rotation limit, the chain energy term (i.e., first term) dominates the argument of the exponential in Eq. (3.3), such that its minimum determines \mathbf{Q} at the saddle point; in the frame averaging limit, the torsional elastic energy term dominates, and it is instead this term whose minimum determines \mathbf{Q} at the saddle point.

Free rotation limit. First assume Eq. (3.5) and Eq. (3.7) hold. In this limit, one can take the saddle point approximation at $\mathbf{Q} = \mathbf{Q}^*$, $\mathbf{y} = \mathbf{y}^*$. Taking the leading order approximation with respect to \mathbf{Q} results in,

$$\mathcal{Z}^{FR}(\mathbf{F}, \mathbf{Q}_0) \approx e^{-U_{\text{net}}(\mathbf{Q}^*)/k_B T} \int_{\mathbf{y} \in \Omega} d\mathbf{y} \exp\left(-\frac{1}{k_B T} \sum_{i=1}^k w_i (|\mathbf{F}\mathbf{Q}^* \mathbf{X}_i - \mathbf{y}|)\right). \quad (3.9)$$

For brevity, let $W_{\text{ch}}(\mathbf{F}, \mathbf{Q}, \mathbf{y}) = \sum_{i=1}^k w_i (|\mathbf{F}\mathbf{Q}\mathbf{X}_i - \mathbf{y}|)$.⁸ Expanding about $\mathbf{y} = \mathbf{y}^*$,

$$\mathcal{Z}^{FR}(\mathbf{F}, \mathbf{Q}_0) \approx e^{-(W_{\text{ch}}(\mathbf{F}, \mathbf{Q}^*, \mathbf{y}^*) + U_{\text{net}}(\mathbf{Q}^*)) / k_B T} \int_{\mathbf{y} \in \Omega} d\mathbf{y} \exp\left(-\frac{1}{2k_B T} (\mathbf{y} - \mathbf{y}^*) \cdot \left. \frac{\partial^2 W_{\text{ch}}}{\partial \mathbf{y} \partial \mathbf{y}} \right|_{\mathbf{Q}=\mathbf{Q}^*, \mathbf{y}=\mathbf{y}^*} (\mathbf{y} - \mathbf{y}^*)\right), \quad (3.10)$$

where higher order terms, $\mathcal{O}((\mathbf{y} - \mathbf{y}^*)^3)$, have been neglected. Extending the domain of integration to $\mathbf{y} \in \mathbb{R}^3$ results in Gaussian integrals such that

$$\mathcal{Z}^{FR}(\mathbf{F}, \mathbf{Q}_0) \approx \left(\frac{(2\pi k_B T)^{3/2}}{\sqrt{\det\left(\left. \frac{\partial^2 W_{\text{ch}}}{\partial \mathbf{y} \partial \mathbf{y}} \right|_{\mathbf{Q}=\mathbf{Q}^*, \mathbf{y}=\mathbf{y}^*}\right)}} \right) \exp\left(-\frac{W_{\text{ch}}(\mathbf{F}, \mathbf{Q}^*, \mathbf{y}^*)}{k_B T} - \frac{U_{\text{net}}(\mathbf{Q}^*)}{k_B T}\right) \quad (3.11)$$

where $\det(\partial^2 W_{\text{ch}} / \partial \mathbf{y} \partial \mathbf{y})$ is the determinant of the Hessian of the free energy of the chains with respect to \mathbf{y} . Then the free energy of a cross-link in the free rotation limit is given by

$$\boxed{W_c^{FR}(\mathbf{F}, \mathbf{Q}_0) = W_{\text{ch}}(\mathbf{F}, \mathbf{Q}^*, \mathbf{y}^*) + U_{\text{net}}(\mathbf{Q}^*) + \frac{k_B T}{2} \ln\left(\det\left(\left. \frac{\partial^2 W_{\text{ch}}}{\partial \mathbf{y} \partial \mathbf{y}} \right|_{\mathbf{Q}=\mathbf{Q}^*, \mathbf{y}=\mathbf{y}^*}\right)\right) - \frac{3k_B T}{2} \ln(2\pi k_B T)}. \quad (3.12)$$

For simplicity, terms that have negligible effect on the mechanics are dropped.

- (1) The last term has no influence on the mechanics.
- (2) The second term is also negligible, by assumption (Eq. (3.7)); and, further, it will be shown that for many networks of interest \mathbf{Q}^* does not change significantly with deformation; thus, even when $\kappa/2k_B T$ is not small, the second term likely has a negligible coupling to mechanics.⁹

⁷ This condition does not necessarily imply $\kappa/k_B T \ll 1$. It could alternatively be met through high enough degeneracy of \mathbf{Q}^* (e.g., due to symmetry) such that for each \mathbf{Q}_0 there is a \mathbf{Q}^* that is sufficiently close.

⁸ The analytical form of the first and second derivatives of W_{ch} with respect to \mathbf{y} is provided in Appendix C for both Gaussian chains and Kuhn and Grün chains.

⁹ The last term may influence thermal properties and the second term may be more relevant for certain multiphysics problems.

- (3) The second-to-last term is related to fluctuations of the cross-link junction position, and is more subtle. It has been argued in previous work that it has no effect on the mechanics of networks of Gaussian chains [4], and that its significance for networks with other types of chains (e.g. Kuhn and Gr \ddot{u} n chains) is also small [8, 9]. Unless otherwise stated, this junction fluctuation term is also dropped. It will, however, be revisited and analyzed when appropriate.

After simplifying, Eq. (3.12) takes the form

$$\boxed{W_c^{FR}(\mathbf{F}) = W_{\text{ch}}(\mathbf{F}, \mathbf{Q}^*, \mathbf{y}^*) = \inf_{\mathbf{Q} \in SO(3), \mathbf{y} \in \Omega} \sum_{i=1}^k w_i (|\mathbf{F}\mathbf{Q}\mathbf{X}_i - \mathbf{y}|)}. \quad (3.13)}$$

Frame averaging limit. Assume Eq. (3.6) and Eq. (3.8) hold. In this limit, one can take the saddle point approximation at $\mathbf{Q} = \mathbf{Q}_0, \mathbf{y} = \mathbf{y}_{\mathbf{Q}_0}^*$. Taking the leading order approximation with respect to \mathbf{Q} results in,

$$\mathcal{Z}^{FA}(\mathbf{F}, \mathbf{Q}_0) \approx \int_{\mathbf{y} \in \Omega} d\mathbf{y} \exp\left(-\frac{W_{\text{ch}}(\mathbf{F}, \mathbf{Q}_0, \mathbf{y})}{k_B T}\right). \quad (3.14)$$

Expanding about $\mathbf{y} = \mathbf{y}_{\mathbf{Q}_0}^*$,

$$\mathcal{Z}^{FA}(\mathbf{F}, \mathbf{Q}_0) \approx e^{-W_{\text{ch}}(\mathbf{F}, \mathbf{Q}_0, \mathbf{y}_{\mathbf{Q}_0}^*)/k_B T} \int_{\mathbf{y} \in \Omega} d\mathbf{y} \exp\left(-\frac{1}{2k_B T} (\mathbf{y} - \mathbf{y}_{\mathbf{Q}_0}^*) \cdot \left. \frac{\partial^2 W_{\text{ch}}}{\partial \mathbf{y} \partial \mathbf{y}} \right|_{\mathbf{Q}=\mathbf{Q}_0, \mathbf{y}=\mathbf{y}_{\mathbf{Q}_0}^*} (\mathbf{y} - \mathbf{y}_{\mathbf{Q}_0}^*)\right), \quad (3.15)$$

where higher order terms, $\mathcal{O}((\mathbf{y} - \mathbf{y}_{\mathbf{Q}_0}^*)^3)$, have been neglected. Extending the domain of integration to $\mathbf{y} \in \mathbb{R}^3$ results in Gaussian integrals such that

$$\mathcal{Z}^{FA}(\mathbf{F}, \mathbf{Q}_0) \approx \left(\frac{(2\pi k_B T)^{3/2}}{\sqrt{\det\left(\left. \frac{\partial^2 W_{\text{ch}}}{\partial \mathbf{y} \partial \mathbf{y}} \right|_{\mathbf{Q}=\mathbf{Q}_0, \mathbf{y}=\mathbf{y}_{\mathbf{Q}_0}^*}\right)}} \right) \exp\left(-\frac{W_{\text{ch}}(\mathbf{F}, \mathbf{Q}_0, \mathbf{y}_{\mathbf{Q}_0}^*)}{k_B T}\right) \quad (3.16)$$

and

$$\boxed{W_c^{FA}(\mathbf{F}, \mathbf{Q}_0) = W_{\text{ch}}(\mathbf{F}, \mathbf{Q}_0, \mathbf{y}_{\mathbf{Q}_0}^*) + \frac{k_B T}{2} \ln\left(\det\left(\left. \frac{\partial^2 W_{\text{ch}}}{\partial \mathbf{y} \partial \mathbf{y}} \right|_{\mathbf{Q}=\mathbf{Q}_0, \mathbf{y}=\mathbf{y}_{\mathbf{Q}_0}^*}\right)\right) - \frac{3k_B T}{2} \ln(2\pi k_B T)}. \quad (3.17)}$$

Similar to Eq. (3.13), the last term is dropped for simplicity, and because it has no bearing on the mechanical behavior. The second term (i.e., the cross-link junction fluctuation term) is also dropped – both for simplicity and because, again, it has been found that it often has a negligible effect on mechanical behavior [4, 8, 9]. After simplifying, Eq. (3.17) takes the form

$$\boxed{W_c^{FA}(\mathbf{F}, \mathbf{Q}_0) = W_{\text{ch}}(\mathbf{F}, \mathbf{Q}_0, \mathbf{y}_{\mathbf{Q}_0}^*) = \inf_{\mathbf{y} \in \Omega} \sum_{i=1}^k w_i (|\mathbf{F}\mathbf{Q}_0\mathbf{X}_i - \mathbf{y}|)}. \quad (3.18)}$$

Fig. 3 displays a schematic physically depicting the free rotation and frame averaging limits. In addition, the nondimensional representation of the cross-link partition function (Eq. (3.11) and Eq. (3.16)) and cross-link free energy (Eq. (3.12) and Eq. (3.17)) for both limits is provided in Appendix D.

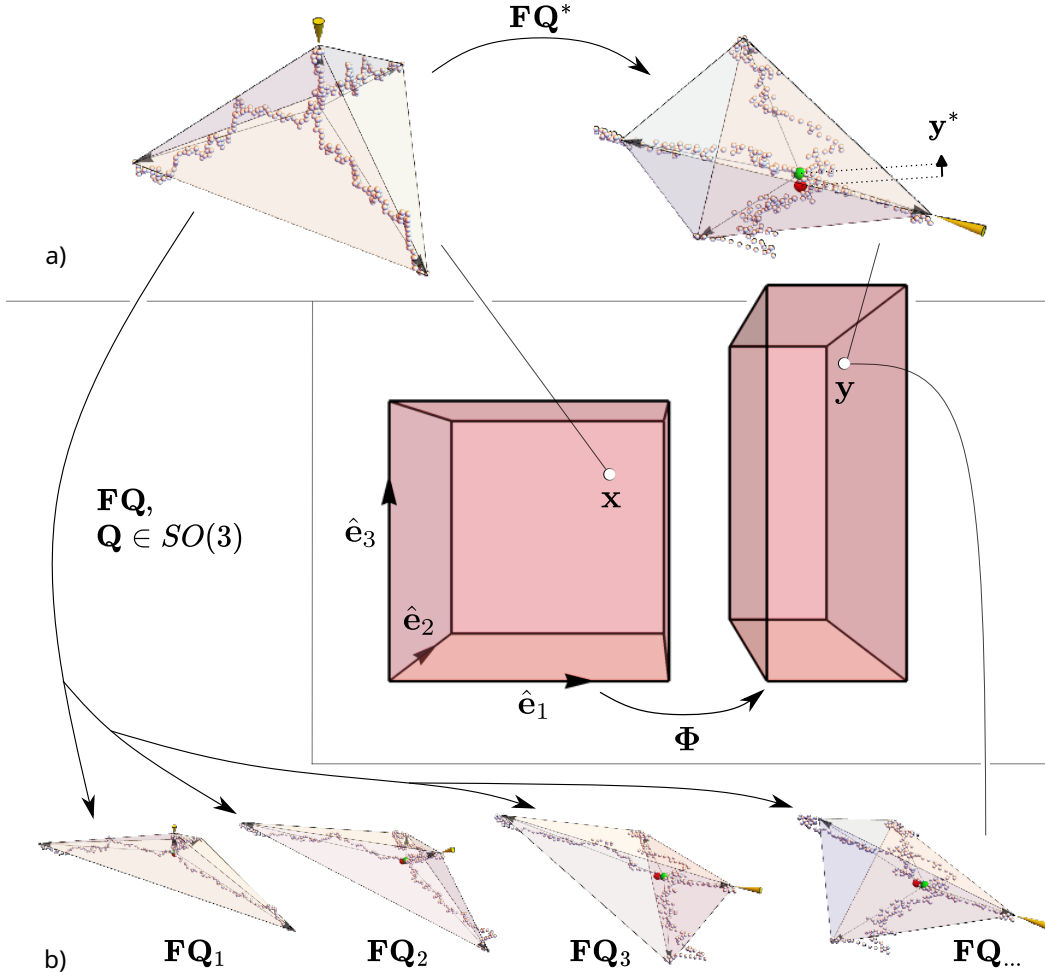


FIG. 3. a) The polydisperse 4-chain RVE gets mapped under FQ^* for the free rotation limit. In the deformed RVE, the origin and cross-link position are denoted by a red ball and green ball, respectively. b) In the frame averaging limit, the RVE response to F is averaged over all possible frames, represented by $Q \in SO(3)$. The chain deformations, stretches, and cross-link position are, in general, different for each Q .

Remark 1. Frame averaging limit for isotropic materials. For isotropic materials, it is often convenient to represent the cross-link free energy of the frame averaging limit as the integral of Eq. (3.18) over all Q_0 . Using Eq. (3.2) from Assumption 3, this leads to the following form

$$W_c^{FA}(\mathbf{F}) = \frac{1}{8\pi^2} \int_{Q_0 \in SO(3)} dQ_0 \left(\inf_{y \in \Omega} \sum_{i=1}^k w_i (|\mathbf{F}Q_0 \mathbf{X}_i - y|) \right). \quad (3.19)$$

In a similar fashion, the frame averaging over all $y_{Q_0}^*$ (from Eq. (3.6)) is given by

$$y^{*FA}(\mathbf{F}) = \frac{1}{8\pi^2} \int_{Q_0 \in SO(3)} dQ_0 y_{Q_0}^*. \quad (3.20)$$

Remark 2. Applicability of the free rotation and frame averaging limits. The free rotation and frame averaging limits may be more or less applicable to different types of polymer networks. For example, some biopolymer networks consisting of semi-flexible polymers with bending rigidity may resist shear and rotation at cross-links [101–103] and, as such, the frame averaging limit may provide

a good model. Meanwhile, many authoritative works on soft polymer networks (e.g., elastomers) make reference to the “locally fluid-like freedom” for molecular motion within the polymer network (e.g., [4, 104]). For soft polymer networks consisting of freely jointed chains, there is experimental evidence that suggests the free rotation limit is a sound approximation [11]. An added benefit of focusing on the limits, beyond computational tractability, is that it also removes the need to fit an additional model parameter, κ .

Remark 3. Relationship to existing polymer network models. The frame averaging limit shares structural similarities with the full network model [12, 13]: both integrate over a continuous uniform distribution (chains over \mathbb{S}^2 vs. cross-link orientations over $SO(3)$) and can employ similar quadrature techniques. However, the frame averaging limit represents a more physical realization – rather than imposing infinite chain connectivity at a single junction, it averages over all orientations of finite cross-link structures where loads are shared among a discrete number of chains.

From a homogenization perspective, the junction relaxation in our framework is analogous to nonlinear RVE methods where boundaries are deformed while interiors equilibrate [105, 106], naturally satisfying force balance. This contrasts with restrictive affine (Voigt-type) or equal-force (Reuss-type) theories [54–56].

Historically, junction relaxation appears in the classical 4-chain [4, 10] and 3-chain models [35, 107]. While earlier discrete models oriented the RVE relative to the principal frame to satisfy frame indifference, Arruda-Boyce [11] was the first to use the orientation that optimally distributes elastic energy across chains, which was later generalized in [80]. Polydispersity in fluctuating-junction models was explored by Kloczkowski et al. [108] for bimodal chains. Our framework unifies these ideas – junction relaxation, rotational fluctuations, and polydispersity – while also satisfying frame indifference. For detailed discussion of historical developments and comparisons with specific models, see Appendix E.

B. Junction position relaxation

Uniqueness. For many networks of interest, the solution to the junction positional relaxation for general \mathbf{F} and \mathbf{Q} is unique.

Proposition 1. *For RVEs consisting of chains with free energies $(w_i, i = 1, \dots, k)$ that are all convex, non-decreasing functions of stretch, with at least 1 that is strictly convex, strictly increasing, the solution to*

$$\inf_{\mathbf{y} \in \Omega} \{W_{ch}(\mathbf{F}, \mathbf{Q}, \mathbf{y})\} \quad (3.21)$$

where

$$W_{ch}(\mathbf{F}, \mathbf{Q}, \mathbf{y}) = \sum_{i=1}^k w_i (|\mathbf{F}\mathbf{Q}\mathbf{X}_i - \mathbf{y}|) \quad (3.22)$$

exists and is unique.

Proof. By construction, Ω_0 is a compact, convex set. The deformed RVE, $\Omega = \mathbf{F}\mathbf{Q}\Omega_0$, is also compact, convex since these properties are conserved under linear transformation. The minimum exists by the extreme value theorem.

Fix \mathbf{F} and \mathbf{Q} . The compositions $w_i (|\mathbf{F}\mathbf{Q}\mathbf{X}_i - \mathbf{y}|)$ are convex (strictly convex), non-decreasing (strictly increasing) functions composed with convex functions; thus, they are each convex (strictly

convex) functions of \mathbf{y} . As a sum of convex functions, with at least 1 strictly convex, W_{ch} is a strictly convex function of \mathbf{y} . A strictly convex function on a compact, convex set has a unique global minimum. \square

This means that, for polydisperse RVEs consisting of Gaussian chains, Kuhn and Grün chains, wormlike chains, and many others, the solution for the junction position is unique (for fixed \mathbf{F} and \mathbf{Q}).

Exact solution for Gaussian RVEs. For RVEs consisting of Gaussian chains, the equilibrium equation for the junction position, $\partial W_{\text{ch}}/\partial \mathbf{y} = \mathbf{0}$ is linear (see Appendix C), allowing the exact solution:

$$\mathbf{y}^* = \mathbf{F}\mathbf{Q} \frac{\left(\sum_{i=1}^k \frac{\mathbf{X}_i}{n_i}\right)}{\left(\sum_{i=1}^k \frac{1}{n_i}\right)}. \quad (3.23)$$

C. Network mechanics and frame indifference

As mentioned previously, we assume that – although the exact structure of each and every individual cross-link is likely unknown – a statistical distribution of cross-link structures may be known. Recall that $\rho_c(c)$ is the probability density of finding a cross-link with structure given by $c = \{(n_i, \ell_i, \mathbf{X}_i, w_i)\}_{i=1}^k$ in the network of interest. Then the free energy density for the network can be modeled as

$$\mathcal{W}_{\mathcal{C}}(\mathbf{F}) = \frac{M}{2} \int_{c \in \mathcal{C}} dc \rho_c W_c = -\frac{M}{2} k_B T \int_{c \in \mathcal{C}} dc \rho_c \ln(\mathcal{Z}(\mathbf{F}, \mathbf{Q}_0)), \quad (3.24)$$

where M is the density of cross-links per unit volume such that the product $M\rho(c)$ equals the number density of cross-link structure c . The factor of 1/2 is here because each chain in the RVE is assumed to be connected to 2 distinct cross-linkers in the network.

Frame indifference. Frame indifference can be shown when the cross-link response utilizes the general partition function, Eq. (3.3), or an approximation thereof which is faithful to its symmetries, and when ρ_c satisfies Assumption 3; that is, where the orientation of cross-links within an elastic embedding is uniformly distributed.

Proof. Given Eq. (3.3) and Assumption 3, it suffices to show that $\mathcal{Z}(\mathbf{F}, \mathbf{Q}_0) = \mathcal{Z}(\mathbf{\Lambda}, \mathbf{Q}'_0)$ where, recall, $\mathbf{\Lambda} = \text{diag}(\lambda_1, \lambda_2, \lambda_3) = \mathbf{P}\mathbf{V}\mathbf{P}^T$ is a diagonalization of the right stretch tensor, \mathbf{V} , and we make the definition $\mathbf{Q}'_0 = \mathbf{P}\mathbf{Q}_0$. Again, $\mathbf{F} = \mathbf{R}\mathbf{V}$. Then

$$\mathcal{Z}(\mathbf{F}, \mathbf{Q}_0) = \int_{\mathbf{y} \in \Omega} d\mathbf{y} \int_{\mathbf{Q} \in SO(3)} d\mathbf{Q} \exp\left(-\frac{1}{k_B T} \sum_{i=1}^k w_i (|\mathbf{R}\mathbf{P}^T \mathbf{\Lambda} \mathbf{P} \mathbf{Q} \mathbf{X}_i - \mathbf{y}|) - \frac{U_{\text{net}}(\mathbf{Q})}{k_B T}\right). \quad (3.25)$$

Let $\mathbf{y}' = (\mathbf{R}\mathbf{P}^T)^{-1} \mathbf{y} = \mathbf{P}\mathbf{R}^T \mathbf{y}$ and $\mathbf{Q}' = \mathbf{P}\mathbf{Q}$. The argument to the chain free energy takes the form

$$|\mathbf{R}\mathbf{P}^T \mathbf{\Lambda} \mathbf{P} \mathbf{Q} \mathbf{X}_i - \mathbf{y}| = |\mathbf{R}\mathbf{P}^T (\mathbf{\Lambda} \mathbf{P} \mathbf{Q} \mathbf{X}_i - \mathbf{y}')| = |\mathbf{\Lambda} \mathbf{Q}' \mathbf{X}_i - \mathbf{y}'| \quad (3.26)$$

and, consequently,

$$\begin{aligned} \mathcal{Z}(\mathbf{F}, \mathbf{Q}_0) &= \int_{\mathbf{y} \in \Omega} d\mathbf{y} \int_{\mathbf{Q} \in SO(3)} d\mathbf{Q} \exp\left(-\frac{1}{k_B T} \sum_{i=1}^k w_i (|\mathbf{\Lambda} \mathbf{Q}' \mathbf{X}_i - \mathbf{y}'|) - \frac{U_{\text{net}}(\mathbf{Q})}{k_B T}\right) \\ &= \int_{\mathbf{y} \in \Omega} d\mathbf{y} \int_{\mathbf{Q} \in SO(3)} d\mathbf{Q} \exp\left(-\frac{1}{k_B T} \sum_{i=1}^k w_i (|\mathbf{\Lambda} \mathbf{Q}' \mathbf{X}_i - \mathbf{y}'|) - \frac{\kappa}{2k_B T} \|\mathbf{P}^T (\mathbf{Q}' - \mathbf{Q}'_0)\|^2\right). \end{aligned} \quad (3.27)$$

The tensor norm, $\|\cdot\|$, has not yet been specified. For norm choices that appropriately model torsional elasticity, we want $\|\mathbf{P}^T(\mathbf{Q}' - \mathbf{Q}'_0)\| = \|\mathbf{Q}' - \mathbf{Q}'_0\|$ to hold. The Frobenius norm is one such example and is also the most natural choice for modeling elasticity. In all such cases,

$$\mathcal{Z}(\mathbf{F}, \mathbf{Q}_0) = \int_{\mathbf{y}' \in \Omega} d\mathbf{y}' \int_{\mathbf{Q}' \in SO(3)} d\mathbf{Q}' \exp\left(-\frac{1}{k_B T} \sum_{i=1}^k w_i (|\boldsymbol{\Lambda} \mathbf{Q}' \mathbf{X}_i - \mathbf{y}'|) - \frac{\kappa}{2k_B T} \|(\mathbf{Q}' - \mathbf{Q}'_0)\|^2\right), \quad (3.28)$$

and, as a result, $\mathcal{Z}(\mathbf{F}, \mathbf{Q}_0) = \mathcal{Z}(\boldsymbol{\Lambda}, \mathbf{Q}'_0)$. Thus, the resulting constitutive model is isotropic and frame indifferent. \square

D. Cross-link structures

Having addressed the response of a cross-link to external loads, we now turn our attention to instantiation of cross-link structures. Per Assumptions 1-3, chains have their expected lengths, r_{rms} , upon cross-linking, and the orientations of chains are maximally spaced out. To construct c , let the junction position at the moment of cross-linking be at the origin. For each $\mathbf{X}_i \in \Omega_0$, define the unit vector $\hat{\mathbf{X}}_i = \mathbf{X}_i / |\mathbf{X}_i|$. We place these unit vectors according to the Thomson problem: the equilibrium configuration of electrostatically repulsive particles on the unit sphere [109]. Ideally, we also place these unit vectors to maximize reflectional symmetry about the origin (especially if the Thomson problem is not able to be satisfied). These two considerations maximize angular separation between chains and produces an isotropic distribution of $\{\hat{\mathbf{X}}_i\}_{i=1}^k$, consistent with excluded volume and entropic considerations prior to cross-linking. The classical 4-chain [6, 10] and 6-chain [80] models correspond to Thomson solutions for $k = 4$ and 6, respectively. The classical 8-chain [11] model does not correspond to the Thomson solution for $k = 8$, but it does maximize the reflectional symmetry of $\{\hat{\mathbf{X}}_i\}_{i=1}^8$ about the origin.

In this work, we construct the polydisperse 4-chain model as $c = \{(n_i, \ell_i, \mathbf{X}_i, w_i)\}_{i=1}^4$ where

$$\begin{aligned} \mathbf{X}_1 &= (r_{rms})_1 (0, 0, 1), & \mathbf{X}_2 &= (r_{rms})_2 \left(0, \frac{2\sqrt{2}}{3}, -\frac{1}{3}\right), \\ \mathbf{X}_3 &= (r_{rms})_3 \left(\sqrt{\frac{2}{3}}, -\frac{\sqrt{2}}{3}, -\frac{1}{3}\right), & \mathbf{X}_4 &= (r_{rms})_4 \left(-\sqrt{\frac{2}{3}}, -\frac{\sqrt{2}}{3}, -\frac{1}{3}\right). \end{aligned} \quad (3.29)$$

This will be the primary RVE of interest throughout. For reference, Appendix B provides polydisperse cross-link RVEs for $k \in [3, 8]$. As in Section II, r_{rms} is calculated as a function of n , ℓ , and w , so c implicitly determines all r_{rms} .

E. Cross-link statistics

We next address parameterization of the probability density, $\rho(c)$. Recall the 3 polydispersity phenomena: scattered chain orientations, unequal chain contour lengths, and variation in the number of chains per cross-link junction. Chain orientation scatter has been addressed in Section III A and Section III C (Assumption 3). To capture dispersity in the latter 2 phenomena, we define probability density functions $\rho_n = \rho_n(n)$ and $\rho_k = \rho_k(k)$ for chain monomer number and cross-linker functionality, respectively.¹⁰ We restrict attention to networks where all monomers have the same

¹⁰ Although n and k are discrete random variables, we use a continuous formulation since they can be represented as weighted sum of Dirac deltas, e.g., $\rho_n(n) = \sum_{i=1}^{\infty} p_{n,i} \delta(n - i)$ and $\rho_k(k) = \sum_{j=1}^{\infty} p_{k,j} \delta(k - j)$ where $\sum_i p_{n,i} = \sum_j p_{k,j} = 1$. Approximating n and k as continuous (e.g., Gaussian) is sometimes convenient.

length, b , so n_i uniquely determines ℓ_i and $|\mathbf{X}_i|$.^{11,12}

To construct $\rho(c)$, we invoke Flory’s ideal network assumptions [110]: during cross-linking, (1) all functional groups of the same type are equally reactive, (2) all groups react independently, and (3) no intramolecular reactions occur in finite species. Consequently, *the number of monomers in each chain are independently and identically distributed* (i.i.d.). Given Assumption 3, the probability density is

$$\rho(c) = \rho(\{(n_i, \ell_i, \mathbf{X}_i, w_i)\}_{i=1}^k) = \rho(\{(n_i, \ell_i, \mathbf{Q}_0 \mathbf{X}_i, w_i)\}_{i=1}^k) = \frac{\rho_k(k)}{8\pi^2} \prod_{i=1}^k \rho_n(n_i). \quad (3.30)$$

Integration over \mathcal{C} follows as

$$\int_{c \in \mathcal{C}} dc \rho(c) = \frac{1}{8\pi^2} \int_{\mathbf{Q}_0 \in SO(3)} d\mathbf{Q}_0 \int_0^\infty dk \rho_k(k) \int_0^\infty \dots \int_0^\infty \prod_{i=1}^k dn_i \rho_n(n_i). \quad (3.31)$$

Characterizing ρ_n experimentally prior to cross-linking is feasible, but whether monomer numbers remain i.i.d. after cross-linking is an open question. Molecular dynamics simulations [94–96, 111] or *in silico* network synthesis (e.g., Monte Carlo methods [112, 113]) could provide insight into realistic cross-link distributions. Alternatively, ρ_k , ρ_n , and ρ might be constructed from polymerization statistics — Miller-Macosko theory [114] or Pearson-Graessely theory [115] for ρ_k , and Flory-Stockmayer theory [110] for ρ_n . For simplicity, we retain the i.i.d. assumption on monomer numbers and assume simple forms for ρ_k and ρ_n . Connecting this framework to experimental or *in silico* network synthesis statistics is left for future work.

IV. FREE ROTATION METHODS

A. $SO(3)$ representations and numerical optimization

There are numerical pathologies associated with the Euler angle representation when optimizing over rotations [116]. We instead use the exponential, or “axis-angle”, representation. The Rodrigues vector, $\boldsymbol{\omega} \in \mathbb{R}^3$, describes the angle of rotation, $\varphi = |\boldsymbol{\omega}|$, and an axis about which to rotate, $\hat{\mathbf{u}} = \boldsymbol{\omega}/\varphi$. The rotation, \mathbf{Q} , is obtained by taking the exponential of the generating skew-symmetric tensor

$$\mathbf{A} = \begin{pmatrix} 0 & -\hat{u}_3 & \hat{u}_2 \\ \hat{u}_3 & 0 & -\hat{u}_1 \\ -\hat{u}_2 & \hat{u}_1 & 0 \end{pmatrix}; \quad \mathbf{Q}(\boldsymbol{\omega}) = \exp(\varphi \mathbf{A}) = \mathbf{I} + \sin \varphi \mathbf{A} + (1 - \cos \varphi) \mathbf{A}^2. \quad (4.1)$$

While the form of W_c^{FR} given by Eq. (3.13) is convenient to work with analytically, we have found that the following equivalent form has better convergence numerically:

$$W_c^{FR}(\mathbf{F}) = \inf_{\boldsymbol{\omega} \in B_{2\pi}(\mathbf{0}), \mathbf{y} \in \Omega} \sum_{i=1}^k w_i (|\mathbf{F} \mathbf{Q} \mathbf{X}_i - \mathbf{Q} \mathbf{y}|), \quad (4.2)$$

where $B_{2\pi}(\mathbf{0})$ is the ball of radius 2π centered at the origin, $\mathbf{0} = (0, 0, 0)$. The key differences in the formulation used for numerics are: (1) the explicit use of the Rodrigues representation and (2) rotating the cross-link along with the chain ends as opposed to only rotating the chain ends. Eq.

¹¹ Although chain ends are placed at $|\mathbf{X}_i| = (r_{rms})_i$ from the origin to establish Ω_0 , the initial chain length $r_i = |\mathbf{X}_i - \mathbf{y}|$ may differ from $(r_{rms})_i$ due to initial relaxation of the cross-link position $\mathbf{y} \in \Omega_0$.

¹² Dispersity in initial chain conformation could be considered within the modeling framework by allowing n_i and $|\mathbf{X}_i|$ (or \mathbf{X}_i , more generally) to vary independently through a joint probability distribution.

(4.2) was approximated in Mathematica using `FindMinimum` for local optimization and `NMinimize` for global optimization. `FindMinimum` uses a series of interior point methods for constrained (local) optimization; and `NMinimize` uses Nelder-Mead methods, supplemented by differential evolution. The local optimization toolset was used for all of the 4-chain numerical results because, as will be elaborated on shortly, the exact solution is known for the monodisperse case, which provides a good initial guess for all of the 4-chain numerical examples presented herein. Global optimization methods were used for the 6-chain models because, in the 6-chain case, the monodisperse solution is not explicitly known. The choices for optimization methods were made for simplicity of implementation; however, we remark that the exponential representation for rotations is also amenable to gradient-based methods [116].

B. Special case of monodispersity

For certain monodisperse networks where the RVEs are given by the classical 4-, 6-, and 8-chain models, the solution to the inner minimization of W_c^{FR} is known in closed form. This solution is useful as a starting point for both analytical approximation of, and as an initial guess for numerical approximation of, the free rotation limit for polydisperse networks.

Proposition 2 (Known solution for inner minimization and unification of discrete, monodisperse polymer network models). *Consider a monodisperse RVE such that $n_1 = \dots = n_k = n$, $\ell_1 = \dots = \ell_k = \ell$, $w_1 = \dots = w_k = w$, and $|\mathbf{X}_1| = \dots = |\mathbf{X}_k| = \tilde{r}_{rms}$ where, without loss of generality, the origin is assumed to coincide with the center of mass, i.e. $\sum_{i=1}^k \mathbf{X}_i = \mathbf{0}$. Let*

$$\gamma^* = \frac{\tilde{r}_{rms}}{\ell} \sqrt{\frac{\lambda_1^2 + \lambda_2^2 + \lambda_3^2}{3}}, \quad (4.3)$$

and

$$\{\mathbf{Q}^*, \mathbf{y}^*\} = \arg \inf_{\mathbf{Q} \in SO(3), \mathbf{y} \in \Omega} \sum_{i=1}^k w (|\mathbf{FQX}_i - \mathbf{y}|) \quad (4.4)$$

be the minimizing rotation and cross-link position, respectively, for a given RVE, $\{(n, \ell, \mathbf{X}_i, w)\}_{i=1}^k$, and deformation pair. Provided the additional following conditions are satisfied:

- (1) the chain free energy is the same convex, non-decreasing function of stretch squared, γ^2 , for each chain, and the chain free energy does not depend on the direction of stretch,
- (2) the chain directions in the RVE, $\mathbf{X}_i/\tilde{r}_{rms}$, are consistent with one of the classical 4-chain, 6-chain, or 8-chain RVEs (e.g., Eq. (3.29), Eq. (B4), Eq. (B6)),¹³

we have the following results:

- i) a solution to the inner optimization problem for W_c^{FR} (i.e., $\{\mathbf{Q}^*, \mathbf{y}^*\}$) is known, and is such that $\gamma_i = |\mathbf{FQ}^* \mathbf{X}_i - \mathbf{y}^*|/\ell = \gamma^*$ for all $i = 1, \dots, k$. It can be formulated explicitly as $\mathbf{y}^* = \mathbf{0}$ for all cases, and

$$\mathbf{Q}^* = \mathbf{Q} \left(\frac{\pi}{4} \hat{e}_1 \right) \mathbf{Q} \left(\arccos \sqrt{\frac{2}{3}} \hat{e}_2 \right) \mathbf{Q} \left(-\frac{\pi}{2} \hat{e}_3 \right) \mathbf{P} \text{ for the 4-chain RVE,} \quad (4.5a)$$

and

$$\mathbf{Q}^* = \mathbf{P} \text{ for the 8-chain RVE.} \quad (4.5b)$$

¹³ The classical 3-chain RVE is not included here because it does not satisfy $\sum_{i=1}^k \mathbf{X}_i = \mathbf{0}$.

ii) all aforementioned RVEs produce the same constitutive model when the network has a consistent density of chains per unit volume (i.e., after an appropriate renormalization of $M \rightarrow M/k$), which is equivalent to the classical 8-chain model (e.g., [11]).

The principal argument is divided into the following parts: (1) the equipartition property of convex functions, (2) there is a lower bound on the sum of square chain stretches, $\sum_i \gamma_i^2$, with respect to both rotations of the RVE and translations of the cross-link junction, and (3) a rotation and cross-link position exist that satisfy an equipartition of stretch.

Lemma (Equipartition property). *Given a convex, non-decreasing function f and n variables, x_1, \dots, x_n , whose sum is bounded from below by y , a solution to*

$$\min_{x_1, \dots, x_n} \sum_{i=1}^n f(x_i) \quad \text{subject to} \quad \sum_{i=1}^n x_i \geq y$$

is $x_1 = \dots = x_n = \frac{y}{n}$.

Proof. This follows from the definition of convexity,

$$\sum_{i=1}^n f(x_i) = n \left(\frac{1}{n} \sum_{i=1}^n f(x_i) \right) \geq n f \left(\frac{1}{n} \sum_{i=1}^n x_i \right) \geq n f \left(\frac{y}{n} \right).$$

and the last step is due to the non-decreasing property of f . \square

The significance of equipartition is that it establishes the optimality of the \mathbf{Q}^* and \mathbf{y}^* where the sum of the chain stretches squared is both minimal and equally partitioned between each of the k chains. We now proceed with the remainder of the proof of Proposition 2.

Proof. The first step is to consider the lower bound on the sum of chain stretches squared. One can show that this quantity is invariant with respect to rotations. Importantly, it establishes that the lower bound is achieved if and only if $\mathbf{y}^* = \mathbf{0}$.

Lower bound on $\sum_i \gamma_i^2$ and a solution for \mathbf{y}^ .* Consider $\sum_i \gamma_i^2$ for general \mathbf{Q} and \mathbf{y} :

$$\sum_{i=1}^k \gamma_i^2 = \frac{1}{\ell^2} \sum_{i=1}^k |\mathbf{FQX}_i - \mathbf{y}|^2 = \frac{1}{\ell^2} \left(\underbrace{\sum_{i=1}^k (\mathbf{FQX}_i) \cdot (\mathbf{FQX}_i)}_{\text{conserved}} - 2 \underbrace{\sum_{i=1}^k (\mathbf{FQX}_i) \cdot \mathbf{y}}_{=0} + \underbrace{\sum_{i=1}^k \mathbf{y} \cdot \mathbf{y}}_{\geq 0} \right). \quad (4.6)$$

The first term in the parentheses is conserved with respect to $\mathbf{Q} \in SO(3)$ [80]. (For completeness, this result is reproduced in Appendix F.) The second term vanishes. Indeed,

$$2 \sum_{i=1}^k (\mathbf{FQX}_i) \cdot \mathbf{y} = 2 \sum_{i=1}^k \mathbf{X}_i \cdot (\mathbf{Q}^T \mathbf{F}^T \mathbf{y}) = 2 (\mathbf{Q}^T \mathbf{F}^T \mathbf{y}) \cdot \underbrace{\left(\sum_{i=1}^k \mathbf{X}_i \right)}_{=0}. \quad (4.7)$$

Finally, the last term is clearly nonnegative. What is instructive about this analysis is that for monodisperse RVEs that satisfy the conditions of the proposition, $\mathbf{y}^* = \mathbf{0}$ is a part of a solution for all possible \mathbf{F} .

\mathbf{Q}^* that satisfies equipartition of stretch. The final step is to establish that, provided $\mathbf{y}^* = \mathbf{0}$, a \mathbf{Q}^* exists such that equipartition of stretch is satisfied. This is indeed the case and, in fact, an explicit solution can be given for the 4- and 8-chain cases [80].

(4-chain case) To show the 4-chain case, we decompose the rotation of interest \mathbf{Q}^* as $\mathbf{Q}^* = \mathbf{Q}'\mathbf{P}$ where, recall, \mathbf{P} rotates the Euclidean basis to align with the principal frame. Then it suffices to show that \mathbf{Q}' exists such that the chain stretches are all equal. Let $\mathbf{Q}' = \mathbf{Q}(\alpha\hat{e}_1)\mathbf{Q}(\beta\hat{e}_2)\mathbf{Q}(\xi\hat{e}_3)$. Then the chain with end-to-end vector $\mathbf{X}_1 (= \tilde{r}_{rms}(0, 0, 1))$ (see Eq. (3.29)) is deformed such that $\mathbf{X}_1 \rightarrow \mathbf{F}\mathbf{Q}'\mathbf{P}\mathbf{X}_1$ and

$$\gamma_1 = \frac{\tilde{r}_{rms}}{\ell} \sqrt{\lambda_1^2 \sin^2 \beta + \lambda_2^2 \sin^2 \alpha \cos^2 \beta + \lambda_3^2 \cos^2 \alpha \cos^2 \beta}. \quad (4.8)$$

Here α and β can be chosen such that $\gamma_1 = \gamma^*$. One such solution is $\alpha = \pi/4$ and $\beta = \arccos \sqrt{2/3}$. Substituting this solution for α and β into \mathbf{Q}' , we see that $\mathbf{X}_2 (= \tilde{r}_{rms}(0, 2\sqrt{2}/3, -1/3))$ is deformed such that

$$\gamma_2 = \frac{\tilde{r}_{rms}}{9\ell} \sqrt{3(\lambda_1 + 4\lambda_1 \sin \xi)^2 + \lambda_2^2 (6 \cos \xi + \sqrt{3}(1 - 2 \sin \xi))^2 + \lambda_3^2 (6 \cos \xi - \sqrt{3}(1 - 2 \sin \xi))^2}. \quad (4.9)$$

Now ξ can be chosen such that $\gamma_2 = \gamma^*$. One such solution is $\xi = -\pi/2$. Substituting into \mathbf{Q}' we see that $\gamma_1 = \dots = \gamma_4 = \gamma^*$.

(6-chain case) The stretch for each chain in the RVE can be formulated as

$$\gamma_i = \frac{1}{\ell} \sqrt{\mathbf{X}_i \cdot \bar{\mathbf{C}} \mathbf{X}_i}, \quad \text{where } \bar{\mathbf{C}} = \mathbf{Q}^T \mathbf{C} \mathbf{Q} \quad (4.10)$$

is a real proper orthogonal similarity transformation of \mathbf{C} . There exists a real proper orthogonal similarity transformation where all of the elements on the diagonal are equal [117]. The existence of this similarity transformation can be understood as follows. Consider rotating the coordinate system about \hat{e}_3 by φ . One can permute \bar{C}_{11} and \bar{C}_{22} by taking $\varphi = \pi/2$. Further, this transformation of \bar{C}_{11} and \bar{C}_{22} is continuous with respect to φ so that there exists a φ such that $\bar{C}_{11} = \bar{C}_{22}$. Similar arguments can be made about \bar{C}_{11} and \bar{C}_{33} (by rotating about \hat{e}_2), and about \bar{C}_{22} and \bar{C}_{33} (by rotating about \hat{e}_1). Thus, there exists a \mathbf{Q}^* such that $\bar{C}_{11} = \bar{C}_{22} = \bar{C}_{33} = 1/3 \text{Tr } \mathbf{C}$. Clearly, in this case, the chain stretches satisfy Eq. (4.3). Unfortunately, the exact form of \mathbf{Q}^* as a function of \mathbf{F} is not known (at least not to the authors).

(8-chain case) The \mathbf{Q}^* which satisfies Eq. (4.3) for the 8-chain RVE is well-known and is given by $\mathbf{Q}^* = \mathbf{P}$ [11]. \square

Remark 4. Implications for some isotropic, monodisperse polymer networks. Common chain free energies are convex, non-decreasing functions of γ^2 [80] (e.g., the Gaussian chain, the Kuhn and Gr \ddot{u} n approximation to the freely jointed chain, and the worm-like chain). This, along with Proposition 2, suggests that isotropic, monodisperse polymer networks which (1) are free to locally rotate and (2) consist of chains with convex free energies have an elastic response which is insensitive to – and potentially invariant with respect to – network topology.

Remark 5. Caveats for polydisperse polymer networks. There are two important differences for polydisperse polymer networks: (1) it is unlikely that $|\mathbf{X}_1| = \dots = |\mathbf{X}_k|$ holds; as a result, $\sum_i \gamma_i^2$ is no longer conserved with respect to rotations and $\mathbf{y}^* = \mathbf{0}$ may no longer be an optimal cross-link position, and (2) the chain free energies differ by chain, so equipartition of stretch is no longer an optimal solution. For instance, if the network consists of Gaussian chains with differing numbers of monomers, then

each chain has a different chain free energy, $w_i(\gamma) = (3/2) n_i k_B T \gamma^2$ (i.e., the entropic springs have different stiffnesses). However, as mentioned, the known solution for monodisperse networks may serve as inspiration towards initial guesses for numerical approximations of W_c^{FR} , and closed-form, analytical approximations of W_c^{FR} .

C. Closed-form approximation

Computation of the free rotation limit may pose some difficulties as it consists of averaging over the space of all cross-link RVEs, and inside the averaging operation is an optimization problem. Further, the representation for RVEs may be high-dimensional. Numerical integration can become prohibitively expensive in such a high-dimensional space, especially when the integrand is expensive to compute. To address these difficulties, we seek to derive analytical, closed-form approximations to the inner optimization problem for W_c^{FR} .

Consider a polydisperse RVE whose monodisperse counterpart has an exact solution to the rotational and cross-link positional relaxation problem (4-chain and 8-chain). We reformulate the inner optimization problem for W_c^{FR} (towards approximation in the limit of a “small” amount of polydispersity) by considering perturbations about the known solution for the monodisperse case. To begin, we assume incompressibility, which implies that $\mathbf{F} = \text{diag}(\lambda_1, \lambda_2, 1/\lambda_1 \lambda_2)$ without loss of generality. This takes the form

$$W_{c,(n_1, \dots, n_k)}^{FR} = \inf_{\mathbf{Q} \in SO(3), \mathbf{y} \in \Omega} \sum_{i=1}^k w_i (|\mathbf{F} \mathbf{Q} \mathbf{X}_i - \mathbf{y}|) = \inf_{\delta \boldsymbol{\omega}, \delta \mathbf{y}} \sum_{i=1}^k w_i (|\mathbf{F} \mathbf{Q}(\delta \boldsymbol{\omega}) \mathbf{Q}_m \mathbf{X}_i - (\mathbf{y}_m + \delta \mathbf{y})|) \quad (4.11)$$

where we introduce $W_{c,(n_1, \dots, n_k)}^{FR}$ to denote the free energy of an RVE in the free rotation limit with n_1, \dots, n_k monomers in its chains, where \mathbf{Q}_m and \mathbf{y}_m are the monodisperse solutions to the rotational and cross-link positional relaxation problem, respectively, and where $\mathbf{Q}(\delta \boldsymbol{\omega})$ is a small additional rotation and $\delta \mathbf{y}$ is a perturbation of the cross-link position. Both $\delta \boldsymbol{\omega}$ and $\delta \mathbf{y}$ are assumed small; that is, $\epsilon = \max(|\delta \boldsymbol{\omega}|, |\delta \mathbf{y}| / (r_{rms})_{\max}) \ll 1$ where $(r_{rms})_{\max} = \max((r_{rms})_1, \dots, (r_{rms})_k)$. For brevity, let the inner free energy cost be denoted by

$$\widehat{W}_c^{FR}(\delta \boldsymbol{\omega}, \delta \mathbf{y}) = \sum_{i=1}^k w_i (|\mathbf{F} \mathbf{Q}(\delta \boldsymbol{\omega}) \mathbf{Q}_m \mathbf{X}_i - (\mathbf{y}_m + \delta \mathbf{y})|), \quad (4.12)$$

and then we approximate derivatives with respect to $\delta \boldsymbol{\omega}$ and $\delta \mathbf{y}$ to linear order in $\delta \boldsymbol{\omega}$ and $\delta \mathbf{y}$ as¹⁴

$$\frac{\partial \widehat{W}_c^{FR}}{\partial(\delta \boldsymbol{\omega})} = \left. \frac{\partial \widehat{W}_c^{FR}}{\partial(\delta \boldsymbol{\omega})} \right|_{(\mathbf{0}, \mathbf{0})} + \left(\left. \frac{\partial^2 \widehat{W}_c^{FR}}{\partial \delta \mathbf{y} \partial \delta \boldsymbol{\omega}} \right|_{(\mathbf{0}, \mathbf{0})} \right) \delta \mathbf{y} + \left(\left. \frac{\partial^2 \widehat{W}_c^{FR}}{\partial \delta \boldsymbol{\omega} \partial \delta \boldsymbol{\omega}} \right|_{(\mathbf{0}, \mathbf{0})} \right) \delta \boldsymbol{\omega} + \mathcal{O}(\epsilon^2), \quad (4.13)$$

$$\frac{\partial \widehat{W}_c^{FR}}{\partial(\delta \mathbf{y})} = \left. \frac{\partial \widehat{W}_c^{FR}}{\partial(\delta \mathbf{y})} \right|_{(\mathbf{0}, \mathbf{0})} + \left(\left. \frac{\partial^2 \widehat{W}_c^{FR}}{\partial \delta \mathbf{y} \partial \delta \mathbf{y}} \right|_{(\mathbf{0}, \mathbf{0})} \right) \delta \mathbf{y} + \left(\left. \frac{\partial^2 \widehat{W}_c^{FR}}{\partial \delta \boldsymbol{\omega} \partial \delta \mathbf{y}} \right|_{(\mathbf{0}, \mathbf{0})} \right) \delta \boldsymbol{\omega} + \mathcal{O}(\epsilon^2). \quad (4.14)$$

Dropping higher order terms (i.e. $\mathcal{O}(\epsilon^2)$), setting Eq. (4.13) and Eq. (4.14) equal to $\mathbf{0}$, and solving for $\delta \boldsymbol{\omega}$ and $\delta \mathbf{y}$, one can arrive at an approximation that minimizes \widehat{W}_c^{FR} . We denote the solution

¹⁴ Note that $\delta \boldsymbol{\omega}$ derivatives are with respect to components of the Rodrigues vector, not rotational derivatives (see [116], for example). The approximation made here can be seen as a leading order perturbation, in contrast to a full iteration of Newton’s method, which can lead to complex and unstable expressions when the initial guess is not “close enough”.

for $\delta\boldsymbol{\omega}$ and $\delta\mathbf{y}$ as $\widetilde{\delta\boldsymbol{\omega}}$ and $\widetilde{\delta\mathbf{y}}$, respectively, such that

$$\widetilde{\delta\boldsymbol{\omega}} = \widetilde{\delta\boldsymbol{\omega}}(n_1, \dots, n_k), \quad (4.15a)$$

$$\widetilde{\delta\mathbf{y}} = \widetilde{\delta\mathbf{y}}(n_1, \dots, n_k). \quad (4.15b)$$

As derived, the approximation above, by itself, does not satisfy material frame indifference. The reason is as follows: the rotation which minimizes the free energy for the monodisperse case is not unique; in other words, there are other equally valid choices of \mathbf{Q}_m to perturb about via $\delta\boldsymbol{\omega}$ (\mathbf{Q}^* as expressed in Eq. (4.5) is only one such choice). Different choices of rotation can result in different approximations for the polydisperse case because the varying chain lengths break some symmetry. For example, consider the rotation of a cube such that its edges are aligned with the principal directions, $\hat{\mathbf{v}}_i$. Naively, one could expand about all rotations that align the chains in the (undeformed) RVE with the diagonals of the cube, and derive an approximate solution for each. Then, the best approximation can be chosen as the one with minimal free energy. Luckily, further derivations are unnecessary. Different choices of \mathbf{Q}_m about which to expand correspond with certain permutations of the monomer numbers, (n_1, \dots, n_k) . Therefore, approximations to the rotational and cross-link position relaxations can be expressed as

$$\sigma^* = \arg \min_{\sigma \in \mathcal{G}} \widetilde{W}_c^{FR}(\widetilde{\delta\boldsymbol{\omega}}(\sigma \cdot (n_1, \dots, n_k)), \widetilde{\delta\mathbf{y}}(\sigma \cdot (n_1, \dots, n_k))) \quad (4.15c)$$

$$\{\delta\boldsymbol{\omega}, \delta\mathbf{y}\} = \{\widetilde{\delta\boldsymbol{\omega}}(\sigma^* \cdot (n_1, \dots, n_k)), \widetilde{\delta\mathbf{y}}(\sigma^* \cdot (n_1, \dots, n_k))\} \quad (4.15d)$$

where $\mathcal{G} \leq \mathbb{S}_k$ is the symmetry group of the RVE structure, which is a subgroup of \mathbb{S}_k , the symmetric group of k elements, and $\sigma \cdot \square$ denotes the group action of σ on \square . In other words, the approximate solution for the cross-link rotational and positional relaxation is taken to be the one for which the inner free energy is minimal, where the minimization is over all permutations of the monomers numbers that are consistent with the underlying symmetry of the RVE. For the 4-chain RVE, $\mathcal{G} \cong \mathbb{S}_4$.

The free energy of the polydisperse RVE, $W_{c,(n_1, \dots, n_k)}^{FR}$, can then be approximated by substituting Eq. (4.15) into Eq. (4.12).

Remark 6. Distinction between linearization about the monodisperse RVE solution and linear elasticity. The closed form approximation given by Eq. (4.15) was obtained by linearization of its governing equations; however, the approximation is distinct from *linear elasticity*. The typical assumption underlying linear elasticity is that $\|\nabla\mathbf{u}\|$ is small such that $\mathcal{O}(\|\nabla\mathbf{u}\|^2)$ terms can be neglected, where \mathbf{u} is the deformation at a material point. Instead, here, *the linearization is about the monodisperse RVE solution, which is known for finite deformations*. The approximation can be expected to be at its most accurate when the amount of polydispersity (i.e. variance in n_i) within the RVE is small enough. We will show through example that this is indeed the case. The closed-form approximation agrees well with numerical solutions at small deformations in all cases. For nearly monodisperse networks, the error increases gradually with deformation. For highly polydisperse networks, the error grows more rapidly.

Gaussian networks with cross-link degree 4 Consider the polydisperse 4-chain RVE (with \mathbf{X}_i given by Eq. (3.29)) consisting of chains with Gaussian free energy given by Eq. (2.5). Here, the closed-form approximation for the rotational and cross-link positional relaxation problem is found

to be

$$\widetilde{\delta\omega}_1(n_1, n_2, n_3, n_4) = 0, \quad (4.16a)$$

$$\widetilde{\delta\omega}_2(n_1, n_2, n_3, n_4) = \frac{a_1(a_4\lambda_1^4\lambda_2^4 - a_2^2\lambda_1^2 - a_3^2\lambda_2^2)}{a_3(a_1^2\lambda_1^4\lambda_2^4 + a_2^2\lambda_1^2 + a_3^2\lambda_2^2)}, \quad (4.16b)$$

$$\widetilde{\delta\omega}_3(n_1, n_2, n_3, n_4) = \frac{a_2(a_1^2\lambda_1^4\lambda_2^4 + a_5\lambda_1^2 + a_3^2\lambda_2^2)}{a_3(a_1^2\lambda_1^4\lambda_2^4 + a_2^2\lambda_1^2 + a_3^2\lambda_2^2)}, \quad (4.16c)$$

$$\widetilde{\delta y}_1(n_1, n_2, n_3, n_4) = -\frac{ba_3a_6\bar{n}_{\text{geo}}^2\lambda_1\lambda_2^2}{\sqrt{3}a_7(a_1^2\lambda_1^4\lambda_2^4 + a_2^2\lambda_1^2 + a_3^2\lambda_2^2)}, \quad (4.16d)$$

$$\widetilde{\delta y}_2(n_1, n_2, n_3, n_4) = \frac{ba_2a_6\bar{n}_{\text{geo}}^2\lambda_1^2\lambda_2}{\sqrt{3}a_7(a_1^2\lambda_1^4\lambda_2^4 + a_2^2\lambda_1^2 + a_3^2\lambda_2^2)}, \quad (4.16e)$$

$$\widetilde{\delta y}_3(n_1, n_2, n_3, n_4) = \frac{ba_1a_6\bar{n}_{\text{geo}}^2\lambda_1^3\lambda_2^3}{\sqrt{3}a_7(a_1^2\lambda_1^4\lambda_2^4 + a_2^2\lambda_1^2 + a_3^2\lambda_2^2)}, \quad (4.16f)$$

$$\sigma^* = \arg \min_{\sigma \in \mathbb{S}^4} \widetilde{W}_c^{FR}(\widetilde{\delta\omega}(\sigma \cdot (n_1, n_2, n_3, n_4)), \widetilde{\delta\mathbf{y}}(\sigma \cdot (n_1, n_2, n_3, n_4))) \quad (4.16g)$$

$$\{\delta\boldsymbol{\omega}, \delta\mathbf{y}\} = \{\widetilde{\delta\omega}(\sigma^* \cdot (n_1, n_2, n_3, n_4)), \widetilde{\delta\mathbf{y}}(\sigma^* \cdot \{n_1, n_2, n_3, n_4\})\}, \quad (4.16h)$$

where

$$a_1 = \sqrt{n_1n_2n_3} - \sqrt{n_1n_2n_4} - \sqrt{n_1n_3n_4} + \sqrt{n_2n_3n_4}, \quad (4.16i)$$

$$a_2 = \sqrt{n_1n_2n_3} - \sqrt{n_1n_2n_4} + \sqrt{n_1n_3n_4} - \sqrt{n_2n_3n_4}, \quad (4.16j)$$

$$a_3 = \sqrt{n_1n_2n_3} + \sqrt{n_1n_2n_4} - \sqrt{n_1n_3n_4} - \sqrt{n_2n_3n_4}, \quad (4.16k)$$

$$a_4 = 2(-2n_2n_3\sqrt{n_1n_4} + n_2n_3n_4 + n_1(n_4(\sqrt{n_2} - \sqrt{n_3})^2 + n_2n_3)), \quad (4.16l)$$

$$a_5 = -2(-2n_2n_4\sqrt{n_1n_3} + n_2n_3n_4 + n_1(-2n_3\sqrt{n_2n_4} + n_3n_4 + n_2(n_3 + n_4))), \quad (4.16m)$$

$$a_6 = 3n_2n_3n_4 - 2\sqrt{n_1}(n_3n_4\sqrt{n_2} + n_2(n_3\sqrt{n_4} + n_4\sqrt{n_3})) \quad (4.16n)$$

$$+ n_1(3n_3n_4 + n_2(-2\sqrt{n_3n_4} + 3n_3 + 3n_4) - 2\sqrt{n_2}(n_3\sqrt{n_4} + n_4\sqrt{n_3})),$$

$$a_7 = n_1n_2n_3 + n_1n_2n_4 + n_1n_3n_4 + n_2n_3n_4, \quad (4.16o)$$

$\bar{n}_{\text{geo}} = (n_1n_2n_3n_4)^{1/4}$ is the geometric mean of monomer number, $\bar{n} = (n_1 + \dots + n_4)/4$ is the arithmetic mean of monomer number, and $\eta = \bar{n}_{\text{geo}}/\bar{n}$ is the ratio of the geometric mean to the arithmetic mean, often referred to as the ‘‘efficiency’’ of a set of values. The efficiency is a measure of the homogeneity of values in a given dataset; it is 1 when all of the values are the same and approaches 0 as the values become increasing disparate. In this context, it is a measure of polydispersity.

V. FRAME AVERAGING METHODS

A. $SO(3)$ representations and numerical optimization

Unlike the free rotation limit, the frame averaging limit does not require optimization over rotations, but instead requires integration over $SO(3)$, as per Eq. (3.19). We approximate integration over $SO(3)$ via numerical quadrature using Euler angle parameterization

$$\frac{1}{8\pi^2} \int_{\mathbf{Q}_0 \in SO(3)} d\mathbf{Q}_0 F(\mathbf{Q}_0) \approx \sum_{i=1}^{N_{SO(3)}} v_i F((\mathbf{Q}_0)_i), \quad (5.1)$$

where F is some general (scalar, vectorial, or tensorial) function of \mathbf{Q}_0 , $\{(\mathbf{Q}_0)_i\}_{i=1}^{N_{SO(3)}}$ is the set of $SO(3)$ quadrature points, $\{w_i\}_{i=1}^{N_{SO(3)}}$ is the set of corresponding weight factors, and $N_{SO(3)}$ is the number of quadrature points. Additional details of $SO(3)$ quadrature are provided in Appendix G. The $SO(3)$ quadrature scheme can be constructed from any spherical quadrature rule. Since full network and microsphere models [12–15] already employ spherical quadrature for integration over chain orientations, existing implementations require only minor modification to perform $SO(3)$ integration.

While the form of W_c^{FA} given by Eq. (3.18) and Eq. (3.19) are convenient to work with analytically, we have found that the following equivalent forms have better convergence numerically:

$$W_c^{FA}(\mathbf{F}, \mathbf{Q}_0) = \inf_{\mathbf{y} \in \Omega} \sum_{i=1}^k w_i (|\mathbf{F}\mathbf{Q}_0\mathbf{X}_i - \mathbf{Q}_0\mathbf{y}|), \quad (5.2)$$

$$W_c^{FA}(\mathbf{F}) = \frac{1}{8\pi^2} \int_{\mathbf{Q}_0 \in SO(3)} d\mathbf{Q}_0 \left(\inf_{\mathbf{y} \in \Omega} \sum_{i=1}^k w_i (|\mathbf{F}\mathbf{Q}_0\mathbf{X}_i - \mathbf{Q}_0\mathbf{y}|) \right). \quad (5.3)$$

Eq. (5.2) and Eq. (5.3) were approximated in Python via the NumPy [118] and SciPy [119] packages. For the $SO(3)$ quadrature involved in Eq. (5.3), we need to define a foundational spherical quadrature scheme and the number of spin discretization points, N_ψ (see Appendix G). We use the 74-point, 13-degree Bažant and Oh [120] formula as the foundational spherical quadrature scheme, along with $N_\psi = 16$, for all frame averaging limit results in this work (due to symmetry considerations, this amounts to $N_{SO(3)} = 592$). For our frame averaging limit results, we use the Constrained Optimization BY Quadratic Approximations (COBYQA) algorithm [121, 122] offered by the `scipy.optimize.minimize` function for local constrained optimization (unless specified otherwise, e.g., Fig. 5). Even though our computational implementation is capable of utilizing other local constrained optimization methods¹⁵ and global constrained optimization methods,¹⁶ we found the results obtained from the COBYQA method to be both efficient and accurate. This computational implementation is provided in a freely available `polydisperse-polymer-networks` GitHub repository [127].

B. Closed-form approximation

As with the free rotation assumption, we outline a procedure for deriving an analytical, closed-form approximation to the inner optimization problem for W_c^{FA} . We propose $\mathbf{y}_m = \mathbf{0}$ as the initial guess for the junction position, motivated by the free rotation monodisperse case. For frame averaging monodisperse RVEs with Gaussian chains and $\sum_{i=1}^k \mathbf{X}_i = \mathbf{0}$, $\mathbf{y}_{\mathbf{Q}_0}^* = \mathbf{0}$ is the exact equilibrium solution (as per Eq. (3.23)). (This also holds exactly for monodisperse 6-chain and 8-chain RVEs with Kuhn-Grün and wormlike chain models.¹⁷) This suggests $\mathbf{y}_m = \mathbf{0}$ provides a reasonable guess about which to expand for approximating a solution to the polydisperse equilibrium equation. This takes the form

$$W_{c,(n_1, \dots, n_k)}^{FA}(\mathbf{F}, \mathbf{Q}_0) = \inf_{\mathbf{y} \in \Omega} \sum_{i=1}^k w_i (|\mathbf{F}\mathbf{Q}_0\mathbf{X}_i - \mathbf{y}|) \approx \inf_{\delta\mathbf{y}_{\mathbf{Q}_0}} \sum_{i=1}^k w_i (|\mathbf{F}\mathbf{Q}_0\mathbf{X}_i - (\mathbf{y}_m + \delta\mathbf{y}_{\mathbf{Q}_0})|), \quad (5.4)$$

$$W_{c,(n_1, \dots, n_k)}^{FA}(\mathbf{F}) = \frac{1}{8\pi^2} \int_{\mathbf{Q}_0 \in SO(3)} d\mathbf{Q}_0 \left(W_{c,(n_1, \dots, n_k)}^{FA}(\mathbf{F}, \mathbf{Q}_0) \right), \quad (5.5)$$

¹⁵ These include the Constrained Optimization BY Linear Approximation (COBYLA) algorithm [123] and the constrained trust region method [124] offered by the `scipy.optimize.minimize` function.

¹⁶ These include the simplicial homology global optimization [125] and differential evolution [126] methods provided by the `scipy.optimize.shgo` and `scipy.optimize.differential_evolution` functions, respectively.

¹⁷ It can be seen that this satisfies force balance for the 6 and 8-chain RVEs because for every chain force $\hat{\mathbf{r}}_i w'_i (\mathbf{F}\mathbf{Q}_0\mathbf{X}_i)$ there is an equal and opposite force. By Proposition 1, this is the unique minimum of W_{ch} .

where we introduce $W_{c,(n_1,\dots,n_k)}^{FA}$ to denote the free energy of an RVE in the frame averaging limit with n_1, \dots, n_k monomers in its chains, $\delta\mathbf{y}_{\mathbf{Q}_0}$ is a small perturbation of the cross-link position, and $|\delta\mathbf{y}_{\mathbf{Q}_0}|/(r_{rms})_{\max} \ll 1$. For brevity, let the inner free energy cost be denoted by

$$\widehat{W}_c^{FA}(\delta\mathbf{y}_{\mathbf{Q}_0}, \mathbf{Q}_0) = \sum_{i=1}^k w_i (|\mathbf{F}\mathbf{Q}_0\mathbf{X}_i - (\mathbf{y}_m + \delta\mathbf{y}_{\mathbf{Q}_0})|), \quad (5.6)$$

and then we approximate the derivative with respect to $\delta\mathbf{y}_{\mathbf{Q}_0}$ to linear order in $\delta\mathbf{y}_{\mathbf{Q}_0}$ as

$$\frac{\partial \widehat{W}_c^{FA}}{\partial (\delta\mathbf{y}_{\mathbf{Q}_0})} = \left. \frac{\partial \widehat{W}_c^{FA}}{\partial (\delta\mathbf{y}_{\mathbf{Q}_0})} \right|_0 + \left(\left. \frac{\partial^2 \widehat{W}_c^{FA}}{\partial \delta\mathbf{y}_{\mathbf{Q}_0} \partial \delta\mathbf{y}_{\mathbf{Q}_0}} \right|_0 \right) \delta\mathbf{y}_{\mathbf{Q}_0} + \mathcal{O}(\epsilon^2). \quad (5.7)$$

To arrive at an approximation that minimizes \widehat{W}_c^{FA} , we solve for $\delta\mathbf{y}_{\mathbf{Q}_0}$ by dropping higher order terms (i.e. $\mathcal{O}(\epsilon^2)$) and setting Eq. (5.7) equal to $\mathbf{0}$,

$$\delta\mathbf{y}_{\mathbf{Q}_0} = - \left(\left. \frac{\partial^2 \widehat{W}_c^{FA}}{\partial \delta\mathbf{y}_{\mathbf{Q}_0} \partial \delta\mathbf{y}_{\mathbf{Q}_0}} \right|_0 \right)^{-1} \left. \frac{\partial \widehat{W}_c^{FA}}{\partial (\delta\mathbf{y}_{\mathbf{Q}_0})} \right|_0. \quad (5.8)$$

The free energy of the polydisperse RVE, $W_{c,(n_1,\dots,n_k)}^{FA}$, can then be approximated by substituting $\delta\mathbf{y}_{\mathbf{Q}_0}$ into Eq. (5.6). Notably, since $\mathbf{y}_m = \mathbf{0}$, then the analytical form of each of the derivatives in Eq. (5.8) is directly given in Appendix C (when swapping $\delta\mathbf{y}_{\mathbf{Q}_0}$ for \mathbf{y}). This convenience can then be utilized in deriving an analytical expression for $\delta\mathbf{y}_{\mathbf{Q}_0}$.

Recall that the exact solution for $\delta\mathbf{y}_{\mathbf{Q}_0}$ for polydisperse RVEs consisting of Gaussian chains is given by Eq. (3.23) (where $\mathbf{Q} = \mathbf{Q}_0$). We supply the analytical form of $\delta\mathbf{y}_{\mathbf{Q}_0}$ for the case of polydisperse Kuhn and Grün chains in Appendix H. But henceforth in this work, we exclusively utilize the form of $\delta\mathbf{y}_{\mathbf{Q}_0}$ supplied in Eq. (3.23).

VI. BIMODAL NETWORKS OF GAUSSIAN CHAINS

In general, the probability density function over RVEs, $\rho(c)$, may be complex (which could render the calculation of the network free energy density, as per Eq. (3.24), computationally costly). In contrast, traditional (discrete) polymer networks only consider a single molecular weight with a fixed RVE geometry, which is equivalent to $\rho_n(n) = \delta(n - n_0)$, and has resulted in models that, in many cases, combine simplicity (i.e., a small number of fitted parameters) with quality fits. Inspired by this, and motivated by the principle of parsimony to keep the number of model parameters as small as possible, we consider the analogous probability density for networks with a bimodal distribution of chain molecular weights that are exclusively joined at tetrafunctional cross-links ($k = 4$). Assuming that the number of monomers in each chain are independent and identically distributed (as discussed in Section III E), we here represent the probability density over RVEs as

$$\rho(c) = \rho_4(k) \prod_{i=1}^4 \rho_n(n_i), \quad (6.1a)$$

$$\rho_4(k) = \delta(k - 4), \quad (6.1b)$$

$$\rho_n(n) = p\delta(n - n_a) + (1 - p)\delta(n - n_b), \quad (6.1c)$$

where the \mathbf{X}_i are related to n_i by Eq. (3.29). To make connections to a realistic bimodal distribution of chain molecular weights, n_a and n_b can be thought of as the peaks of the distribution, and p can

be tuned to account for the relative probability masses (i.e. integration of density “local” to each peak) between the peaks. In a discrete random variable sense, p is the probability of a given chain having n_a monomers and $1 - p$ is the probability of a given chain having n_b monomers.

Given the independence and discreteness of monomer numbers, the free energy density takes the simplified form,

$$\begin{aligned} \mathcal{W}_C(\mathbf{F}) = \frac{M}{2} & \left(p^4 \binom{4}{4} W_{c,(n_a,n_a,n_a,n_a)} + p^3 (1-p) \binom{4}{3} W_{c,(n_a,n_b,n_b,n_b)} + p^2 (1-p)^2 \binom{4}{2} W_{c,(n_a,n_a,n_b,n_b)} \right. \\ & \left. + p(1-p)^3 \binom{4}{1} W_{c,(n_a,n_a,n_a,n_b)} + (1-p)^4 \binom{4}{0} W_{c,(n_b,n_b,n_b,n_b)} \right), \end{aligned} \quad (6.2)$$

where the binomial coefficients account for all of the permutations of monomers which give equivalent RVEs by symmetry (e.g., $W_{c,(n_a,n_b,n_b,n_b)} = W_{c,(n_b,n_a,n_b,n_b)} = W_{c,(n_b,n_b,n_a,n_b)} = W_{c,(n_b,n_b,n_b,n_a)}$ by symmetry, etc.). By considering Gaussian chains, the above model given by Eq. (6.2) allows one to characterize the structure of a bimodal polymer network through n_a , n_b , p , M , and b .

Before considering Eq. (6.2) in any more depth, we first turn our attention to the three distinct classes of 4-chain RVEs that constitute it: the monodisperse RVE ($W_{c,(n_a,n_a,n_a,n_a)}$ and $W_{c,(n_b,n_b,n_b,n_b)}$), which is already known to have the equipartition of stretch solution (Proposition 2) for the free rotation limit and $\mathbf{y}_m = \mathbf{0}$ for the frame averaging limit; the RVE with one chain of different length ($W_{c,(n_a,n_b,n_b,n_b)}$ and $W_{c,(n_a,n_a,n_a,n_b)}$); and the RVE with two of each chain length $W_{c,(n_a,n_a,n_b,n_b)}$. For brevity, we will refer to the second and third 4-chain RVE classes as the 1-3 and 2-2 RVEs, respectively. Since the monodisperse RVE is well-known and exactly characterized, we will focus primarily on the 1-3 and 2-2 RVEs (and refer back to the monodisperse RVE only for comparison).

In what follows, we first investigate the behavior of these RVEs in the free rotation limit, and then briefly highlight the corresponding frame averaging limit behavior.

A. Free rotation limit

Closed-form approximation for the 1-3 RVE in the free rotation limit. For the 1-3 RVE, Eq. (4.16) takes on the considerably simpler form:

$$\delta\omega_1 = 0, \quad (6.3a)$$

$$\delta\omega_2 = s_2 \left(\frac{3(\lambda_1^2 + \lambda_2^2)}{\lambda_1^2 + \lambda_2^2 + \lambda_1^4 \lambda_2^4} - 2 \right), \quad (6.3b)$$

$$\delta\omega_3 = s_3 \left(\frac{3\lambda_1^2}{\lambda_1^2 + \lambda_2^2 + \lambda_1^4 \lambda_2^4} - 1 \right), \quad (6.3c)$$

$$\delta y_1 = s_2 s_3 b \frac{\sqrt{3n_\alpha n_\beta} (\sqrt{n_\beta} - \sqrt{n_\alpha}) \lambda_1 \lambda_2 (\lambda_1 + \lambda_2)}{2(3n_\alpha + n_\beta) (\lambda_1^2 + \lambda_2^2 + \lambda_1^4 \lambda_2^4)}, \quad (6.3d)$$

$$\delta y_2 = s_2 b \frac{\sqrt{3n_\alpha n_\beta} (\sqrt{n_\beta} - \sqrt{n_\alpha}) \lambda_1 \lambda_2 (\lambda_1 + \lambda_2)}{2(3n_\alpha + n_\beta) (\lambda_1^2 + \lambda_2^2 + \lambda_1^4 \lambda_2^4)}, \quad (6.3e)$$

$$\delta y_3 = s_3 b \frac{\sqrt{3n_\alpha n_\beta} (\sqrt{n_\beta} - \sqrt{n_\alpha}) \lambda_1^3 \lambda_2^3}{2(3n_\alpha + n_\beta) (\lambda_1^2 + \lambda_2^2 + \lambda_1^4 \lambda_2^4)}, \quad (6.3f)$$

where n_α and n_β refer to the number of monomers in the 1-3 RVE with multiplicity 1 and 3, respectively; and where $s_2 = \pm 1$, and $s_3 = \pm 1$ can vary independently to give 4 different solutions. Remarkably, the free energies that result from the 4 different solutions are all identical.¹⁸ Similarly, the magnitudes of cross-link displacement and RVE rotations are invariant as

$$|\delta\boldsymbol{\omega}| = \sqrt{5 - \frac{3(4\lambda_1^2\lambda_2^2 + (1 + 6\lambda_1^6)\lambda_2^4 + 4\lambda_1^4\lambda_2^6)}{(\lambda_1^2 + \lambda_2^2 + \lambda_1^4\lambda_2^4)^2}}, \quad (6.3g)$$

$$|\delta\mathbf{y}| = \frac{b|\sqrt{n_\alpha} - \sqrt{n_\beta}|\lambda_1\lambda_2}{3n_\alpha + n_\beta} \sqrt{\frac{3n_\alpha n_\beta}{(\lambda_1^2 + \lambda_2^2 + \lambda_1^4\lambda_2^4)}}. \quad (6.3h)$$

Closed-form approximation for the 2-2 RVE in the free rotation limit. Likewise, Eq. (4.16) takes on the simplified form for the 2-2 RVE,

$$\delta\boldsymbol{\omega} = \mathbf{0}, \quad (6.4a)$$

$$\delta y_i = \pm \frac{b\eta}{2\sqrt{3}} (\sqrt{n_b} - \sqrt{n_a}) \lambda_i, \quad (6.4b)$$

$$\delta y_j = 0, \quad (6.4c)$$

where $\eta = \bar{n}_{\text{geo}}/\bar{n}$. Here, there are 6 separate solutions as $i = 1, 2, 3$ and $j \neq i$. For the 2-2 RVE, the free energy can be formulated concisely as

$$k_B T \left((1 + \eta) \lambda_i^2 + 2 \sum_{j=1, j \neq i}^3 \lambda_j^2 \right), \quad (6.5)$$

where $i = 1, 2, 3$ and $\lambda_3 = 1/\lambda_1^2\lambda_2^2$; of the 6 solutions for $\delta\boldsymbol{\omega}$ and $\delta\mathbf{y}$, there are only 3 associated forms of the free energy that are unique. Of the 3, the minimum free energy is always given by the case where $\lambda_i = \max(\lambda_1, \lambda_2, \lambda_3)$. This is because $\eta \leq 1$. Note that equality $\eta = 1$ occurs if and only if $n_a = n_b$, recovering the Neo-Hookean model. The factor $(1 + \eta)$ in front of the maximum principal stretch is reduced relative to the factor 2 in front of the other principal stretches when $\eta < 1$ (i.e., when polydispersity is significant). This indicates that the 2-2 RVE exhibits reduced stiffness in the maximum principal stretch direction, with the degree of reduction determined by the polydispersity parameter η . Physically, the RVE allows relaxation by preferentially aligning softer chains (those with smaller monomer number n) along the maximum stretch direction, thereby reducing resistance to deformation in that direction.

Junction fluctuation term. For networks of Gaussian chains, the junction fluctuation term takes a form that is invariant with respect to the macroscopic deformation (e.g., see Eq. (C2)). This invariance can be physically understood as follows: the Hessian of the cross-link junction positional energy is determined by the tangent stiffnesses of the connected polymer chains about the optimal position, \mathbf{y}^* . Because Gaussian chains exhibit a constant stiffness – lacking the strain stiffening or softening observed in finite extensibility models – the Hessian remains constant regardless of the individual chain stretches. Consequently, the fluctuation term is independent of the continuum-scale deformation, thereby justifying its exclusion from the mechanical stress analysis presented in

¹⁸ Verified in the Mathematica notebook that can be found at <https://github.com/grasingerm/polydisperse-network-models>.

this work. Indeed, the determinants of the Hessians for the 1-3 and 2-2 RVEs are given by

$$\det \left(\frac{\partial^2 W_{\text{ch}}}{\partial \mathbf{y} \partial \mathbf{y}} \Big|_{\mathbf{Q}=\mathbf{Q}^*, \mathbf{y}=\mathbf{y}^*} \right) = \frac{27 (k_B T)^3}{b^6} \left(\frac{3}{n_\alpha} + \frac{1}{n_\beta} \right)^3, \quad (6.6a)$$

$$\det \left(\frac{\partial^2 W_{\text{ch}}}{\partial \mathbf{y} \partial \mathbf{y}} \Big|_{\mathbf{Q}=\mathbf{Q}^*, \mathbf{y}=\mathbf{y}^*} \right) = \frac{27 (k_B T)^3}{b^6} \left(\frac{2}{n_a} + \frac{2}{n_b} \right)^3, \quad (6.6b)$$

respectively. Note that each of the terms in the parentheses of Eq. (6.6) appear as a ratio of a monomer number to the number of chains in the RVE with that particular monomer number (e.g., for the 1-3 RVE, there are 3 chains with n_α monomers and 1 chain with n_β monomers).

Accuracy of closed-form approximations. The closed-form approximation agrees well with the numerical solutions for the examples considered herein. First consider the uniaxial deformation, $\mathbf{F} = \text{diag}(\lambda, 1/\sqrt{\lambda}, 1/\sqrt{\lambda})$. Fig. 4 a) shows $W_{c,(.)}$ as a function of λ for (130, 90, 90, 90) (\triangle), (70, 110, 110, 110) (\diamond), (40, 120, 120, 120) (\square), (50, 50, 150, 150) ($*$), and (25, 25, 175, 175) (\circ). Numerical solutions are represented by markers, whereas closed-form approximations are given by a solid line of the corresponding color. For the 1-3 RVEs, the approximation is nearly exact for the two cases with lower variance, but there is some disagreement at higher stretches for the (40, 120, 120, 120) case. Despite the high variance, the 2-2 RVEs ((50, 50, 150, 150) and (25, 25, 175, 175)) show almost exact agreement at all the deformations considered. Note that, for the 1-3 RVEs, the amount of variance in n_i seems to drive behavior more than whether the 1 chain length is greater than or less than the length of the remaining 3 chains. In fact, the behavior of the (130, 90, 90, 90) and (70, 110, 110, 110) are nearly identical, as are the pair (40, 120, 120, 120) and (50, 50, 150, 150). The two classes of behavior here appear to be organized primarily by the amount of variance in n_i (and, correspondingly, η). The free energy response of a second deformation mode, simple shear, is shown in Fig. 4 b). Here $\mathbf{F} = \mathbf{I} + s \hat{e}_1 \otimes \hat{e}_3$, and the principal stretches are $\lambda_1 = \sqrt{2 + s^2 + s\sqrt{4 + s^2}}/\sqrt{2}$, $\lambda_2 = 1$, and $\lambda_3 = \sqrt{2 + s^2 - s\sqrt{4 + s^2}}/\sqrt{2}$. Similar phenomena can be observed for simple shear, illustrating their generality to other types of deformation.

Degree of polydispersity. To highlight some additional phenomena, Fig. 6 shows the free energy response of polydisperse free rotation RVEs with a fixed \bar{n} and wider range of monomer number variances when subjected to a) uniaxial deformation and b) simple shear deformation. An increase in monomer number variance leads to lower free energies, and broader, flatter free energy curves, which has some correspondence with softer networks. We point to the (10, 130, 130, 130) cross-link RVE as an example where free energy minima do not occur at $\lambda = 1$; it is also clearly nonconvex. The free energy in the free rotation limit can exhibit nonconvexity because it is approximated as the minimum over 4 candidate equilibria, each corresponding to a local minima of the rotation optimization. Although each candidate free energy function appears convex, their pointwise minimum is not guaranteed to preserve convexity. Nonconvexity occurs when the global minimum switches from one candidate to another as the deformation varies. This is a potential limitation with either the approximation in the free rotation limit, the method developed herein for the construction of polydisperse RVEs, or both; however, we note that these cases appear isolated to RVEs with large variance, and where at least 1 of the chains has a small number of monomers (i.e. $n_i/n_j \ll 1$ for some i and j). Fig. 6 c) shows the rotated and deformed (40, 120, 120, 120) RVE when uniaxially deformed with $\lambda = 1.25, 1.5, 1.75$, and 2.0. The cross-link position in the reference configuration and the deformed configuration are denoted by red and green points, respectively. The rotation and displacement of the cross-link increase with deformation. Fig. 6 d) and e) show the magnitude of cross-link displacement, $|\mathbf{y}|/b$, as a function of deformation. The relationship appears nearly linear, where the RVEs with a higher degree of polydispersity have a higher slope; that is, the cross-link displaces more with deformation when there is more variance in $(n_i)_{i=1}^4$.

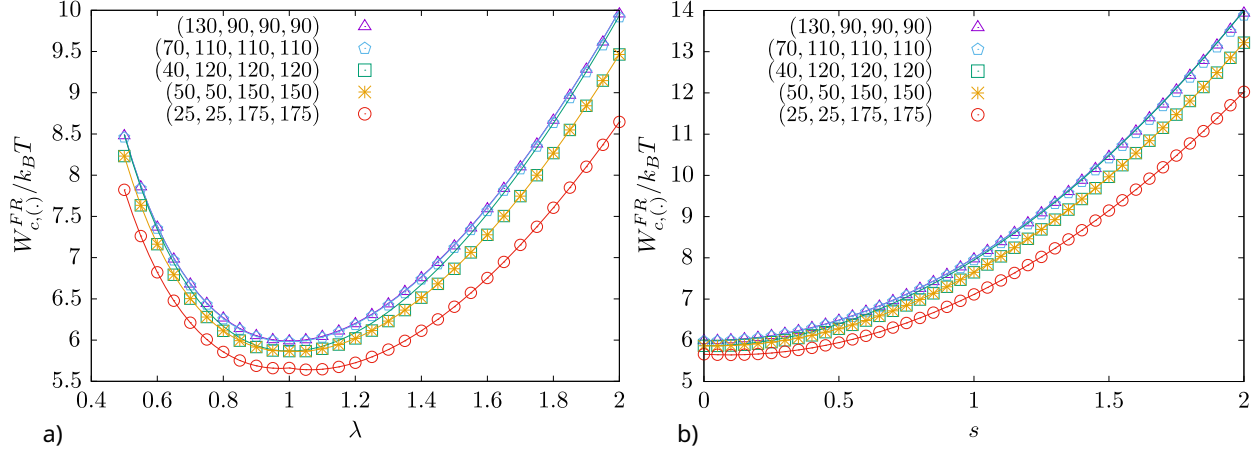


FIG. 4. Agreement of closed-form approximation for free rotation RVEs with various degrees of polydispersity undergoing uniaxial a) and simple shear b) deformations.

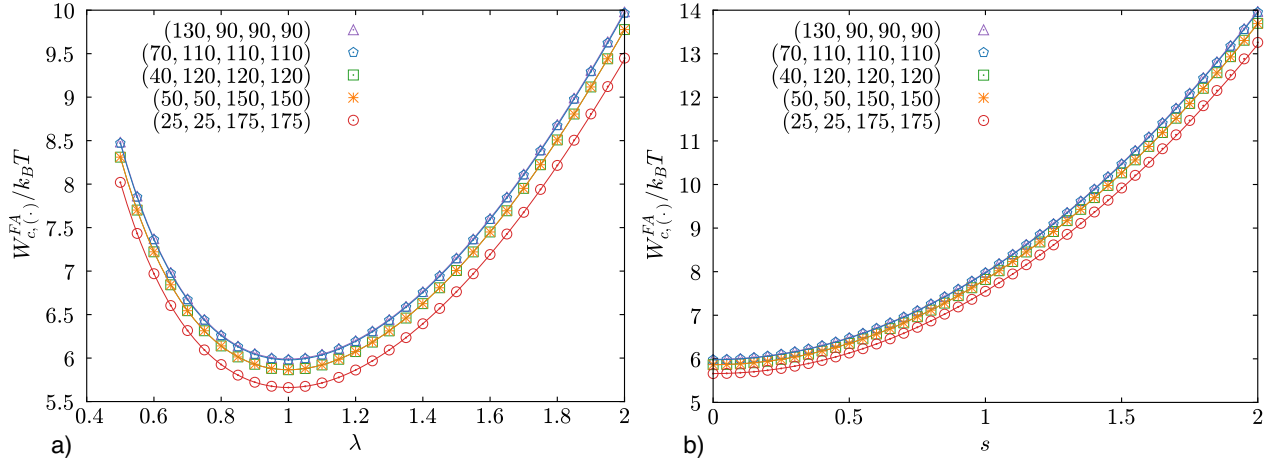


FIG. 5. Agreement of closed-form approximation for frame averaging RVEs with various degrees of polydispersity undergoing uniaxial a) and simple shear b) deformations. Note that the Constrained Optimization BY Linear Approximation (COBYLA) algorithm [123] (offered by the `scipy.optimize.minimize` function) was used here for local constrained optimization to produce these particular frame averaging numerical results.

The change in mechanical properties with polydispersity can be made more precise by investigating the tangent stiffness modulus, $E_{(.)} = \partial^2 W_{c(.)} / \partial \lambda^2$, with respect to uniaxial deformation. For simplicity, we only derive an expression for the tangent stiffness modulus of the 1-3 RVE for 1 of the 4 candidate minima with respect to rotations. (The chosen minima corresponds with $s_2 = -s_3 = 1$ in Eq. (6.3).) The tangent stiffness modulus for the 1-3 RVE is

$$E_{(n_\alpha, n_\beta, n_\beta, n_\beta)} \Big|_{\lambda=1} = 3k_B T \left(\frac{15n_\alpha + 7n_\beta - 6\sqrt{n_\alpha n_\beta}}{3n_\alpha + n_\beta} \right), \quad (6.7)$$

and, for the 2-2 RVE is

$$E_{(n_a, n_a, n_b, n_b)} \Big|_{\lambda=1} = 2k_B T (5 + \eta), \quad (6.8)$$

where, again, $\eta = \sqrt{n_a n_b} / \bar{n}$ is the efficiency. If the average monomer number is constrained such that $4\bar{n} = n_\alpha + 3n_\beta$ for the 1-3 RVE and $4\bar{n} = 2n_a + 2n_b$ for the 2-2 RVE, then, in either case, the

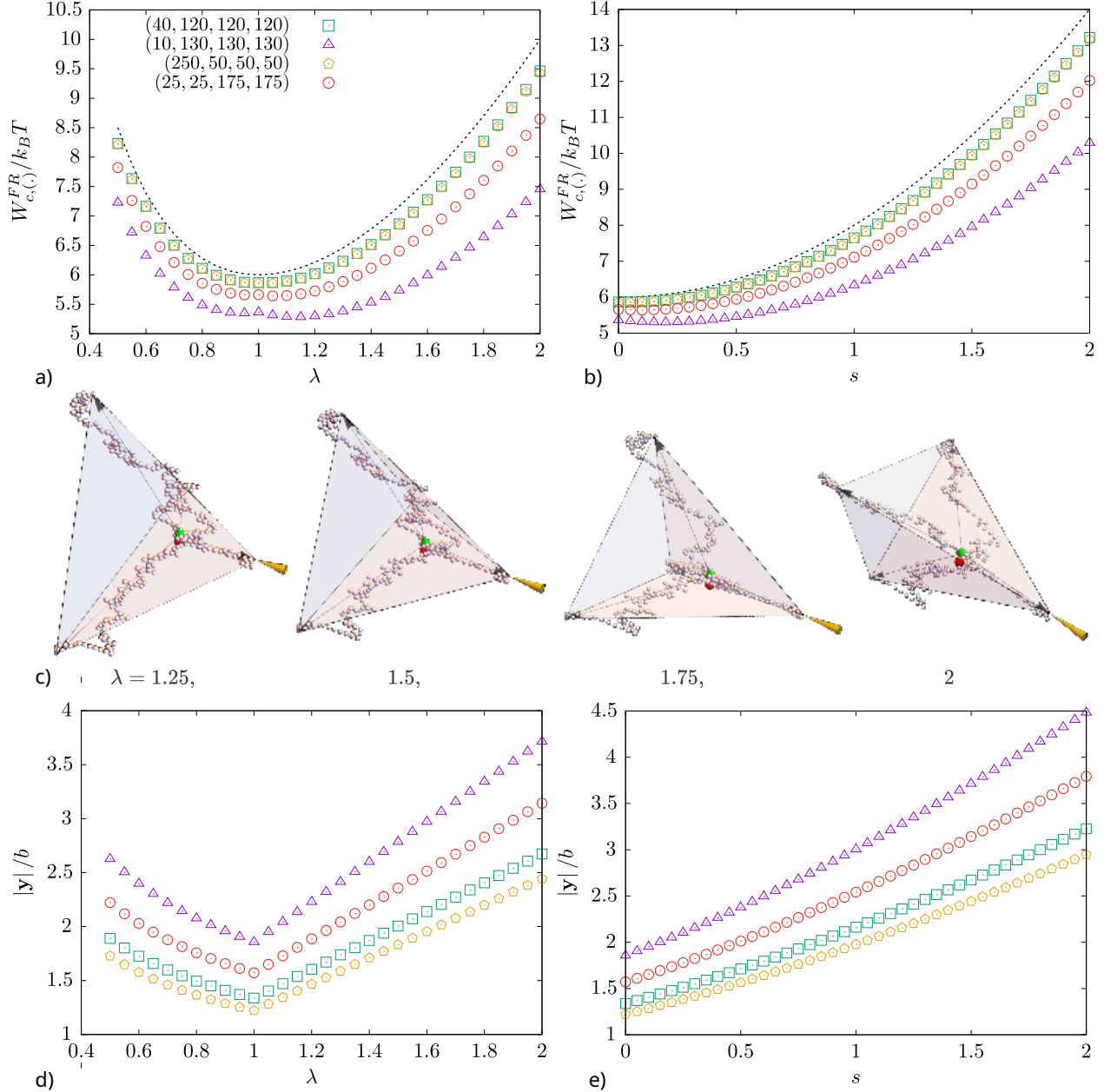


FIG. 6. Free energy response for free rotation RVEs with various degrees of polydispersity for a) uniaxial and b) simple shear deformations. c) (40, 120, 120, 120) free rotation RVEs under uniaxial deformations of $\lambda = 1.25, 1.5, 1.75,$ and 2 . Cross-link displacements for polydisperse free rotation RVEs under d) uniaxial and e) simple shear deformations.

stiffness modulus is an extrema if and only if $n_\alpha = n_\beta = \bar{n}$ and $n_a = n_b = \bar{n}$, respectively; that is, when the RVE is monodisperse. Upon inspection of the second derivatives of E with respect to monomer numbers, it is seen that the monodisperse case is indeed a maxima for the 2-2 RVE, but, surprisingly, a minima for the 1-3 RVE. This can also be seen in Fig. 8, which shows the tangent stiffness modulus as a function of λ for various polydisperse a) 1-3 and b) 2-2 RVEs. Although the monodisperse case is a minima for 1-3 RVEs, the difference in stiffness is small between the RVEs considered. Thus, in a full bimodal network model of the form Eq. (6.2), a net softening may

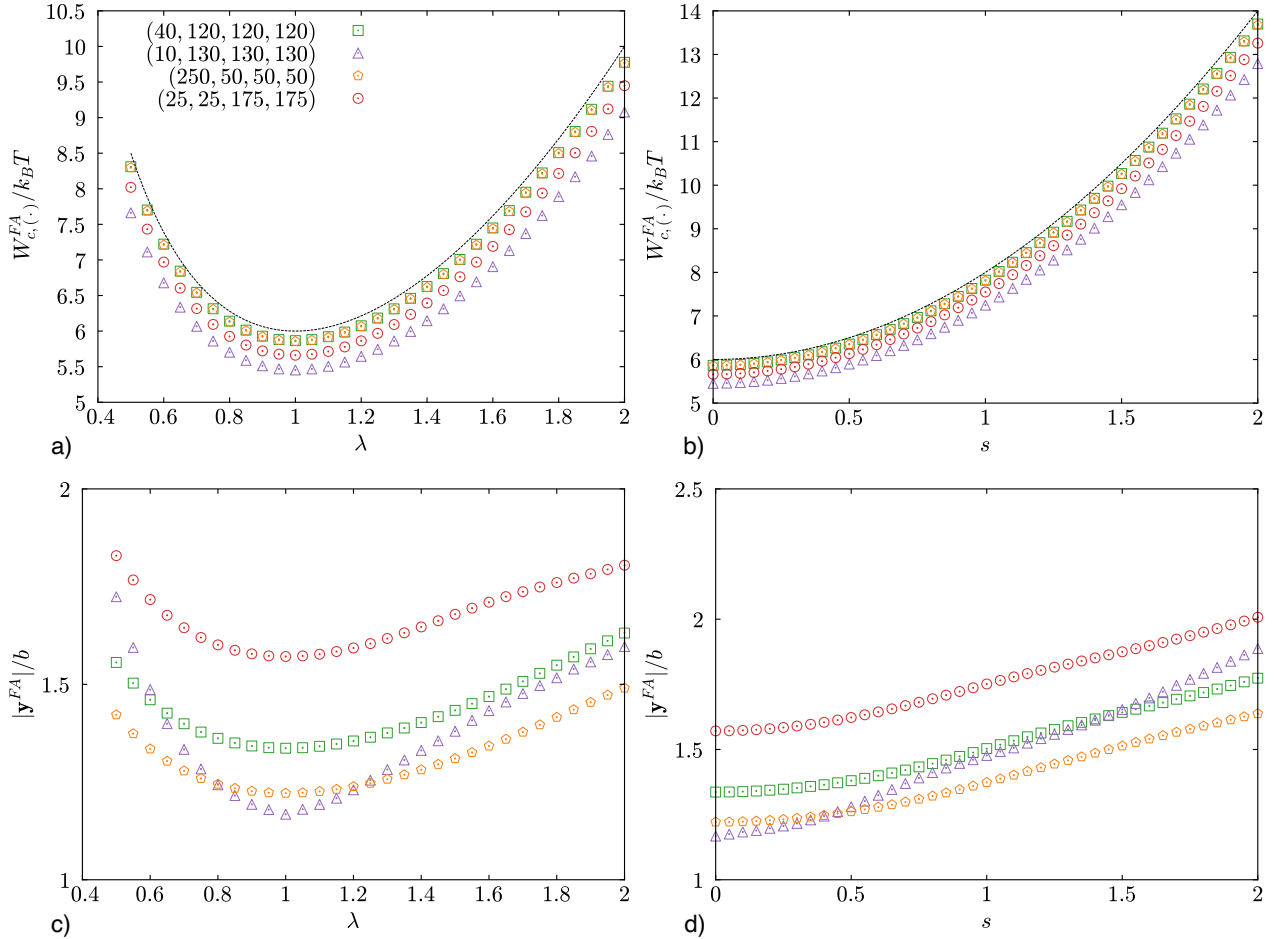


FIG. 7. Free energy response for frame averaging RVEs with various degrees of polydispersity for a) uniaxial and b) simple shear deformations. Cross-link displacements for polydisperse frame averaging RVEs under c) uniaxial and d) simple shear deformations.

often occur with increasing polydispersity. This agrees qualitatively with the results of mesoscale simulations [66].

Cross-links with degree 4 versus degree 6. For a monodisperse network consisting of FJC (or WLC) chains, the 4-, 6-, and 8-chain RVEs produce the same constitutive model (see e.g., Remark 4 or [80]). Here, we consider the implications of topological differences on polydisperse networks. Fig. 9 shows the per-chain free energy response for polydisperse 4- and 6-chain RVEs undergoing uniaxial deformations. The average number of monomers, \bar{n} , is held fixed at 100. For a), in both the 4- and 6-chain RVEs, half of the chains are shorter and half are longer. The behavior is identical. However, in b) only 1 chain is of a smaller number of monomers, 40. In this case, the per-chain free energy response is different depending on whether the cross-link consists of 4 chains or 6 chains.

B. Frame averaging limit

In Fig. 5, we present both the closed-form approximation (Eq. (3.23) where $\mathbf{Q} = \mathbf{Q}_0$) and the numerical solution for several different polydisperse frame averaging RVEs in a) uniaxial deformation and b) simple shear deformation. Here, the closed-form approximation agrees very well with the

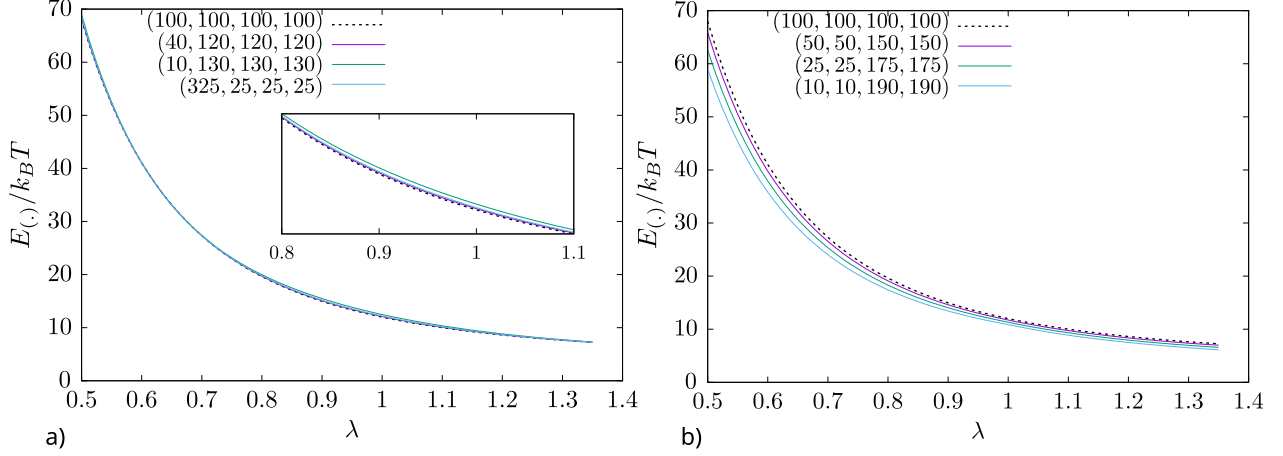


FIG. 8. Tangent stiffness modulus, $E = \partial^2 W_{c(.)}/\partial \lambda^2$ for various polydisperse a) 1-3 and b) 2-2 free rotation RVEs.

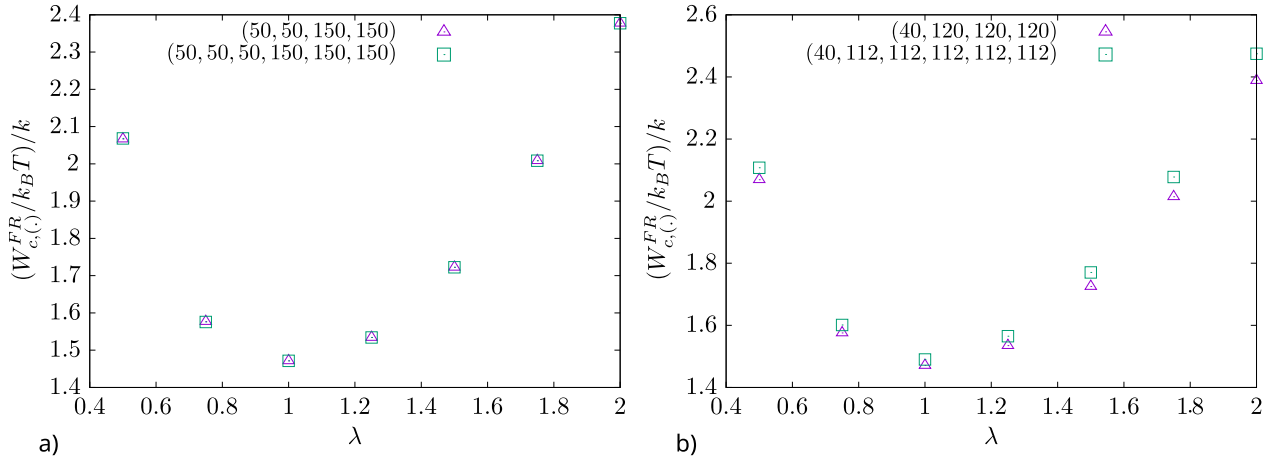


FIG. 9. Comparison between 4-chain and 6-chain free rotation RVEs. a) For the cases where half of the chains are of one length, and half the other, the behavior is the same. b) However, for fixed average but one chain of a different length, there is a difference in behavior between the 4-chain and 6-chain RVEs.

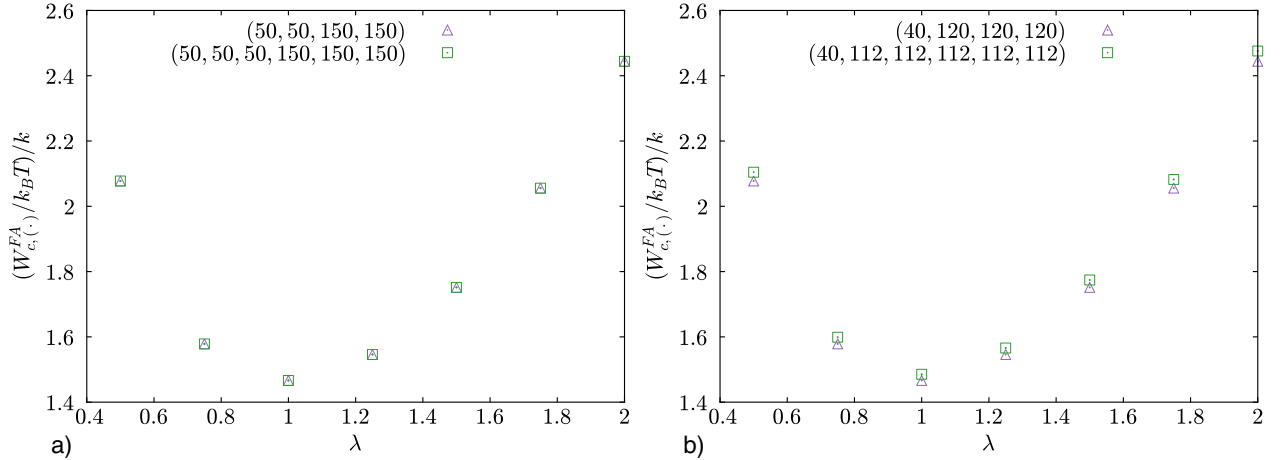


FIG. 10. Comparison between 4-chain and 6-chain frame averaging RVEs. The trends analogously follow those from the free rotation RVEs in Fig. 9.

corresponding numerical solutions. The free energy minima for each frame averaging RVE also occurs at $\lambda = 1$ in uniaxial deformation and $s = 0$ in simple shear. When compared with the analogous results for the free rotation model in Fig. 4, it is clear that free energy state of each frame averaging RVE is, at all deformation states, equal to or greater than the free energy state of its free rotation counterpart.

To highlight some additional phenomena, Fig. 7 shows the free energy response of polydisperse frame averaging RVEs with a fixed \bar{n} and wider range of monomer number variances when subjected to a) uniaxial deformation and b) simple shear deformation. Moreover, Fig. 7 c) and d) show the magnitude of frame averaging cross-link displacement, $|\mathbf{y}^{FA}|/b$, as a function of deformation. When comparing Fig. 7 c) and d) to the analogous free rotation results in Fig. 6 d) and e), several intriguing observations can be made. First, it is clear that, during deformation, less cross-link displacement takes place in the frame averaging limit as compared to the free rotation limit. With less cross-link displacement under the same macroscopically-imposed deformation conditions, the chains in the frame averaging limit are thus more deformed than their free rotation counterparts, which leads to the frame averaging RVE free energy state being greater than that for the free rotation limit. Second, there seems to be a rather non-linear relationship between deformation and cross-link displacement in the frame averaging limit (which could possibly be attributed to numerical approximation error from using $SO(3)$ quadrature to approximately integrate over all possible cross-link orientations). This is in contrast to the very nearly linear relationship between deformation and cross-link displacement in the free rotation limit. Third, in the free rotation RVE, cross-link displacement increases when there is more variance in $(n_i)_{i=1}^4$. This trend clearly does not hold for the frame averaging limit.

Finally, Fig. 10 shows the per-chain free energy response for polydisperse 4- and 6-chain frame averaging RVEs undergoing uniaxial deformations. These frame averaging RVEs exhibit similar behavior when compared to their free rotation counterparts in Fig. 9.

VII. FINITE EXTENSIBILITY AND STRAIN STIFFENING

The elastic response of many soft polymer networks consists of an initial Neo-Hookean regime followed by strain stiffening. The result is a stress-strain curve that takes a characteristic ‘S’ shape. The Gaussian model for chain free energies, together with polymer network models, can recover the Neo-Hookean regime and help to elucidate the implications of macromolecular and network structure within this regime [4]; however, this combination cannot resolve the strain stiffening regime. In contrast, the Kuhn and Gr \ddot{u} n chain free energy, w_{KG} , takes into account the finite extensibility of the FJC and, as a result, captures a strain stiffening regime at large deformations (see [11]). Ideally, a closed-form approximation would be obtained using the chain free energy w_{KG} within each RVE of interest, following the procedure outlined in Section IV C for the free rotation limit and Section V B for the frame averaging limit. However, for the free rotation limit, this proves intractable because w_{KG} involves the inverse Langevin function, for which the exact analytical formula does not exist and approximations are often complex. Complicating matters further, the inverse Langevin function is nested within csch and ln functions. Instead, we take advantage of the fact that the Gaussian chain is a leading order approximation of w_{KG} . The approximations $\delta\omega$ and $\delta\mathbf{y}$ derived for Gaussian chains in Eq. (6.3) and Eq. (6.4) naturally serve as leading order approximations for free rotation RVEs with Kuhn and Gr \ddot{u} n chains. A key consideration here is that Eq. (6.3) represents 4 different approximate solutions for the 1-3 RVE and Eq. (6.4) represents 6 for the 2-2 RVE. As before, the best approximation for a given deformation in either case is the one that results in the minimum

free energy. For the 1-3 RVE, provided one follows the convention¹⁹ that the chain with unique monomer number is taken to be chain 1 (i.e. along $(0, 0, 1)$), then numerical results reveal that Eq. (6.3) with $s_2 = -1$ and $s_3 = 1$ is the optimal approximation for the examples presented herein. For the 2-2 RVE, provided the convention (n_a, n_a, n_b, n_b) is used for the undeformed chain orientations,

$$\delta\boldsymbol{\omega} = \mathbf{0}, \quad (7.1a)$$

$$\delta y_1 = \delta y_2 = 0, \quad (7.1b)$$

$$\delta y_3 = \frac{b\eta(\sqrt{n_a} - \sqrt{n_b})}{2\sqrt{3}(\lambda_1\lambda_2)}, \quad (7.1c)$$

is optimal for the examples presented herein. A comparison of the closed-form approximation in the free rotation limit with numerical results is given in Fig. 11 for a) 1-3 RVEs and b) 2-2 RVEs. As expected, the approximation remains very accurate at moderate strains (e.g. $\lambda \lesssim 1.3$). The error increases with the combination of variance in the monomer numbers and large deformations. While, in this case, there is a slight over prediction of the strain energies, the closed-form solution remains a good leading order approximation for the influence of polydispersity on the elasticity of the network.

Although a closed-form approximation using the Kuhn-Grün chain free energy can be obtained for the frame averaging limit (Eq. (H4)), we instead use the Gaussian-based approximation from Eq. (3.23). This choice ensures direct comparability between the two limits and simplifies implementation, as the Gaussian approximation serves as the leading-order term for Kuhn-Grün chains at moderate deformations. Fig. 12 shows this approximation agrees well with numerical solutions for both a) 1-3 and b) 2-2 RVEs across all strains considered. As in the Gaussian case, the frame averaging limit consistently predicts equal or higher free energies than the free rotation limit.

‘S’-curves. Next we consider the features of the ‘S’ shaped stress-strain curves that can be captured with the approach developed herein. Qualitatively, the 2 limits agree; a discussion of where and why they diverge will be discussed in the next paragraph. Since the strain stiffening regime in the ‘S’ is due to the finite extensibility of the chains, we again consider RVEs consisting of Kuhn and Grün chains. Let \mathcal{W}_C be given by Eq. (6.2). For the free rotation limit, the 1-3 RVEs are approximated by Eq. (6.3) with $s_2 = -1$ and $s_3 = 1$, and the 2-2 RVEs are approximated by Eq. (7.1). For the frame averaging limit, we again follow the approximation provided in Eq. (3.23) for all polydisperse RVEs. Fig. 13 shows $\boldsymbol{\Sigma} = \partial\mathcal{W}_C/\partial\mathbf{F}$ for the uniaxial stretch, λ . Recall that p represents the probability that a chain has n_a monomers, and $1 - p$ is the probability of a chain with n_b monomers. In Fig. 13 a), p and \bar{n} are fixed at $p = 0.5$ and $\bar{n} = 75$, respectively, and the network has increasing disparities between n_a and n_b , corresponding to increasing degrees of network polydispersity. Notice that increasing polydispersity leads to the strain stiffening regime (i.e. sharp increase in stress) occurring at lower stretches and lower stresses. In Fig. 13 b), n_a and n_b are fixed at 50 and 100, respectively, and p varies as 0.1, 0.25, 0.5, 0.75, and 0.9. Although strain stiffening occurs near the same stretch, the shape of the strain stiffening regime changes with p . More precisely, the onset of strain stiffening is more gradual, and less sharp with increasing p . A takeaway here is that the minimum n_i appears to controls the stretch at which strain stiffening begins to occur, and p modulates how sharply the stress begins to diverge within that regime. The bimodal polymer network model developed herein is one that can capture more complex features in ‘S’ stress-strain curves while only introducing a few additional model parameters that have clear

¹⁹ The conventions chosen here are without loss of generality. Recall: a permutation of monomer numbers is equivalent to changing the frame about which we expand to obtain the closed-form approximation. Fixing a particular permutation and minimizing over the finite number of frames that are optimal for the monodisperse case is sufficient to satisfy material frame indifference.

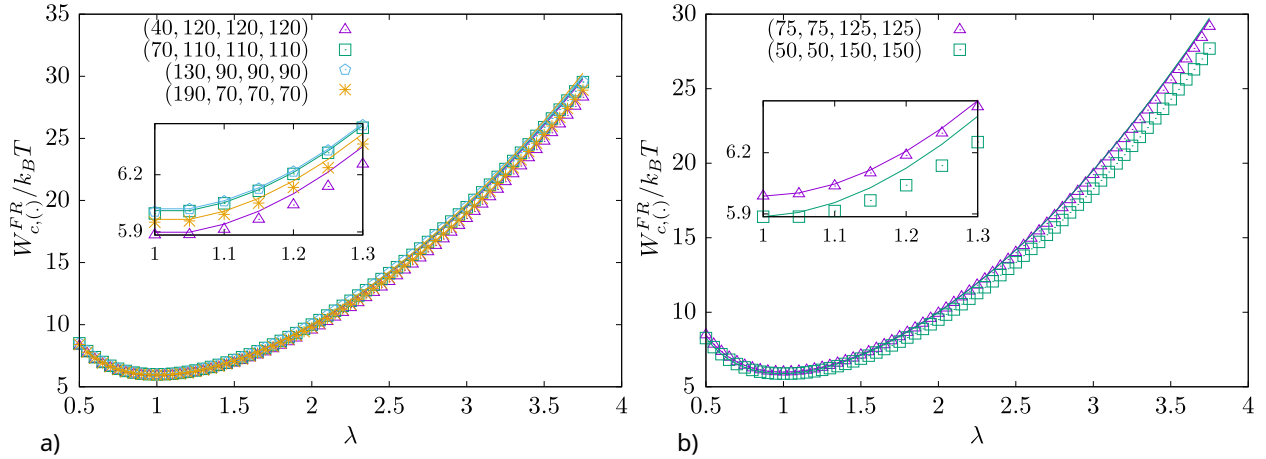


FIG. 11. Agreement of closed-form approximation for free rotation RVEs with Kuhn and Gr\u00fcn chains (exhibiting finite extensibility) in uniaxial deformation for the a) 1-3 RVEs and b) 2-2 RVEs.

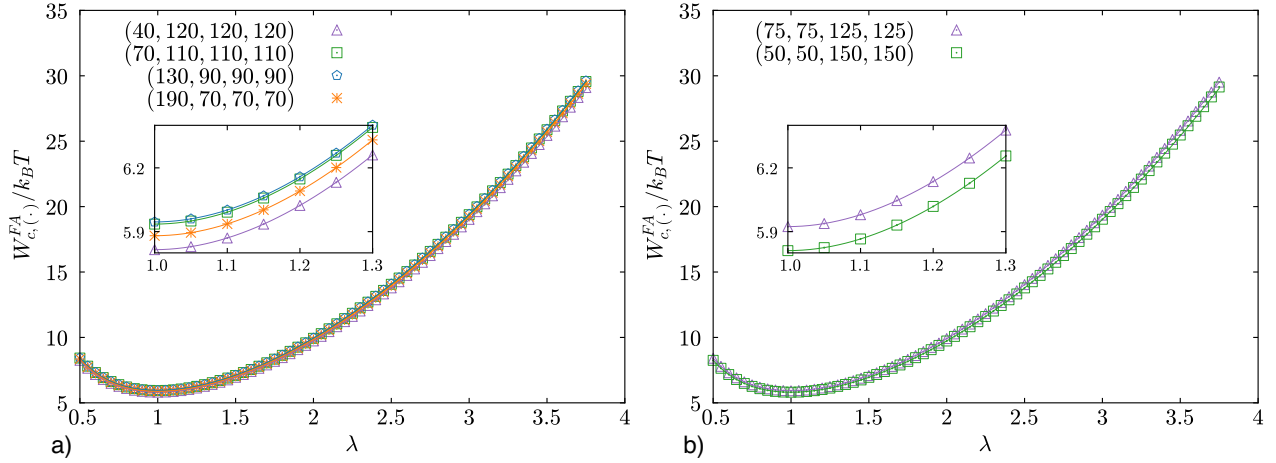


FIG. 12. Agreement of closed-form approximation for frame averaging RVEs with Kuhn and Gr\u00fcn chains (exhibiting finite extensibility) in uniaxial deformation for the a) 1-3 RVEs and b) 2-2 RVEs.

physical meanings, are directly tied to the structure of the polymer network, and can potentially be measured, designed, and perhaps even synthesized with a certain degree of control.

Comparison of free rotation and frame averaging limits. In principle, the free rotation limit has access to a greater number of relaxation modes than the frame averaging limit; consequently, the free energy and stress predicted by the free rotation limit should theoretically always be less than or equal to its frame averaging counterpart. Surprisingly, Fig. 13 shows that, in many cases, the opposite trend is observed. This remarkable observation is not derived from physical reasons, but is instead an artifact of approximation error inherent to the closed-form solutions derived for the minimum energy frame. To be specific, there is an error in the approximation for the optimal frame that grows with both increasing deformation and an increasing degree of polydispersity. When the approximation for the optimal frame in the free rotation limit is expected to be accurate – such as when the degree of polydispersity is low – the free rotation and frame averaging limits agree nearly exactly. Altogether, this suggests that for the elasticity of polydisperse networks, averaging over all frames is generally as effective as minimizing over frames for modeling soft networks; furthermore, averaging over all frames tends to be superior to attempting to approximate the optimal frame for

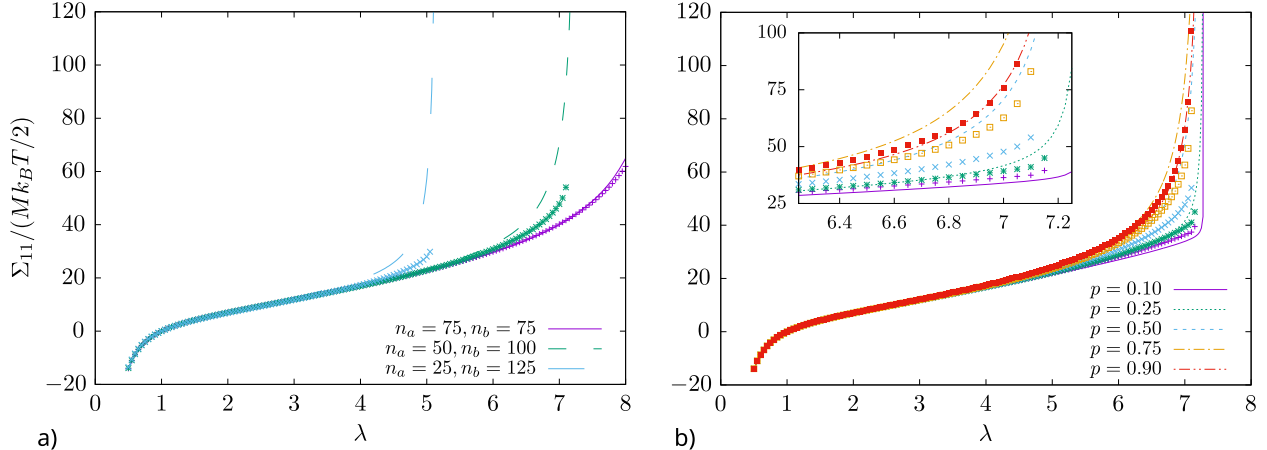


FIG. 13. ‘S’ shaped stress-strain curves common in soft polymer network elasticity. a) Stress-strain curves for bimodal networks with $p = 0.5$, $\bar{n} = 75$, and varying n_a and n_b (lines: free rotation limit; markers: frame averaging limit). Greater disparity between n_a and n_b leads to earlier onset of strain stiffening. b) Stress-strain curves for networks with $n_a = 50$, $n_b = 100$, and varying p , where p is the probability that a chain has n_a monomers and $1 - p$ the probability of n_b monomers (lines: free rotation limit; markers: frame averaging limit). Increasing p leads to a more gradual, less sharp stress increase in the strain stiffening regime.

networks with larger degrees of polydispersity and at larger deformations. This, combined with the simplicity of its formulation, make it an advantageous approach for modeling the elasticity of polydisperse networks. It remains open how the two limits compare for polydisperse networks with multiphysics loadings, such as electroelasticity (e.g., [44, 53, 80]). This presents an interesting topic for future work.

VIII. CONCLUSION

Summary. In this work, we introduce a new approach to polymer network modeling that shifts the perspective from polymer chains as the basic unit to cross-links and their connected chains. A central feature of this framework is that cross-link junction positions are allowed to relax to satisfy local force balance. Regarding the frame (orientation) of the Representative Volume Element (RVE), we explored two distinct limiting behaviors: the free rotation limit and the frame averaging limit. The free rotation limit assumes the cross-link rotates to an optimal orientation that minimizes free energy, offering a physically intuitive mechanism that aligns well with quintessential experimental data for unimodal networks. Conversely, the frame averaging limit incorporates structural heterogeneity by averaging over all possible cross-link orientations. This dual perspective allows for a more general distribution of stretches and forces within the network compared to more restrictive assumptions like equal stretch or equal force theories, enabling the direct linking of statistical descriptors of the network structure to macroscopic mechanical response.

To address potential computational challenges of integrating and optimizing in high-dimensional parameter spaces, we derived closed-form approximations for both limits. While the free rotation model appeals to some physical intuition for soft networks, the frame averaging limit proved to be cleaner to work with both analytically and numerically. Physical insights gained from this framework reveal that greater variance in monomer numbers typically leads to a softening at the RVE level. Furthermore, topological differences are shown to fundamentally alter the mechanical response even when the average chain length is conserved. Finally, by investigating ‘S’-shaped stress-strain curves

for bimodal networks, it was found that the onset of strain stiffening is governed by the shorter chains, while the sharpness of the stiffening reflects their proportion.

Outlook. Given the observation that the frame averaging limit generally provides a good approximation to the free rotation limit, a potential simple heuristic for modeling “soft” polymer networks may be to define the free energy of a RVE as the minimum of their respective predictions. Such an approach would naturally bound the energy of the system, leveraging the strengths of the frame averaging limit in regimes of high polydispersity while retaining the physical intuition of the free rotation limit where applicable. While the main thrust of this work was to proceed analytically, it could prove to be both fruitful and interesting to explore the implications of this framework numerically.

A potential issue with the numerical approximation of stress in this context is the difficulty of approximating derivatives of the free energy density via finite differences. Although possible, this approach is likely computationally expensive because the formulation involves optimization problems nested within multidimensional integration. The core difficulty lies in the fact that the derivatives are currently “outside” these operations. Ideally, derivatives would be “pushed inside” the operators; while this can be readily done with respect to the integrals for non-pathological networks, derivatives cannot be brought inside the inner optimization problems. To address this, we propose an approximation inspired by the concept of a “soft max” (or “soft min”), as popularized by the machine learning community (e.g., [128]). Here, the optimization problem is regularized and reposed as an integration, resembling Boltzmann statistics where a computational parameter, β , takes the place of inverse temperature:

$$\inf_x W(x) \approx \frac{\int dx (W e^{-\beta W})}{\int dx e^{-\beta W}}, \quad (8.1)$$

$$\arg \inf_x W(x) \approx \frac{\int dx (x e^{-\beta W})}{\int dx e^{-\beta W}}, \quad (8.2)$$

provided $\beta \gg 1$. As β increases, the approximation approaches the true minimum, though numerical stability must be carefully managed. The key advantage of replacing the optimization problem with an integral is that it allows one to push derivatives all the way down to the integrand, where they can be taken analytically or handled more easily by alternative means, such as automatic differentiation. While the motivating example was an approximation of stress, this idea applies to the many quantities of interest that can be posed as derivatives of the free energy density.

Closure. Despite the focus on relatively simple polydisperse chain and cross-link distributions, this work opens new possibilities for investigating synthesis-morphology-property relationships in polymer networks in a rational and efficient manner. Future research directions include incorporating a distribution of chain conformations within the polymer network homogenization framework, investigating the implications of polydispersity on fracture mechanics and toughness in heterogeneous networks, polydisperse multifunctional polymer networks, and phase transitions in polydisperse biopolymer networks. The ability to model these networks on the basis of the statistical descriptors of the structure of the network represents a step toward the targeted design of polymer networks with specific mechanical properties.

SOFTWARE AVAILABILITY

The code(s) used for analysis and generation of data for this work is available at <https://github.com/grasingerm/polydisperse-network-models> and <https://github.com/jasonmulderrig/polydisperse-polymer-networks>.

ACKNOWLEDGMENTS

MG thanks Gal deBotton and Kaushik Dayal for insightful discussions and their encouragement in pursuit of the topic. MG acknowledges the support of the Air Force Research Laboratory. JPM gratefully acknowledges the support of the National Research Council (NRC) Research Associateship Program (administered by the National Academies of Sciences, Engineering, and Medicine). MB acknowledges the support of Sandia National Laboratories. Sandia National Laboratories is a multi-mission laboratory managed and operated by National Technology and Engineering Solutions of Sandia, LLC, a wholly owned subsidiary of Honeywell International, Inc., for the U.S. Department of Energy's National Nuclear Security Administration under Contract No. DE-NA0003525. Any subjective views or opinions expressed in the paper do not necessarily represent the views of the U.S. Department of Energy or the U.S. Government. The U.S. Government retains and the publisher, by accepting the article for publication, acknowledges that the U.S. Government retains a non exclusive, paid-up, irrevocable, world-wide license to publish or reproduce the published form of this manuscript, or allow others to do so, for U.S. Government purposes.

Appendix A: Numerical implementation of the inverse Langevin function

In this work, we numerically approximate the inverse Langevin function $\mathcal{L}^{-1}(x)$ with the Jedynak $R_{9,2}$ approximant [129],

$$\mathcal{L}^{-1}(x) = \frac{x(3 - 1.00651x^2 - 0.96225x^4 + 1.47353x^6 - 0.48953x^8)}{(1-x)(1+1.01524x)}. \quad (\text{A1})$$

Using this inverse Langevin approximant, we obtain the following approximation to the Kuhn and Grün chain free energy in Eq. (2.6) (as per [129]),

$$\begin{aligned} \frac{w_{\text{KG}}(r)}{nk_B T} = & -0.015 + 0.0072\left(\frac{r}{\ell}\right) + 0.4887\left(\frac{r}{\ell}\right)^2 - 0.0025\left(\frac{r}{\ell}\right)^3 - 0.0035\left(\frac{r}{\ell}\right)^4 - 0.0015\left(\frac{r}{\ell}\right)^5 \\ & - 0.1627\left(\frac{r}{\ell}\right)^6 + 0.001\left(\frac{r}{\ell}\right)^7 + 0.0603\left(\frac{r}{\ell}\right)^8 - \ln\left(1 - \frac{r}{\ell}\right) - 0.992 \ln\left(0.985 + \frac{r}{\ell}\right). \end{aligned} \quad (\text{A2})$$

The above is correspondingly employed within the Kuhn and Grün polymer chain conformation probability density $p_{\text{KG}}(r)$ in Eq. (2.2).

The derivative of the inverse Langevin function, $(\mathcal{L}^{-1})'(x)$, is also of importance in this work. We approximate $(\mathcal{L}^{-1})'(x)$ by taking the derivative of the Jedynak $R_{9,2}$ approximant,

$$\begin{aligned} (\mathcal{L}^{-1})'(x) &= \frac{\partial \mathcal{L}^{-1}(x)}{\partial x} = \frac{(\mathcal{L}^{-1})'(x)_{\text{num}}}{(\mathcal{L}^{-1})'(x)_{\text{denom}}}, \quad (\text{A3}) \\ (\mathcal{L}^{-1})'(x)_{\text{num}} &= (3 - 3.01953x^2 - 4.81125x^4 + 10.31471x^6 - 4.40577x^8)(1-x)(1+1.01524x) \\ &\quad - x(0.01524 - 2.03048x)(3 - 1.00651x^2 - 0.96225x^4 + 1.47353x^6 - 0.48953x^8), \\ (\mathcal{L}^{-1})'(x)_{\text{denom}} &= ((1-x)(1+1.01524x))^2. \end{aligned}$$

Appendix B: Recommended chain end positions for polydisperse cross-link RVEs

In this Appendix section, we apply the principles introduced in Section IIID to define the set of chain end positions, $\{\mathbf{X}_i\}_{i=1}^k$, and the corresponding set of unit vectors, $\{\hat{\mathbf{X}}_i\}_{i=1}^k$ ($\hat{\mathbf{X}}_i = \mathbf{X}_i/|\mathbf{X}_i|$),

for polydisperse cross-link RVEs where $k \in [3, 8]$. Recall that we place these unit vectors according to the Thomson problem: the equilibrium configuration of electrostatically repulsive particles on the unit sphere [109]. Ideally, we also place these unit vectors to maximize reflectional symmetry about the origin (especially if the Thomson problem is not able to be satisfied). In what follows, we provide $\{\mathbf{X}_i\}_{i=1}^k$ that either satisfies or closely satisfies these two considerations for $k \in [3, 8]$. For each case where $\{\mathbf{X}_i\}_{i=1}^k$ does not exactly satisfy both of these considerations, it is not known (at least not to the authors) if there even exists some $\{\mathbf{X}_i\}_{i=1}^k$ that does.

- $k = 3$: There are many choices for $\{\hat{\mathbf{X}}_i\}_{i=1}^3$ that solve the Thomson problem and maximize reflectional symmetry, where $\{\hat{\mathbf{X}}_i\}_{i=1}^3$ define the vertices of an equilateral triangle that rests on some equatorial plane in a unit sphere. One such example, inspired by the 3-chain models of [5], [35], and [107] is provided below²⁰

$$\begin{aligned} \mathbf{X}_1 &= (r_{rms})_1 \left(\sqrt{\frac{2}{3}}, -\sqrt{\frac{1}{6}}, -\sqrt{\frac{1}{6}} \right), & \mathbf{X}_2 &= (r_{rms})_2 \left(-\sqrt{\frac{1}{6}}, \sqrt{\frac{2}{3}}, -\sqrt{\frac{1}{6}} \right), \\ \mathbf{X}_3 &= (r_{rms})_3 \left(-\sqrt{\frac{1}{6}}, -\sqrt{\frac{1}{6}}, \sqrt{\frac{2}{3}} \right). \end{aligned} \quad (\text{B1})$$

Remark 7. Special considerations for the $k = 3$ RVE domain. Recall that Ω_0 is defined such that $\Omega_0 \subset \mathbb{R}^3$ (Ω is defined similarly). However, for the $k = 3$ RVE, the three chains $\{\mathbf{X}_i\}_{i=1}^3$ always lie on some shared plane, and thus, $\Omega_0 \subset \mathbb{R}^2$. We rectify this conflict by noting that (1) there exists a rectangular prism (in \mathbb{R}^3) tightly bounding $\{\mathbf{X}_i\}_{i=1}^3$, and (2) the boundary of said rectangular prism is taken as Ω_0 .²¹

- $k = 4$: The Thomson problem is solved and reflectional symmetry is maximized by taking $\{\hat{\mathbf{X}}_i\}_{i=1}^4$ to be coincident with the vertices of a regular tetrahedron. This aligns with the topology of the 4-chain model [6, 10]:

$$\begin{aligned} \mathbf{X}_1 &= (r_{rms})_1 (0, 0, 1), & \mathbf{X}_2 &= (r_{rms})_2 \left(0, \frac{2\sqrt{2}}{3}, -\frac{1}{3} \right), \\ \mathbf{X}_3 &= (r_{rms})_3 \left(\sqrt{\frac{2}{3}}, -\frac{\sqrt{2}}{3}, -\frac{1}{3} \right), & \mathbf{X}_4 &= (r_{rms})_4 \left(-\sqrt{\frac{2}{3}}, -\frac{\sqrt{2}}{3}, -\frac{1}{3} \right). \end{aligned} \quad (\text{B2})$$

- $k = 5$: The Thomson problem is solved by taking $\{\hat{\mathbf{X}}_i\}_{i=1}^5$ to be coincident with the vertices of an equilateral triangular bipyramid:

$$\begin{aligned} \mathbf{X}_1 &= (r_{rms})_1 (0, 0, 1), & \mathbf{X}_2 &= (r_{rms})_2 (1, 0, 0), \\ \mathbf{X}_3 &= (r_{rms})_3 \left(-\frac{1}{2}, \frac{\sqrt{3}}{2}, 0 \right), & \mathbf{X}_4 &= (r_{rms})_4 \left(-\frac{1}{2}, -\frac{\sqrt{3}}{2}, 0 \right), \\ \mathbf{X}_5 &= (r_{rms})_5 (0, 0, -1). \end{aligned} \quad (\text{B3})$$

²⁰ This RVE was formulated through the following procedure: (i) As per the 3-chain model [5], initially $\{\hat{\mathbf{X}}_i = \hat{\mathbf{e}}_i\}_{i=1}^3$ and $\mathbf{y} = \mathbf{0}$; (ii) translate $\{\hat{\mathbf{X}}_1, \hat{\mathbf{X}}_2, \hat{\mathbf{X}}_3\}$ by $(-\frac{1}{3}, -\frac{1}{3}, -\frac{1}{3})$ so that $\mathbf{y} = \mathbf{0}$ is now coincident with the center-of-mass of the RVE; and (iii) dilate the cube coinciding with the translated $\{\hat{\mathbf{X}}_1, \hat{\mathbf{X}}_2, \hat{\mathbf{X}}_3\}$ such that $\{|\hat{\mathbf{X}}_i - \mathbf{y}| = 1\}_{i=1}^3$.

²¹ During deformation, Ω is defined analogously.

- $k = 6$: The Thomson problem is solved and reflectional symmetry is maximized by taking $\{\hat{\mathbf{X}}_i\}_{i=1}^6$ to be coincident with the vertices of a regular octahedron. This aligns with the topology of the 6-chain model [80]:

$$\mathbf{X}_i = \begin{cases} (r_{rms})_i \hat{\mathbf{e}}_i, & i = 1, 2, 3 \\ -(r_{rms})_i \hat{\mathbf{e}}_{i-3}, & i = 4, 5, 6 \end{cases} \quad (\text{B4})$$

- $k = 7$: The Thomson problem is solved by taking $\{\hat{\mathbf{X}}_i\}_{i=1}^7$ to be coincide with the vertices of an equilateral pentagonal bipyramid:

$$\begin{aligned} \mathbf{X}_1 &= (r_{rms})_1 (0, 0, 1), & \mathbf{X}_2 &= (r_{rms})_2 (1, 0, 0), \\ \mathbf{X}_3 &= (r_{rms})_3 \left(\frac{1}{4} (\sqrt{5} - 1), \sqrt{\frac{5}{8} + \frac{\sqrt{5}}{8}}, 0 \right), & \mathbf{X}_4 &= (r_{rms})_4 \left(\frac{1}{4} (-1 - \sqrt{5}), \sqrt{\frac{5}{8} - \frac{\sqrt{5}}{8}}, 0 \right), \\ \mathbf{X}_5 &= (r_{rms})_5 \left(\frac{1}{4} (-1 - \sqrt{5}), -\sqrt{\frac{5}{8} - \frac{\sqrt{5}}{8}}, 0 \right), & \mathbf{X}_6 &= (r_{rms})_6 \left(\frac{1}{4} (\sqrt{5} - 1), -\sqrt{\frac{5}{8} + \frac{\sqrt{5}}{8}}, 0 \right), \\ \mathbf{X}_7 &= (r_{rms})_7 (0, 0, -1). \end{aligned} \quad (\text{B5})$$

- $k = 8$: Reflectional symmetry is maximized by taking $\{\hat{\mathbf{X}}_i\}_{i=1}^8$ to be coincident with the vertices of a regular cube. This aligns with the topology of the 8-chain model [11]:

$$\mathbf{X}_i = \frac{(r_{rms})_i}{\sqrt{3}} (\pm 1, \pm 1, \pm 1), \quad i = 1, 2, \dots, 8. \quad (\text{B6})$$

The Thomson problem is solved by taking $\{\hat{\mathbf{X}}_i\}_{i=1}^8$ to be coincident with the vertices of a regular square anti-prism. One can realize such an RVE by twisting any one of the cube faces in the 8-chain model by $\pi/4$. We provide one such solution below:

$$\mathbf{X}_i = \begin{cases} \frac{(r_{rms})_i}{\sqrt{3}} (1, \pm 1, \pm 1), & i = 1, 2, 3, 4 \\ \frac{(r_{rms})_i}{\sqrt{2}} (-1, \pm 1, 0), & i = 5, 6 \\ \frac{(r_{rms})_i}{\sqrt{2}} (-1, 0, \pm 1), & i = 7, 8 \end{cases} \quad (\text{B7})$$

Appendix C: Derivatives of cross-link chain free energy with respect to junction position

Recall $W_{\text{ch}}(\mathbf{F}, \mathbf{Q}, \mathbf{y}) = \sum_{i=1}^k w_i (|\mathbf{F}\mathbf{Q}\mathbf{X}_i - \mathbf{y}|)$. Also, recall here that $\mathbf{r}_i = \mathbf{F}\mathbf{Q}\mathbf{X}_i - \mathbf{y}$, and thus, $r_i = |\mathbf{r}_i| = |\mathbf{F}\mathbf{Q}\mathbf{X}_i - \mathbf{y}|$. For Gaussian chains,

$$\frac{\partial W_{\text{ch}}}{\partial \mathbf{y}} = -\frac{3k_B T}{b} \sum_{i=1}^k \frac{\mathbf{r}_i}{\ell_i}, \quad (\text{C1})$$

$$\frac{\partial^2 W_{\text{ch}}}{\partial \mathbf{y} \partial \mathbf{y}} = \frac{3k_B T}{b^2} \sum_{i=1}^k \frac{1}{n_i} \mathbf{I}. \quad (\text{C2})$$

For Kuhn and Grün chains,

$$\frac{\partial W_{\text{ch}}}{\partial \mathbf{y}} = -\frac{k_B T}{b} \sum_{i=1}^k \mathcal{L}^{-1} \left(\frac{r_i}{\ell_i} \right) \frac{\mathbf{r}_i}{r_i}, \quad (\text{C3})$$

$$\frac{\partial^2 W_{\text{ch}}}{\partial \mathbf{y} \partial \mathbf{y}} = \frac{k_B T}{b^2} \sum_{i=1}^k \frac{1}{n_i} \left((\mathcal{L}^{-1})' \left(\frac{r_i}{\ell_i} \right) \left(\frac{\mathbf{r}_i \otimes \mathbf{r}_i}{r_i^2} \right) + \left(\frac{\mathcal{L}^{-1} \left(\frac{r_i}{\ell_i} \right)}{\frac{r_i}{\ell_i}} \right) \left(\mathbf{I} - \left(\frac{\mathbf{r}_i \otimes \mathbf{r}_i}{r_i^2} \right) \right) \right), \quad (\text{C4})$$

where $r_i > 0$ must hold. The numerical implementation of \mathcal{L}^{-1} and $(\mathcal{L}^{-1})'$ is detailed in Appendix A.

Appendix D: Nondimensional representation of the cross-link partition function and cross-link free energy

It is often times convenient (especially for numerical implementation) to represent free energies and their derivatives as nondimensional quantities. With this convention, Eq. (3.11) and Eq. (3.12) from the free rotation limit each take the following form,

$$\mathcal{Z}^{FR}(\mathbf{F}, \mathbf{Q}_0) \approx \left(\frac{(2\pi)^{3/2} b^3}{\sqrt{\det \left(\frac{b^2}{k_B T} \frac{\partial^2 W_{\text{ch}}}{\partial \mathbf{y} \partial \mathbf{y}} \Big|_{\mathbf{Q}=\mathbf{Q}^*, \mathbf{y}=\mathbf{y}^*} \right)}} \right) \exp \left(-\frac{W_{\text{ch}}(\mathbf{F}, \mathbf{Q}^*, \mathbf{y}^*)}{k_B T} - \frac{U_{\text{net}}(\mathbf{Q}^*)}{k_B T} \right), \quad (\text{D1})$$

$$\begin{aligned} \frac{W_c^{FR}(\mathbf{F}, \mathbf{Q}_0)}{k_B T} &= \frac{W_{\text{ch}}(\mathbf{F}, \mathbf{Q}^*, \mathbf{y}^*)}{k_B T} + \frac{U_{\text{net}}(\mathbf{Q}^*)}{k_B T} + \frac{1}{2} \ln \left(\det \left(\frac{b^2}{k_B T} \frac{\partial^2 W_{\text{ch}}}{\partial \mathbf{y} \partial \mathbf{y}} \Big|_{\mathbf{Q}=\mathbf{Q}^*, \mathbf{y}=\mathbf{y}^*} \right) \right) \\ &\quad - \frac{3}{2} \ln(2\pi) - 3 \ln(b). \end{aligned} \quad (\text{D2})$$

In the same vein, Eq. (3.16) and Eq. (3.17) from the frame averaging limit each take the following form,

$$\mathcal{Z}^{FA}(\mathbf{F}, \mathbf{Q}_0) \approx \left(\frac{(2\pi)^{3/2} b^3}{\sqrt{\det \left(\frac{b^2}{k_B T} \frac{\partial^2 W_{\text{ch}}}{\partial \mathbf{y} \partial \mathbf{y}} \Big|_{\mathbf{Q}=\mathbf{Q}_0, \mathbf{y}=\mathbf{y}_{\mathbf{Q}_0}^*} \right)}} \right) \exp \left(-\frac{W_{\text{ch}}(\mathbf{F}, \mathbf{Q}_0, \mathbf{y}_{\mathbf{Q}_0}^*)}{k_B T} \right), \quad (\text{D3})$$

$$\begin{aligned} \frac{W_c^{FA}(\mathbf{F}, \mathbf{Q}_0)}{k_B T} &= \frac{W_{\text{ch}}(\mathbf{F}, \mathbf{Q}_0, \mathbf{y}_{\mathbf{Q}_0}^*)}{k_B T} + \frac{1}{2} \ln \left(\det \left(\frac{b^2}{k_B T} \frac{\partial^2 W_{\text{ch}}}{\partial \mathbf{y} \partial \mathbf{y}} \Big|_{\mathbf{Q}=\mathbf{Q}_0, \mathbf{y}=\mathbf{y}_{\mathbf{Q}_0}^*} \right) \right) \\ &\quad - \frac{3}{2} \ln(2\pi) - 3 \ln(b). \end{aligned} \quad (\text{D4})$$

The last two terms in Eq. (D2) and Eq. (D4) each have no influence on the mechanics.

Appendix E: Historical development and related approaches

1. Historical precedent

Historically, some of the core ideas of the current approach have been developed elsewhere, albeit separately. For instance, the influential work of Flory and Rehner [10], and later Treloar [4, 6–9], developed a series of 4-chain polymer network models that included a relaxation of the cross-link junction position. Later on, Kloczkowski, Erman, and Mark [108] extended this fluctuating-junction 4-chain model to account for chains with a bimodal distribution of contour lengths. Adolf and Curro [107] also incorporated a relaxation of the cross-link junction position in the 3-chain model setting. All of these works utilized versions of Assumptions 1, 4, 7, and, to some extent, 5, to establish their models. However, these RVEs were each fixed relative to a chosen coordinate system and the resulting constitutive models did not satisfy frame indifference. Considering this context, the work of Elías-Zúñiga [35] is noteworthy; here, a fluctuating-junction 3-chain model is formulated (similar to Adolf and Curro [107]), where in the undeformed state, the chain ends are located at the vertices of an equilateral tetrahedron cell, and the junction point is located on its centroid. The tetrahedron is further assumed to be contained inside a regular cube. During deformation, the cube subsuming the 3-chain tetrahedron cell adheres to the principal frame assumption [80] while the junction point relaxes to its equilibrium position. In the same way, adherence to the principal frame assumption is enforced on the 4-chain tetrahedron cell in the work of Xing [33] (here, the junction position does not fluctuate). Finally, the seminal work by Arruda and Boyce [11] – the “8-chain model” – highlighted the importance of considering “cooperative” behaviors in polymer networks by allowing the cross-link to rotate to optimally distribute elastic energy across its chains. This idea was recently extended to cross-links consisting of differing numbers of chains: 3, 4, and 6 [80]. However, neither Arruda and Boyce [11] nor Grasinger [80] considered polydispersity, or fluctuation and relaxation of the junction position. This work incorporates each of these ideas, as well as introducing rotational (i.e. twisting) fluctuations of the cross-link.

2. Relationship with prior discrete polymer network models

Our proposed approach aims to model the mechanics of any arbitrary polydisperse cross-link structure. Because of this, many past discrete polymer network models are captured, in a generalized sense, by our framework. Several examples are provided as follows:

- *Fluctuating-junction 4-chain model.* The classical 4-chain model [4, 6–10] is instantiated via our modeling framework with a tetrafunctional cross-link of uniform Gaussian or Kuhn and Grün polymer chains in the absence of a free rotation assumption (i.e., fluctuations due to cross-link rotations are not accounted for). By amending the aforementioned instantiation such that some chains in the cross-link are long and Gaussian while other chains are short and non-Gaussian, the bimodal 4-chain model from Kloczkowski, Erman, and Mark [108] is captured.
- *Fluctuating-junction 3-chain model.* The 3-chain model from Adolf and Curro [107] is instantiated with a trifunctional cross-link of uniform Gaussian polymer chains in the absence of a free rotation assumption. The 3-chain model from Elías-Zúñiga [35] is also able to be instantiated by our modeling framework via a trifunctional cross-link of uniform Kuhn and Grün polymer chains. Here, instead of an absence of a free rotation assumption, a restrictive principal frame (rotation) assumption is enforced.

- *Arruda-Boyce 8-chain model.* As shown in Section IV B, the Arruda-Boyce 8-chain model is instantiated by our modeling framework via an octafunctional cubic cross-link (see Eq. (B6)) of uniform Kuhn and Gr \ddot{u} n polymer chains in the free rotation limit.
- *Free rotation assumption from Grasinger [80].* By assuming uniform polymer chains in the absence of cross-link junction fluctuations, we recover the free rotation assumption from Grasinger [80].

3. Comparing the frame averaging limit with the full network model

The full network model consists of a continuous uniform distribution of chain end-to-end vectors on the sphere of radius r_{rms} , i.e., $\mathbb{S}^2(r_{rms}) = \{\mathbf{r}_{rms} \in \mathbb{R}^3 : |\mathbf{r}_{rms}| = r_{rms}\}$. In the original formulation [12, 13], the chain end-to-end vectors are assumed to deform affinely under \mathbf{F} (other deformation assumptions for the full network model have since been formulated, e.g., [15, 50, 60, 61, 75–77, 130]). Considering this, the full network model RVE free energy is

$$W^{FN}(\mathbf{F}) = \frac{1}{4\pi} \int_{\mathbb{S}^2} dA w\left(r_{rms} \sqrt{\hat{\mathbf{v}} \cdot \mathbf{C} \hat{\mathbf{v}}}\right), \quad (\text{E1})$$

where $\hat{\mathbf{v}} \in \mathbb{S}^2$ is the chain orientation.

When comparing Eq. (E1) with Eq. (3.19), an interesting similarity is observed between the full network model and the frame averaging limit: both frameworks consider a continuous (uniform) probability distribution of polymer network constituents to determine the free energy of the RVE. Because of this, similar quadrature techniques can be used to evaluate the integration required for each framework.²²

The two frameworks differ in several respects. The frame averaging limit RVE permits chains with varying monomer numbers, while the full network model RVE assumes uniform chains. The fluctuating cross-link junction allows non-affine chain deformations in the frame averaging limit, whereas the full network model assumes affine deformation. One difference merits further discussion. The full network model RVE comprises infinitely many polymer chains emanating spherically from a common junction point (via the continuous uniform distribution of chains on \mathbb{S}^2) [80]. While this accounts for chains oriented in all directions, the construction is non-physical – no cross-link connects to infinitely many chains. The frame averaging limit instead uses a continuous distribution of real cross-link structures (each with finitely many chains) over all possible orientations. This also accounts for chains in all directions, but as a consequence of averaging over orientations of physical cross-link geometries rather than by artificially imposing infinite functionality. One could argue that the frame averaging limit is a more physically realistic realization of the full network model.

4. Connections to composite homogenization

It is instructive to briefly consider the proposed modeling approach through the lens of homogenization theory. A common starting point for polymer networks is the affine deformation assumption, where end-to-end vectors deform directly with the macroscopic deformation gradient, \mathbf{F} . This is analogous to the Voigt (constant strain) approximation in composites, which is known to provide an upper bound on both the free energy density and the homogenized mechanical response.

²² Spherical quadrature is needed to evaluate the integration over \mathbb{S}^2 for the full network model. For the frame averaging limit, we develop a bespoke quadrature technique for integration over $SO(3)$ (interestingly, this $SO(3)$ quadrature is built directly on top of any arbitrary spherical integration technique). We discuss this $SO(3)$ quadrature in Section V A and Appendix G.

While suitable for some monodisperse networks, this approximation can be poor for systems with chains of different lengths or orientations, as it enforces the development of unequal tensions, leading to unbalanced forces and inefficient distribution of elastic energy. An alternative is provided by equal-force theories [50, 54–56], which assume chains aligned in the same direction share the same tension, analogous to the Reuss (constant stress) approximation. Although this can better match experimental data for polydisperse networks, the Reuss assumption can also be too restrictive. In contrast, the proposed model – which involves relaxing the junction position – is analogous to more advanced nonlinear homogenization techniques where the boundary of an RVE is deformed while its interior relaxes to equilibrium [105, 106]. The junction relaxation naturally satisfies the force balance at each cross-link and, we postulate, permits a more realistic stress distribution than either the equal-strain or equal-force theories.

Appendix F: Proof of the conservation of sum of stretches squared with respect to rotations, Proposition 3

This result was first proved in [80]. It is reproduced here for completeness.

Proposition 3 (Conservation property). *The sum of squares of the chain stretches, i.e. $\sum_{i=1}^k \gamma_i^2$, is conserved relative to general rotations*

a) *for all of the classical 3, 4, 6, and 8-chain RVEs and*

b) *provided the RVE has reflection symmetries about planes (passing through the origin) normal to three orthogonal directions, $\hat{\nu}_j$, $j = 1, 2, 3$, and, $\sum_{i=1}^k (\mathbf{X}_i \cdot \hat{\nu}_j)^2 = C$ for all j .*

While there is some overlap between a) and b), they are considered separately because a) establishes the conservation property for well known discrete polymer networks while b) is a sufficient condition for constructing new polymer network models with the same conservation property.

Proof. a) Let the coordinate systems for the RVEs be chosen such that

$$\mathbf{X}_i = \tilde{r}_{rms} \hat{\mathbf{e}}_i, \quad i = 1, 2, 3, \quad (\text{F1a})$$

for the 3-chain RVE;

$$\begin{aligned} \mathbf{X}_1 &= \tilde{r}_{rms} (0, 0, 1), & \mathbf{X}_2 &= \tilde{r}_{rms} \left(0, \frac{2\sqrt{2}}{3}, -\frac{1}{3} \right) \\ \mathbf{X}_3 &= \tilde{r}_{rms} \left(\sqrt{\frac{2}{3}}, -\frac{\sqrt{2}}{3}, -\frac{1}{3} \right), & \mathbf{X}_4 &= \tilde{r}_{rms} \left(-\sqrt{\frac{2}{3}}, -\frac{\sqrt{2}}{3}, -\frac{1}{3} \right) \end{aligned} \quad (\text{F1b})$$

for the 4-chain RVE;

$$\mathbf{X}_i = \begin{cases} \tilde{r}_{rms} \hat{\mathbf{e}}_i, & i = 1, 2, 3 \\ -\tilde{r}_{rms} \hat{\mathbf{e}}_{i-3}, & i = 4, 5, 6 \end{cases} \quad (\text{F1c})$$

for the 6-chain RVE; and

$$\mathbf{X}_i = \frac{\tilde{r}_{rms}}{\sqrt{3}} (\pm 1, \pm 1, \pm 1), \quad i = 1, 2, \dots, 8 \quad (\text{F1d})$$

for the 8-chain RVE. In each case,

$$\sum_{i=1}^k \gamma_i^2 = \frac{1}{\ell^2} \sum_{i=1}^k (\mathbf{F}\mathbf{Q}\mathbf{X}_i) \cdot (\mathbf{F}\mathbf{Q}\mathbf{X}_i) = \frac{1}{\ell^2} \sum_{i=1}^k \mathbf{X}_i \cdot \bar{\mathbf{C}}\mathbf{X}_i, \quad (\text{F2})$$

where again by $\bar{\mathbf{C}}$ we mean a similarity transformation of \mathbf{C} . Using Eq. (F1) and Eq. (F2), it can be shown directly that

$$\sum_{i=1}^k \gamma_i^2 = \text{const} \times \text{Tr } \bar{\mathbf{C}} \quad (\text{F3})$$

for each case, which is invariant with respect to \mathbf{Q} , as desired.²³

b) Expand each \mathbf{X} in the orthonormal basis, $\hat{\nu}_j$, $j = 1, 2, 3$. Let $\mathbf{X}_m = (\tilde{r}_{rms})_{m1} \hat{\nu}_1 + (\tilde{r}_{rms})_{m2} \hat{\nu}_2 + (\tilde{r}_{rms})_{m3} \hat{\nu}_3$ where $(\tilde{r}_{rms})_{mj} = (\mathbf{X}_m \cdot \hat{\nu}_j)$. Then

$$\sum_{m=1}^k \gamma_m^2 = \frac{1}{\ell^2} \sum_{m=1}^k \mathbf{X}_m \cdot \bar{\mathbf{C}}\mathbf{X}_m = \frac{1}{\ell^2} \sum_{i=1, j=1}^{3,3} \sum_{m=1}^k (\tilde{r}_{rms})_{mi} \bar{C}_{ij} (\tilde{r}_{rms})_{mj} = \frac{1}{\ell^2} \sum_{i=1}^3 \bar{C}_{ii} \sum_{m=1}^k (\tilde{r}_{rms})_{mi}^2, \quad (\text{F4})$$

where $\bar{\bar{\mathbf{C}}}$ is a similarity transformation of $\bar{\mathbf{C}}$ (and, consequently, is a similarity transformation of \mathbf{C}) and the last step is due to the reflection symmetries. Clearly $\sum_{i=1}^k \gamma_i^2 = (C/\ell^2) \text{Tr } \bar{\bar{\mathbf{C}}} = (C/\ell^2) \text{Tr } \mathbf{C}$, as desired. \square

Appendix G: $SO(3)$ quadrature formulation and instantiation

In this work, integration over $SO(3)$ (the proper orthogonal group of rotations in 3 dimensions) is evaluated via a numerical quadrature technique we call $SO(3)$ quadrature

$$\frac{1}{8\pi^2} \int_{\mathbf{Q}_0 \in SO(3)} d\mathbf{Q}_0 F(\mathbf{Q}_0) \approx \sum_{i=1}^{N_{SO(3)}} v_i F((\mathbf{Q}_0)_i), \quad (\text{G1})$$

where F is some general (scalar, vectorial, or tensorial) function of orientation \mathbf{Q}_0 , $\{(\mathbf{Q}_0)_i\}_{i=1}^{N_{SO(3)}}$ is the set of $SO(3)$ quadrature points, $\{v_i\}_{i=1}^{N_{SO(3)}}$ is the set of corresponding weight factors, and $N_{SO(3)}$ is the number of quadrature points. To instantiate the $SO(3)$ quadrature, we follow the sequential procedure provided below:

- (1) Select your spherical quadrature scheme of choice, with N_{sph} spherical quadrature points and $\{v_j\}_{j=1}^{N_{sph}}$ corresponding weight factors. Common spherical quadrature schemes used in mechanics modeling have included those by Bažant and Oh [120], Sloan and Womersley [131], and Lebedev [132–137] (although many others can be used [138–148]).
- (2) Extract the set of spherical coordinates $\{(1, \theta_j, \phi_j)\}_{j=1}^{N_{sph}}$ from the spherical quadrature scheme. Here, we use the ISO 80000-2:2019 [149] convention (also called the physics convention) for spherical coordinates, where θ is the polar angle (with respect to the positive polar axis) and ϕ is the azimuthal angle (the angle of rotation of the radial line about the polar axis). Depending on the coordinate system used to provide the spherical quadrature points, a coordinate system conversion may need to be performed at this step (e.g., a Cartesian-to-spherical coordinate conversion).

²³ The algebra was verified in the Mathematica notebook, MPS-D-22-01011.nb, that can be found at <https://github.com/grasingerm/MPS-D-22-01011/>

- (3) Spherical quadrature is able to be extended to $SO(3)$ quadrature via the following simple step: at each j th orientation dictated by the j th spherical quadrature integration point, (θ_j, ϕ_j) , we must further integrate over all “spin orientations”. We capture this concept of “spin orientation” via the spin angle ψ , where $\psi \in [0, 2\pi)$. In $SO(3)$ quadrature, we must discretize the spin domain of ψ . In this work, we choose a simple method where we discretize the spin domain into N_ψ evenly-spaced points, starting at 0 radians. Thus, associated with each j th spherical quadrature integration point are N_ψ discretized spins. The weight factor that corresponds with each of these discretized spin points is equal to ν_j/N_ψ .
- (4) In light of the details provided in step (3), we begin instantiating $SO(3)$ quadrature by building the following two sets: $\{(\psi_i, \theta_i, \phi_i)\}_{i=1}^{N_{SO(3)}}$ and $\{v_i\}_{i=1}^{N_{SO(3)}}$, where $N_{SO(3)} = N_{sph} * N_\psi$, and each v is appropriately calculated with respect to ν/N_ψ .
- (5) At this point, we reveal that the set $\{(\psi_i, \theta_i, \phi_i)\}_{i=1}^{N_{SO(3)}}$ is actually a collection of Euler angles that discretizes rotations in $SO(3)$. We thus convert $\{(\psi_i, \theta_i, \phi_i)\}_{i=1}^{N_{SO(3)}}$ to $\{(\mathbf{Q}_0)_i\}_{i=1}^{N_{SO(3)}}$ via the ZYZ 3D rotation convention, as follows:

$$(\mathbf{Q}_0)_i = \mathbf{R}_z(\psi_i)\mathbf{R}_y(\theta_i)\mathbf{R}_z(\phi_i), \quad (\text{G2})$$

with corresponding rotation matrices

$$\mathbf{R}_z(\alpha) = \begin{pmatrix} \cos \alpha & -\sin \alpha & 0 \\ \sin \alpha & \cos \alpha & 0 \\ 0 & 0 & 1 \end{pmatrix}, \quad \mathbf{R}_y(\beta) = \begin{pmatrix} \cos \beta & 0 & \sin \beta \\ 0 & 1 & 0 \\ -\sin \beta & 0 & \cos \beta \end{pmatrix}. \quad (\text{G3})$$

- (6) When appropriate, exploit symmetry in the $SO(3)$ quadrature (stemming from symmetry in the foundational spherical quadrature scheme) for enhanced computational efficiency.

Appendix H: Closed-form approximation for the cross-link position in the frame averaging limit for polydisperse Kuhn and Grün chains

Consider a polydisperse RVE consisting of chains with Kuhn and Grün free energy in the frame averaging limit. We here seek an analytical form for $\delta\mathbf{y}_{\mathbf{Q}_0}$ as per Eq. (5.8),

$$\delta\mathbf{y}_{\mathbf{Q}_0} = - \left(\frac{\partial^2 \widehat{W}_c^{FA}}{\partial \delta\mathbf{y}_{\mathbf{Q}_0} \partial \delta\mathbf{y}_{\mathbf{Q}_0}} \Big|_0 \right)^{-1} \frac{\partial \widehat{W}_c^{FA}}{\partial (\delta\mathbf{y}_{\mathbf{Q}_0})} \Big|_0. \quad (\text{H1})$$

Also recall the form for the chain end-to-end vector,

$$\mathbf{r}_i = \mathbf{F}\mathbf{Q}_0\mathbf{X}_i - (\mathbf{y}_m + \delta\mathbf{y}_{\mathbf{Q}_0}), \quad (\text{H2})$$

where $\mathbf{y}_m = \mathbf{0}$. To denote the fact that \mathbf{r}_i is evaluated at $\delta\mathbf{y}_{\mathbf{Q}_0} = \mathbf{0}$, as per Eq. (H1), we define the following shorthand notation:

$$\mathbf{r}_i|_0 = \mathbf{F}\mathbf{Q}_0\mathbf{X}_i, \quad r_i|_0 = |\mathbf{r}_i|_0| = |\mathbf{F}\mathbf{Q}_0\mathbf{X}_i|. \quad (\text{H3})$$

Given all of this, the analytical form for $\delta\mathbf{y}_{\mathbf{Q}_0}$ is found to be

$$\delta\mathbf{y}_{\mathbf{Q}_0} = \left(\sum_{i=1}^k \frac{1}{n_i} \left((\mathcal{L}^{-1})' \left(\frac{r_i|_0}{\ell_i} \right) \left(\frac{\mathbf{r}_i|_0 \otimes \mathbf{r}_i|_0}{(r_i|_0)^2} \right) + \left(\frac{\mathcal{L}^{-1} \left(\frac{r_i|_0}{\ell_i} \right)}{\frac{r_i|_0}{\ell_i}} \right) \left(\mathbf{I} - \left(\frac{\mathbf{r}_i|_0 \otimes \mathbf{r}_i|_0}{(r_i|_0)^2} \right) \right) \right) \right)^{-1} \left(\sum_{i=1}^k \mathcal{L}^{-1} \left(\frac{r_i|_0}{\ell_i} \right) \frac{\mathbf{r}_i|_0}{r_i|_0} \right), \quad (\text{H4})$$

where $r_i|_{\mathbf{0}} > 0$ must hold.

-
- [1] Melvin Mooney. A theory of large elastic deformation. *Journal of applied physics*, 11(9):582–592, 1940.
 - [2] Ronald S Rivlin. Large elastic deformations of isotropic materials iv. further developments of the general theory. *Philosophical transactions of the royal society of London. Series A, Mathematical and physical sciences*, 241(835):379–397, 1948.
 - [3] Raymond William Ogden. Large deformation isotropic elasticity—on the correlation of theory and experiment for incompressible rubberlike solids. *Proceedings of the Royal Society of London. A. Mathematical and Physical Sciences*, 326(1567):565–584, 1972.
 - [4] L R G Treloar. *The physics of rubber elasticity*. Oxford University Press, 1975.
 - [5] Hubert M James and Eugene Guth. Theory of the elastic properties of rubber. *The Journal of Chemical Physics*, 11(10):455–481, 1943.
 - [6] LRG Treloar. The elasticity of a network of long-chain molecules. i. *Transactions of the Faraday Society*, 39:36–41, 1943.
 - [7] Leslie RG Treloar. The elasticity of a network of long-chain molecules—ii. *Transactions of the Faraday Society*, 39:241–246, 1943.
 - [8] LRG Treloar. The elasticity of a network of long-chain molecules.—iii. *Transactions of the Faraday Society*, 42:83–94, 1946.
 - [9] LRG Treloar. The photoelastic properties of short-chain molecular networks. *Transactions of the Faraday Society*, 50:881–896, 1954.
 - [10] Paul J Flory and John Rehner Jr. Statistical mechanics of cross-linked polymer networks i. rubberlike elasticity. *The journal of chemical physics*, 11(11):512–520, 1943.
 - [11] Ellen M Arruda and Mary C Boyce. A three-dimensional constitutive model for the large stretch behavior of rubber elastic materials. *Journal of the Mechanics and Physics of Solids*, 41(2):389–412, 1993.
 - [12] PD Wu and Erik van der Giessen. On improved 3-d non-gaussian network models for rubber elasticity. *Mechanics research communications*, 19(5):427–433, 1992.
 - [13] PD Wu and Erik Van Der Giessen. On improved network models for rubber elasticity and their applications to orientation hardening in glassy polymers. *Journal of the Mechanics and Physics of Solids*, 41(3):427–456, 1993.
 - [14] LRG Treloar and G Riding. A non-gaussian theory for rubber in biaxial strain. i. mechanical properties. *Proceedings of the Royal Society of London. A. Mathematical and Physical Sciences*, 369(1737):261–280, 1979.
 - [15] C Miehe, S Göktepe, and F Lulei. A micro-macro approach to rubber-like materials—part i: the non-affine micro-sphere model of rubber elasticity. *Journal of the Mechanics and Physics of Solids*, 52(11):2617–2660, 2004.
 - [16] B Erman, PJ Flory, and JP Hummel. Moments of the end-to-end vectors for p-phenylene polyamides and polyesters. *Macromolecules*, 13(3):484–491, 1980.
 - [17] H Bechir, Luc Chevalier, and M Idjeri. A three-dimensional network model for rubber elasticity: The effect of local entanglements constraints. *International journal of engineering science*, 48(3):265–274, 2010.
 - [18] Ziyu Xing, Xiaodong Wang, Xiaoling Hu, and Rongguo Zhao. A multi-well energy landscape strategy of the rubber-like polymers undergoing intermolecular interactions for exploring rubber elasticity. *International Journal of Engineering Science*, 220:104438, 2026.
 - [19] Dmitri Miroshnychenko and WA Green. Heuristic search for a predictive strain-energy function in nonlinear elasticity. *International Journal of Solids and Structures*, 46(2):271–286, 2009.
 - [20] Yuhai Xiang, Danming Zhong, Peng Wang, Guoyong Mao, Honghui Yu, and Shaoxing Qu. A general constitutive model of soft elastomers. *Journal of the Mechanics and Physics of Solids*, 117:110–122, 2018.
 - [21] Martin Kroon. An 8-chain model for rubber-like materials accounting for non-affine chain deformations and topological constraints. *Journal of elasticity*, 102(2):99–116, 2011.

- [22] Lin Zhan, Siyu Wang, Shaoxing Qu, Paul Steinmann, and Rui Xiao. A new micro–macro transition for hyperelastic materials. *Journal of the Mechanics and Physics of Solids*, 171:105156, 2023.
- [23] Jacob D Davidson and Nakhiah C Goulbourne. A nonaffine network model for elastomers undergoing finite deformations. *Journal of the Mechanics and Physics of Solids*, 61(8):1784–1797, 2013.
- [24] Vu Ngoc Khiêm and Mikhail Itskov. Analytical network-averaging of the tube model:: Rubber elasticity. *Journal of the Mechanics and Physics of Solids*, 95:254–269, 2016.
- [25] Mikhail Itskov and Vu Ngoc Khiêm. Review of the analytical network-averaging: part i—theoretical foundation. *Mechanics of Soft Materials*, 6(1):5, 2024.
- [26] Jamil Mirzapour. A micro-mechanically-based constitutive model for hyperelastic rubber-like materials considering the topological constraints. *International Journal of Solids and Structures*, 275:112299, 2023.
- [27] Jinglei Yang, Kaijuan Chen, Chao Yu, Kun Zhou, and Guozheng Kang. A hyperelastic constitutive model for soft elastomers considering the entanglement-dependent finite extensibility. *Journal of the Mechanics and Physics of Solids*, 196:106000, 2025.
- [28] Zichuan Li, Jiajie Fan, and Guoqi Zhang. A new physics-motivated constitutive model of hyperelastic polymer networks. *International Journal of Mechanical Sciences*, page 111366, 2026.
- [29] Víctor Jesús Amores, José María Benítez, and Francisco Javier Montáns. Average-chain behavior of isotropic incompressible polymers obtained from macroscopic experimental data. a simple structure-based wpyiwg model in julia language. *Advances in Engineering Software*, 130:41–57, 2019.
- [30] Víctor Jesús Amores, Khanh Nguyen, and Francisco Javier Montáns. On the network orientational affinity assumption in polymers and the micro–macro connection through the chain stretch. *Journal of the Mechanics and Physics of Solids*, 148:104279, 2021.
- [31] Victor Jesus Amores, Laura Moreno, Jose Maria Benitez, and Francisco Javier Montans. A model for rubber-like materials with three parameters obtained from a tensile test. *European Journal of Mechanics-A/Solids*, 100:104931, 2023.
- [32] Ian Tan, John S Biggins, and Thierry Savin. New two-parameter constitutive models for rubber-like materials: Revisiting the relationship between single chain stretch and continuum deformation. *European Journal of Mechanics-A/Solids*, 108:105398, 2024.
- [33] Ziyu Xing. A pseudo-compressible dual 4-chain model of polymer networks for exploring rubber elasticity. *International Journal of Non-Linear Mechanics*, 175:105122, 2025.
- [34] Alex Elías-Zúñiga and Millard F Beatty. Constitutive equations for amended non-gaussian network models of rubber elasticity. *International journal of engineering science*, 40(20):2265–2294, 2002.
- [35] A Elias-Zuniga. A non-gaussian network model for rubber elasticity. *Polymer*, 47(3):907–914, 2006.
- [36] Ayoub Ouardi, Abdellah Hamdaoui, Makrem Arfaoui, Adnane Boukamel, and Nouredine Damil. A 3d micromechanical model for hyperelastic rubber-like materials and its numerical resolution by the asymptotic numerical method (anm). *European Journal of Mechanics-A/Solids*, 111:105594, 2025.
- [37] Tiankai Zhao, Jinrui Cao, Xin Li, Mingyong Xia, Bing Xue, and Hongyan Yuan. A network-based visco-hyperelastic constitutive model for optically clear adhesives. *Extreme Mechanics Letters*, 51:101594, 2022.
- [38] Georgios Grekas, Maria Proestaki, Phoebus Rosakis, Jacob Notbohm, Charalambos Makridakis, and Guruswami Ravichandran. Cells exploit a phase transition to mechanically remodel the fibrous extracellular matrix. *Journal of the Royal Society Interface*, 18(175):20200823, 2021.
- [39] Dawei Song, Assad A Oberai, and Paul A Janmey. Hyperelastic continuum models for isotropic athermal fibrous networks. *Interface Focus*, 12(6):20220043, 2022.
- [40] V Alastrué, MA Martinez, M Doblaré, and Andreas Menzel. Anisotropic micro-sphere-based finite elasticity applied to blood vessel modelling. *Journal of the Mechanics and Physics of Solids*, 57(1):178–203, 2009.
- [41] Samuel C Lamont, Jason Mulderrig, Nikolaos Bouklas, and Franck J Vernerey. Rate-dependent damage mechanics of polymer networks with reversible bonds. *Macromolecules*, 54(23):10801–10813, 2021.
- [42] Miguel Angel Moreno-Mateos, Maria Luisa Lopez-Donaire, Mokarram Hossain, and Daniel Garcia-Gonzalez. Effects of soft and hard magnetic particles on the mechanical performance of ultra-soft magnetorheological elastomers. *Smart Materials and Structures*, 2022.
- [43] Matthew Grasinger, Carmel Majidi, and Kaushik Dayal. Nonlinear statistical mechanics drives intrinsic electrostriction and volumetric torque in polymer networks. *Physical Review E*, 103:042504, 2021.

- [44] Matthew Grasinger, Kosar Mozaffari, and Pradeep Sharma. Flexoelectricity in soft elastomers and the molecular mechanisms underpinning the design and emergence of giant flexoelectricity. *Proceedings of the National Academy of Sciences*, 118(21), 2021. ISSN 0027-8424.
- [45] Matthew Grasinger. *Multiscale Modeling and Theoretical Design of Dielectric Elastomers*. PhD thesis, Carnegie Mellon University, 2019.
- [46] Noy Cohen, Kaushik Dayal, and Gal deBotton. Electroelasticity of polymer networks. *Journal of the Mechanics and Physics of Solids*, 92:105–126, 2016.
- [47] Idan Z Friedberg and Gal deBotton. Electroelasticity of copolymer networks. *Journal of the Mechanics and Physics of Solids*, 175:105295, 2023.
- [48] Jorgen S Bergström and Mary C Boyce. Constitutive modeling of the large strain time-dependent behavior of elastomers. *Journal of the Mechanics and Physics of Solids*, 46(5):931–954, 1998.
- [49] Pratik Khandagale, Timothy Breitzman, Carmel Majidi, and Kaushik Dayal. Statistical field theory for nonlinear elasticity of polymer networks with excluded volume interactions. *Physical Review E*, 107(6):064501, 2023.
- [50] Jason Mulderrig, Bin Li, and Nikolaos Bouklas. Affine and non-affine microsphere models for chain scission in polydisperse elastomer networks. *Mechanics of Materials*, 160:103857, 2021.
- [51] Yunwei Mao, Brandon Talamini, and Lallit Anand. Rupture of polymers by chain scission. *Extreme Mechanics Letters*, 13:17–24, 2017.
- [52] Michael R Buche and Meredith N Silberstein. Chain breaking in the statistical mechanical constitutive theory of polymer networks. *Journal of the Mechanics and Physics of Solids*, 156:104593, 2021.
- [53] Matthew Grasinger and Kaushik Dayal. Architected elastomer networks for optimal electromechanical response. *Journal of the Mechanics and Physics of Solids*, 146:104171, 2021. ISSN 0022-5096.
- [54] PR Von Lockette, EM Arruda, and Y Wang. Mesoscale modeling of bimodal elastomer networks: constitutive and optical theories and results. *Macromolecules*, 35(18):7100–7109, 2002.
- [55] E Verron and A Gros. An equal force theory for network models of soft materials with arbitrary molecular weight distribution. *Journal of the Mechanics and Physics of Solids*, 106:176–190, 2017.
- [56] Bin Li and Nikolaos Bouklas. A variational phase-field model for brittle fracture in polydisperse elastomer networks. *International Journal of Solids and Structures*, 182:193–204, 2020.
- [57] Lin Zhan, Siyu Wang, Rui Xiao, Shaoxing Qu, and Paul Steinmann. Statistical theory for polymer elasticity: From molecular kinematics to continuum behavior. *Physical Review E*, 112(2):025404, 2025.
- [58] Siyu Wang, Heng Xiao, and Lin Zhan. On the statistical physics and thermodynamics of polymer networks: An eulerian theory for entropic elasticity. *Journal of the Mechanics and Physics of Solids*, page 106382, 2025.
- [59] Lucas Mangas Araujo and Laurence Brassart. Force-biased chemical degradation in rubbery networks: Insights from discrete network simulations. *Extreme Mechanics Letters*, page 102344, 2025.
- [60] Lucas Mangas Araujo, Ivan Kryven, and Laurence Brassart. Micromechanical modelling of rubbery networks: The role of chain pre-stretch. *International Journal of Non-Linear Mechanics*, 166:104834, 2024.
- [61] Lucas Mangas Araujo and Laurence Brassart. The role of chain stretch heterogeneity on the uniaxial failure response of rubbery networks. *Mechanics of Materials*, 215:105599, 2026.
- [62] Robert J Wagner, Ethan Hobbs, and Franck J Vernerey. A network model of transient polymers: exploring the micromechanics of nonlinear viscoelasticity. *Soft Matter*, 17(38):8742–8757, 2021.
- [63] Robert J Wagner, Jinyue Dai, Xinfu Su, and Franck J Vernerey. A mesoscale model for the micromechanical study of gels. *Journal of the Mechanics and Physics of Solids*, 167:104982, 2022.
- [64] Robert J Wagner and Meredith N Silberstein. A foundational framework for the mesoscale modeling of dynamic elastomers and gels. *Journal of the Mechanics and Physics of Solids*, 194:105914, 2025.
- [65] Jincheng Lei, Ziqian Li, Shuai Xu, and Zishun Liu. A mesoscopic network mechanics method to reproduce the large deformation and fracture process of cross-linked elastomers. *Journal of the Mechanics and Physics of Solids*, 156:104599, 2021.
- [66] Jincheng Lei and Zishun Liu. A network mechanics method to study the mechanism of the large-deformation fracture of elastomers. *Journal of Applied Physics*, 132(13):135101, 2022.
- [67] Konik Kothari, Yuhang Hu, Sahil Gupta, and Ahmed Elbanna. Mechanical response of two-dimensional polymer networks: role of topology, rate dependence, and damage accumulation. *Journal of Applied Mechanics*, 85(3):031008, 2018.

- [68] Ahmed Ghareeb and Ahmed Elbanna. An adaptive quasicontinuum approach for modeling fracture in networked materials: Application to modeling of polymer networks. *Journal of the Mechanics and Physics of Solids*, 137:103819, 2020.
- [69] Sara Cardona, Mathias Peirlinck, and Behrooz Fereidoonzhad. Topogen: Topology-driven microstructure generation for in silico modeling of fiber network mechanics. *Journal of the Mechanics and Physics of Solids*, page 106257, 2025.
- [70] Juntao Huang, Jiabin Liu, and Shaoting Lin. Topological mechanics of entangled networks. *arXiv preprint arXiv:2509.17813*, 2025.
- [71] Chase M Hartquist, Shu Wang, Bolei Deng, Haley K Beech, Stephen L Craig, Bradley D Olsen, Michael Rubinstein, and Xuanhe Zhao. Fracture of polymer-like networks with hybrid bond strengths. *Journal of the Mechanics and Physics of Solids*, 195:105931, 2025.
- [72] Bolei Deng, Shu Wang, Chase Hartquist, and Xuanhe Zhao. Nonlocal intrinsic fracture energy of polymerlike networks. *Physical Review Letters*, 131(22):228102, 2023.
- [73] Chase Hartquist, Shu Wang, Qiaodong Cui, Wojciech Matusik, Bolei Deng, and Xuanhe Zhao. Scaling law for intrinsic fracture energy of diverse stretchable networks. *Physical Review X*, 15(1):011002, 2025.
- [74] Hao You, Shoujing Zheng, and Hua Li. A network graph entropy-based general model for soft polymer networks. *International Journal of Mechanical Sciences*, page 110732, 2025.
- [75] Mykola Tkachuk and Christian Linder. The maximal advance path constraint for the homogenization of materials with random network microstructure. *Philosophical Magazine*, 92(22):2779–2808, 2012.
- [76] Reza Rastak and Christian Linder. A non-affine micro-macro approach to strain-crystallizing rubber-like materials. *Journal of the Mechanics and Physics of Solids*, 111:67–99, 2018.
- [77] Mykola Tkachuk. Elastic homogenization of materials with composite network structures. *Journal of Mathematical Sciences*, 263(1):104–119, 2022.
- [78] Ellen Kuhl, Krishna Garikipati, Ellen M Arruda, and Karl Grosh. Remodeling of biological tissue: mechanically induced reorientation of a transversely isotropic chain network. *Journal of the Mechanics and Physics of Solids*, 53(7):1552–1573, 2005.
- [79] Noy Cohen. A generalized electro-elastic theory of polymer networks. *Journal of the Mechanics and Physics of Solids*, 110:173–191, 2018.
- [80] Matthew Grasinger. Polymer networks which locally rotate to accommodate stresses, torques, and deformation. *Journal of the Mechanics and Physics of Solids*, 175:105289, 2023.
- [81] Werner Kuhn and F Grün. Beziehungen zwischen elastischen konstanten und dehnungsdoppelbrechung hochelastischer stoffe. *Kolloid-Zeitschrift*, 101(3):248–271, 1942.
- [82] Jason Mulderrig, Brandon Talamini, and Nikolaos Bouklas. A statistical mechanics framework for polymer chain scission, based on the concepts of distorted bond potential and asymptotic matching. *Journal of the Mechanics and Physics of Solids*, 174:105244, 2023.
- [83] Masao Doi, Samuel Frederick Edwards, and Samuel Frederick Edwards. *The theory of polymer dynamics*, volume 73. oxford university press, 1988.
- [84] Michael R Buche, Meredith N Silberstein, and Scott J Grutzik. Freely jointed chain models with extensible links. *Physical Review E*, 106(2):024502, 2022.
- [85] Ehsan Darabi and Mikhail Itskov. A generalized tube model of rubber elasticity. *Soft Matter*, 17(6):1675–1684, 2021.
- [86] Gordon Kumar and Laurence Brassart. On tube models of rubber elasticity: fitting performance in relation to sensitivity to the invariant i_2 . *Mechanics of Soft Materials*, 5(1):6, 2023.
- [87] John F Marko and Eric D Siggia. Stretching dna. *Macromolecules*, 28(26):8759–8770, 1995.
- [88] Andrew Marantan and L Mahadevan. Mechanics and statistics of the worm-like chain. *American Journal of Physics*, 86(2):86–94, 2018.
- [89] Matthew Grasinger and Kaushik Dayal. Statistical mechanical analysis of the electromechanical coupling in an electrically-responsive polymer chain. *Soft Matter*, 16:6265–6284, 2020.
- [90] Matthew Grasinger, Kaushik Dayal, Gal deBotton, and Prashant K Purohit. Statistical mechanics of a dielectric polymer chain in the force ensemble. *Journal of the Mechanics and Physics of Solids*, 158:104658, 2022.
- [91] Pratik Khandagale, Carlos Garcia-Cervera, Gal DeBotton, Timothy Breitzman, Carmel Majidi, and Kaushik Dayal. Statistical field theory of polarizable polymer chains with nonlocal dipolar interactions. *Physical Review E*, 109(4):044501, 2024.

- [92] Steve Plimpton. Fast parallel algorithms for short-range molecular dynamics. *Journal of computational physics*, 117(1):1–19, 1995.
- [93] Aidan P Thompson, H Metin Aktulga, Richard Berger, Dan S Bolintineanu, W Michael Brown, Paul S Crozier, Pieter J In't Veld, Axel Kohlmeyer, Stan G Moore, Trung Dac Nguyen, et al. LAMMPS—a flexible simulation tool for particle-based materials modeling at the atomic, meso, and continuum scales. *Computer physics communications*, 271:108171, 2022.
- [94] Ziyu Ye and Robert A Riggleman. Molecular view of cavitation in model-solvated polymer networks. *Macromolecules*, 53(18):7825–7834, 2020.
- [95] Christopher W Barney, Ziyu Ye, Ipek Sacligil, Kelly R McLeod, Han Zhang, Gregory N Tew, Robert A Riggleman, and Alfred J Crosby. Fracture of model end-linked networks. *Proceedings of the National Academy of Sciences*, 119(7):e2112389119, 2022.
- [96] Han Zhang and Robert A Riggleman. Predicting failure locations in model end-linked polymer networks. *Physical Review Materials*, 8(3):035604, 2024.
- [97] Paul J Flory. Molecular theory of rubber elasticity. *Polymer journal*, 17(1):1–12, 1985.
- [98] Paul J Flory. Network topology and the theory of rubber elasticity. *British polymer journal*, 17(2):96–102, 1985.
- [99] Prince E Rouse Jr. A theory of the linear viscoelastic properties of dilute solutions of coiling polymers. *The Journal of Chemical Physics*, 21(7):1272–1280, 1953.
- [100] Masao Doi. *Introduction to polymer physics*. Oxford university press, 1996.
- [101] Cornelis Storm, Jennifer J Pastore, Fred C MacKintosh, Tom C Lubensky, and Paul A Janmey. Non-linear elasticity in biological gels. *Nature*, 435(7039):191–194, 2005.
- [102] Chase P Broedersz and Fred C MacKintosh. Modeling semiflexible polymer networks. *Reviews of Modern Physics*, 86(3):995–1036, 2014.
- [103] H Hatami-Marbini. Effect of crosslink torsional stiffness on elastic behavior of semiflexible polymer networks. *Physical Review E*, 97(2):022504, 2018.
- [104] Mark Warner and Eugene Michael Terentjev. *Liquid crystal elastomers*, volume 120. Oxford university press, 2007.
- [105] Graeme W Milton. *The theory of composites*. SIAM, 2022.
- [106] PJ Caulfield and P Ponte Castañeda. Twinning in porous elastomers. *Journal of the Mechanics and Physics of Solids*, 193:105896, 2024.
- [107] DB Adolf and JG Curro. Computer simulation of an entangled micronetwork: analysis of junction fluctuations in uniaxial extension. *Macromolecules*, 20(7):1646–1650, 1987.
- [108] A Kloczkowski, Burak Erman, and JE Mark. Effect of non-gaussian chains on fluctuations of junctions in bimodal networks. *Polymer*, 43(8):2569–2574, 2002.
- [109] Joseph John Thomson. Xxiv. on the structure of the atom: an investigation of the stability and periods of oscillation of a number of corpuscles arranged at equal intervals around the circumference of a circle; with application of the results to the theory of atomic structure. *The London, Edinburgh, and Dublin Philosophical Magazine and Journal of Science*, 7(39):237–265, 1904.
- [110] Paul J Flory. *Principles of Polymer Chemistry*. Cornell University Press, 1953.
- [111] Changwoon Jang, Timothy W Sirk, Jan W Andzelm, and Cameron F Abrams. Comparison of crosslinking algorithms in molecular dynamics simulation of thermosetting polymers. *Macromolecular Theory and Simulations*, 24(3):260–270, 2015.
- [112] Tim Bernhard and Andrei A Gusev. Phantom force balance procedure for predicting the modulus of entangled polymer networks. *ACS Polymers Au*, 5(5):500–513, 2025.
- [113] Tim Bernhard, Fabian Schwarz, and Andrei A Gusev. polymer-tools: A python package for generating and analyzing bead-spring polymer networks. *arXiv preprint arXiv:2508.11509*, 2025.
- [114] Douglas R Miller and Christopher W Macosko. A new derivation of postgel properties of network polymers. *Macromolecules*, 9(2):206–211, 1976.
- [115] Dale S Pearson and William W Graessley. The structure of rubber networks with multifunctional junctions. *Macromolecules*, 11(3):528–533, 1978.
- [116] Frank O Kuehnel. On the minimization over $SO(3)$ manifolds. Technical report, Citeseer, 2003.
- [117] Roger A Horn and Charles R Johnson. *Matrix analysis*. Cambridge university press Cambridge, 1985.
- [118] Charles R. Harris, K. Jarrod Millman, Stéfan J. van der Walt, Ralf Gommers, Pauli Virtanen, David Cournapeau, Eric Wieser, Julian Taylor, Sebastian Berg, Nathaniel J. Smith, Robert Kern, Matti

- Picus, Stephan Hoyer, Marten H. van Kerkwijk, Matthew Brett, Allan Haldane, Jaime Fernández del Río, Mark Wiebe, Pearu Peterson, Pierre Gérard-Marchant, Kevin Sheppard, Tyler Reddy, Warren Weckesser, Hameer Abbasi, Christoph Gohlke, and Travis E. Oliphant. Array programming with NumPy. *Nature*, 585(7825):357–362, September 2020. doi:10.1038/s41586-020-2649-2. URL <https://doi.org/10.1038/s41586-020-2649-2>.
- [119] Pauli Virtanen, Ralf Gommers, Travis E. Oliphant, Matt Haberland, Tyler Reddy, David Cournapeau, Evgeni Burovski, Pearu Peterson, Warren Weckesser, Jonathan Bright, Stéfan J. van der Walt, Matthew Brett, Joshua Wilson, K. Jarrod Millman, Nikolay Mayorov, Andrew R. J. Nelson, Eric Jones, Robert Kern, Eric Larson, C J Carey, İlhan Polat, Yu Feng, Eric W. Moore, Jake VanderPlas, Denis Laxalde, Josef Perktold, Robert Cimrman, Ian Henriksen, E. A. Quintero, Charles R. Harris, Anne M. Archibald, Antônio H. Ribeiro, Fabian Pedregosa, Paul van Mulbregt, and SciPy 1.0 Contributors. SciPy 1.0: Fundamental Algorithms for Scientific Computing in Python. *Nature Methods*, 17:261–272, 2020. doi: 10.1038/s41592-019-0686-2.
- [120] P Bažant and BH838076 Oh. Efficient numerical integration on the surface of a sphere. *ZAMM-Journal of Applied Mathematics and Mechanics/Zeitschrift für Angewandte Mathematik und Mechanik*, 66(1): 37–49, 1986.
- [121] T. M. Ragonneau. *Model-Based Derivative-Free Optimization Methods and Software*. PhD thesis, Department of Applied Mathematics, The Hong Kong Polytechnic University, Hong Kong, China, 2022. URL <https://theses.lib.polyu.edu.hk/handle/200/12294>.
- [122] T. M. Ragonneau and Z. Zhang. COBYQA Version 1.1.3, 2025. URL <https://www.cobyqa.com>.
- [123] Z. Zhang. PRIMA: Reference Implementation for Powell’s Methods with Modernization and Amelioration. available at <http://www.libprima.net>, DOI: 10.5281/zenodo.8052654, 2023.
- [124] Andrew R Conn, Nicholas IM Gould, and Philippe L Toint. *Trust region methods*. SIAM, 2000.
- [125] Stefan C Endres, Carl Sandrock, and Walter W Focke. A simplicial homology algorithm for lipschitz optimisation. *Journal of Global Optimization*, 72(2):181–217, 2018.
- [126] Rainer Storn and Kenneth Price. Differential evolution—a simple and efficient heuristic for global optimization over continuous spaces. *Journal of global optimization*, 11(4):341–359, 1997.
- [127] Jason Mulderrig. [jasonmulderrig/polydisperse-polymer-networks](https://github.com/jasonmulderrig/polydisperse-polymer-networks). URL <https://github.com/jasonmulderrig/polydisperse-polymer-networks>.
- [128] Yann LeCun, Sumit Chopra, Raia Hadsell, M Ranzato, Fufei Huang, et al. A tutorial on energy-based learning. *Predicting structured data*, 1(0), 2006.
- [129] Radosław Jedynek. New facts concerning the approximation of the inverse langevin function. *Journal of Non-Newtonian Fluid Mechanics*, 249:8–25, 2017.
- [130] J Diani and Patrick Le Tallec. A fully equilibrated microsphere model with damage for rubberlike materials. *Journal of the Mechanics and Physics of Solids*, 124:702–713, 2019.
- [131] Ian H Sloan and Robert S Womersley. Extremal systems of points and numerical integration on the sphere. *Advances in Computational Mathematics*, 21(1):107–125, 2004.
- [132] Vyacheslav Ivanovich Lebedev. Values of the nodes and weights of ninth to seventeenth order gauss-markov quadrature formulae invariant under the octahedron group with inversion. *USSR Computational Mathematics and Mathematical Physics*, 15(1):44–51, 1975.
- [133] Vyacheslav Ivanovich Lebedev. Quadratures on a sphere. *USSR Computational Mathematics and Mathematical Physics*, 16(2):10–24, 1976.
- [134] Vyacheslav Ivanovich Lebedev. Spherical quadrature formulas exact to orders 25–29. *Siberian Mathematical Journal*, 18(1):99–107, 1977.
- [135] Vyacheslav Ivanovich Lebedev and AL Skorokhodov. Quadrature formulas of orders 41, 47, and 53 for the sphere. In *Russian Acad. Sci. Dokl. Math*, volume 45, pages 587–592, 1992.
- [136] Valentin Ivanovich Lebedev. A quadrature formula for a sphere that is the 59th algebraic order of accuracy. In *Doklady Akademii Nauk*, volume 338, pages 454–456. Russian Academy of Sciences, 1994.
- [137] Vyacheslav Ivanovich Lebedev and Dimitri N Laikov. A quadrature formula for the sphere of the 131st algebraic order of accuracy. In *Doklady Mathematics*, volume 59, pages 477–481. Pleiades Publishing, Ltd., 1999.
- [138] Sangwoo Heo and Yuan Xu. Constructing fully symmetric cubature formulae for the sphere. *Mathematics of computation*, 70(233):269–279, 2001.

- [139] Jörg Fliege and Ulrike Maier. *A two-stage approach for computing cubature formulae for the sphere*. Inst. für Mathematik, 1996.
- [140] Jörg Fliege and Ulrike Maier. The distribution of points on the sphere and corresponding cubature formulae. *IMA Journal of Numerical Analysis*, 19(2):317–334, 1999.
- [141] AH Stroud. *Approximate Calculation of Multiple Integrals*. Prentice-Hall, 1971.
- [142] Alexander D McLaren. Optimal numerical integration on a sphere. *Mathematics of Computation*, 17(84):361–383, 1963.
- [143] J Albrecht and L Collatz. Zur numerischen auswertung mehrdimensionaler integrale. *ZAMM-Journal of Applied Mathematics and Mechanics/Zeitschrift für Angewandte Mathematik und Mechanik*, 38(1-2): 1–15, 1958.
- [144] Casper HL Beentjes. Quadrature on a spherical surface. *Working note available on the website <http://people.maths.ox.ac.uk/beentjes/Essays>*, 2015.
- [145] Pierre-Bernard Badel and Jean-Baptiste Leblond. A note on integration schemes for the microplane model of the mechanical behaviour of concrete. *Communications in numerical methods in engineering*, 20(1):75–81, 2004.
- [146] Wolfram Neutsch. Optimal spherical designs and numerical integration on the sphere. *Journal of Computational Physics*, 51(2):313–325, 1983.
- [147] JH Hannay and JF Nye. Fibonacci numerical integration on a sphere. *Journal of Physics A: Mathematical and General*, 37(48):11591, 2004.
- [148] Sergei L’vovich Sobolev. The number of nodes in cubature formulas on the sphere. In *Selected Works of SL Sobolev: Volume I: Mathematical Physics, Computational Mathematics, and Cubature Formulas*, pages 467–471. Springer, 1962.
- [149] ISO/TC 12 Committee et al. Iso 80000-2: 2019 quantities and units—part 2: Mathematics, aug. 2019.